PROARRHYTHMIC DEFECTS IN TIMOTHY SYNDROME REQUIRE CALMODULIN KINASE II

By

William Howard Thiel

Dissertation

Submitted to the Faculty of the

Graduate School of Vanderbilt University

in partial fulfillment of the requirements

for the degree of

DOCTOR OF PHILOSOPHY

in

Pharmacology

December, 2008

Nashville, Tennessee

Approved:

Professor Mark E. Anderson, M.D. Ph.D.

Professor Alfred George, M.D.

Professor Roger Colbran, Ph.D.

Professor Dan M. Roden, M.D.

Professor Brian Wadzinski, Ph.D.

To my wife, my family, my lab and my dog. Thank you for all of your help.

ACKNOWLEDGMENTS

I would like to acknowledge the support from Mark Anderson's lab and all of the people I worked with at Vanderbilt University and University of Iowa. I would also like to thank the American Heart Association for funding my work with a predoctoral training grant and for granting me a renewal. I would like to thank my wife, Kristi, and my family for all of their support scientifically and beyond.

I would like to give a special thanks to those that helped me with the Timothy Syndrome project. To my committee members Roger Colbran, Al George, Dan Roden and Brian Wadzinski thank you for your patience and guidance. To Biyi Chen and Long-Sheng Song thank you for your help in the Ca^{2+} imaging and for teaching me how to analyze that data. To Olha Koval and Anil Purohit thank you for helping me patch myocytes. To Thomas Hund thank you for creating the mathematical model of Timothy Syndrome. To Peter Mohler thank you for your help and guidance in lenti virus and immuno-fluorescence. Lastly, to Mark Anderson thank you for making me a scientist I am proud to be.

TABLE OF CONTENTS

Page

LIST OF TABLES

LIST OF FIGURES

CHPATER I

INTRODUCTION

The heart: the body's electric pump

Cardiovascular disease is the leading cause of death in developed countries. To treat cardiovascular disease we must better understand how the heart functions. The heart's primary function is to move blood around the body, de-oxygenated blood to the lungs and oxygenated blood to all of the body's tissues. To accomplish this task the heart is organized with four chambers (Figure 1-1A). De-oxygenated blood (Figure 1-1A, blue) returns to the heart into the right atrium (RA), which contracts to fill the right ventricle (RV). When the RV contracts blood is sent to the lungs, becomes oxygenated (Figure 1-1A, red) and returns to the heart's left atrium (LA). The LA contraction fills the left ventricle, which contracts to send oxygenated blood throughout body. All of the chambers, atria and ventricles, are separated by one-way valves that keep the blood moving in the correct direction and prevent any back flow.

To move blood efficiently the heart's chambers must contract in a coordinated manner for several important reasons. A coordinated contraction prevents any single chamber from contracting out of synchrony with the other chambers. To best fill the ventricles the atria should contract just before the ventricles. Ventricular contraction begins on the inside (endocardium) and bottom (apex) of the heart and move towards the outside (epicardium) of the

heart. The heart comes equipped with a conduction system, similar to nerve fibers, which facilitate coordinated contraction. The electrical signal to contract

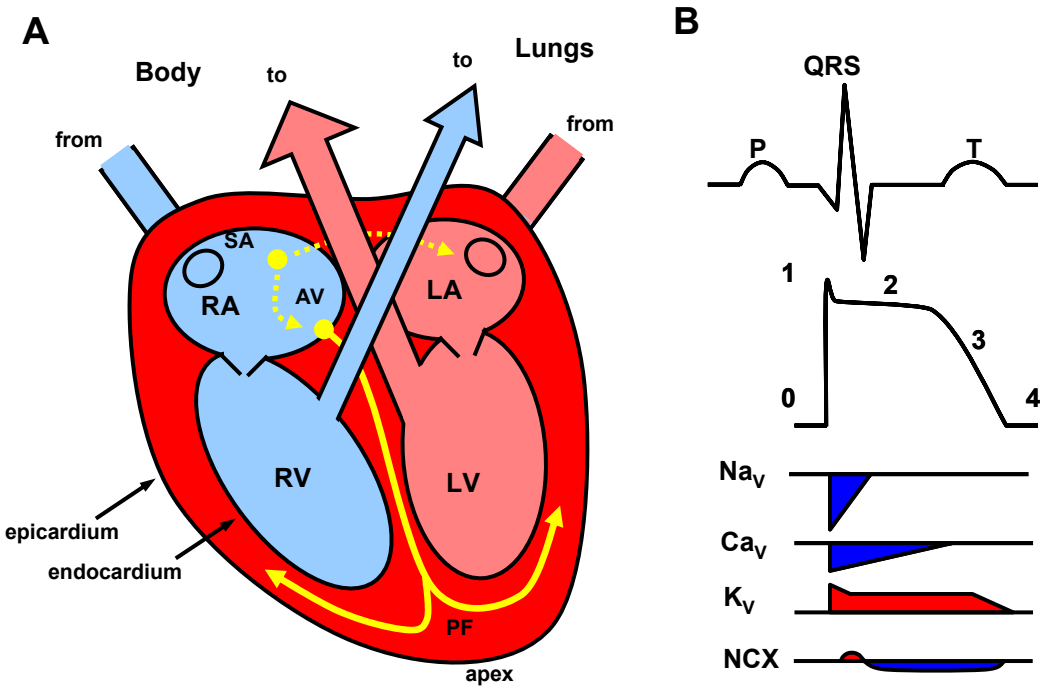

Figure 1-1: A) Schematic of the heat (RA = right atrium, RV = right ventricle, LA = left atrium, LV = left ventricle) showing blood flow (blue = deoxygenated, red = oxygenated) and conduction system (SA = sinoatrial node, AV = atrioventricular node, PF = purkinje fibers). **B)** Schematic of an electrocardiogram (ECG) depicting the electrical activity of the heat as related to a ventricular myocyte action potential and with corresponding ionic currents (red = repolarizing, blue = depolarizing).

begins in the RA with the sinoatrial (SA) node (Figure 1-1A), which sets the rate of contraction for the entire heart. The electrical signal from the SA node moves unimpeded to the LA (Figure 1-1A) but is slowed in reaching the ventricles by the

atrioventricular (AV) node (Figure 1-1A). The AV node allows the atria to contract and fill the ventricles with blood before the ventricles contract. After passing the AV node the electrical signal moves rapidly through the Purkinje fibers (PF) (Figure 1-1A) located within the RV and LV. The PF permit the ventricles to move blood efficiently by optimizing ventricular contraction.

If the electrical activity of the heart becomes irregular (arrhythmia) the heart does not move blood properly, a condition that can lead to reduced cardiac performance, loss of consciousness and death. Electrical activity of the heart may be observed by an electrocardiogram (ECG), which is an electrical readout of the heart's activity (Figure 1-1B). The P wave is the electrical representation of atrial systole, the QRS represents ventricular systole and the T wave represents ventricular repolarization.

The heart is made up of contractile cells called myocytes, specialized conduction cells (SA nodal, AV nodal, Purkinjie Fibers) and support cells including fibroblasts and endothelial cells. Cardiomyocytes are highly structured, electrically excitable and contractile. Each myocyte responds to, generates and propagates action potentials (Figure 1-1B), which are created by the movement of ions across the cell membrane (Figure 1-1B). An action potential begins when the cell membrane depolarization reaches a threshold (about -40 mV) that allows Na^+ conducting voltage gated channels (Na_V) to open and allow Na^+ ions to move into the cell down an electrochemical gradient (Figure 1-1B, phase 0) as depolarizing current. Despite only being open briefly (Figure 1-1B, phase 1), the Na^+ channels depolarize the myocyte membrane and trigger Ca^{2+} conducting

voltage gated channels (Ca_V) and K^+ conducting voltage gated channels (K_V) to open (Figure 1-1B). The electrochemical gradient for Ca^{2+} causes Ca^{2+} ions to move into the cell as a depolarizing current (Figure 1-1B) and the electrochemical gradient for potassium causes K^+ ions move out of the cell (Figure 1-1B) as a repolarizing current (positive). The depolarizing Ca^{2+} current elongates the action potential contributing to the plateau phase (Figure 1-1B, phase 2). When the Ca^{2+} channels close, the K^+ current repolarizes the cellular membrane (Figure 1-1B, phase 3). The cell membrane voltage will return to the resting membrane potential (Figure 1-1B, phase 4), a negative value near the equilibrium potential of K^+ (about -90mV) as predicted by the Nernst equation. The Nernst equation calculates the membrane potential necessary for no net movement of an ion based upon the concentration of that ion inside and outside the cell. The myocyte will remain quiescent until another electrical signal triggers an action potential.

Long QT Syndrome and afterdepolarizations

The cardiac action potential relies on a careful balance between depolarizing and repolarizing currents. Defective ventricular repolarization causes a long QT interval, Long QT Syndrome, and is a precursor to life-threatening arrhythmias (Figure 1-2A). Long QT Syndrome may trigger

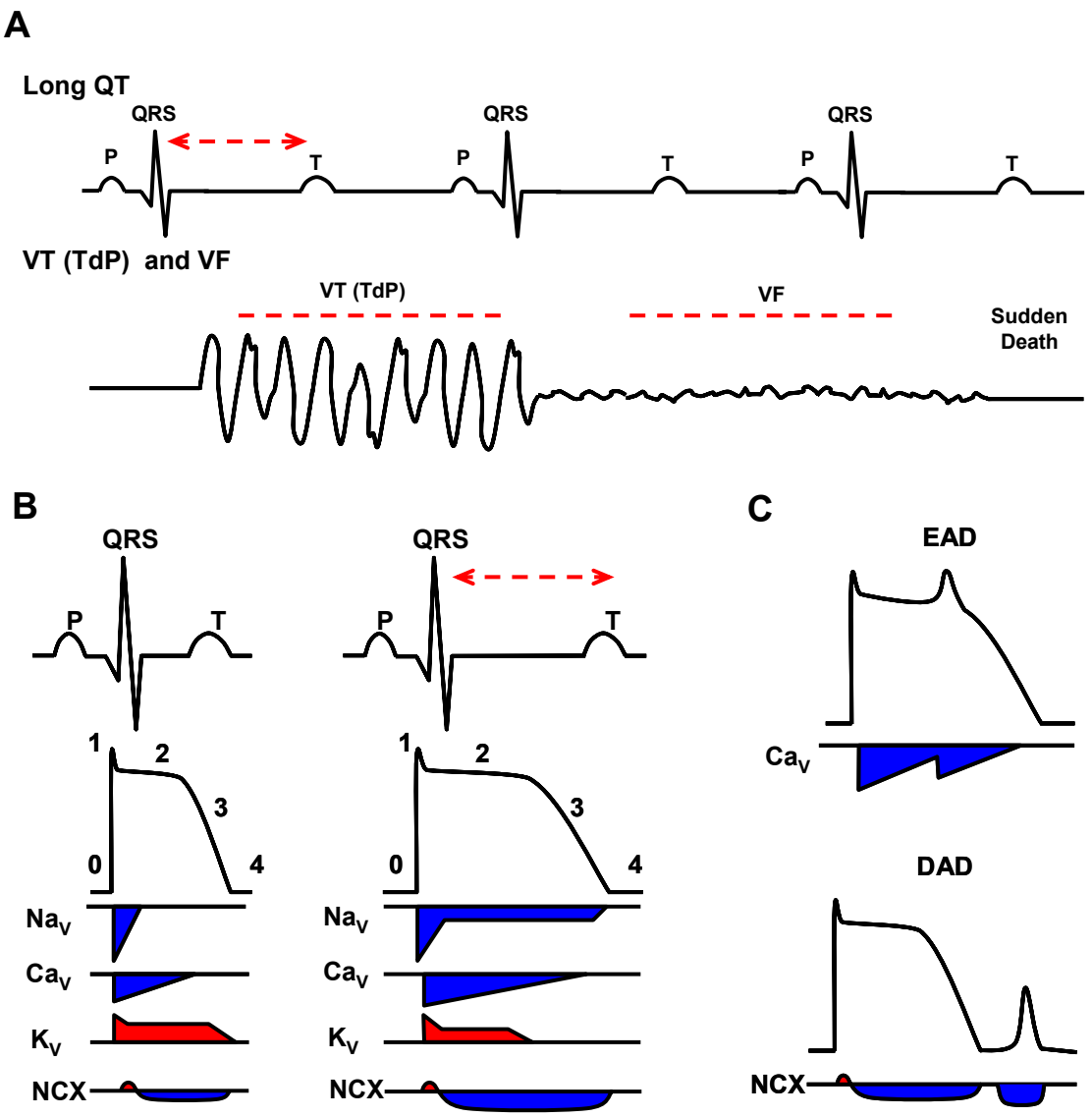

Figure 1-2: A) A prolonged QT interval can trigger ventricular tachycardia (VT) known as Torsades de Pointes (TdP), which may lead to ventricular fibrillation (VF) and sudden death. During VT (TdP) the ventricle is rapidly contracting and for VF ventricle contraction is completely uncoordinated. **B)** The increased duration of the QT interval corresponds to a prolonged action potential with a net loss of repolarizing current (i.e. decreased repolarizing current or increased depolarizing current). **C)** Proarrhythmic action potential early afterdepolarizations (EAD) and delayed afterdepolarization (DAD). EADs are associated with enhanced Ca_V activity and DADs are associated with increased Na^+/Ca^{2+} exchanger (NCX) activity causing an inward I_{Na}.

ventricular tachycardia that may degenerate into ventricular fibrillation (Figure 1-2A). Ventricular tachycardia initiated by a Long QT arrhythmia is referred to as Torsades de Pointes (TdP). Long QT Syndrome is either acquired or inherited. Acquired Long QT Syndrome results from external stimuli most commonly adverse drug interactions. Whereas inherited Long QT Syndrome results from genetic mutations that may be passed to the next generation.

Inherited Long QT Syndrome is caused by genetic mutations that produce a net loss of repolarizing current during the action potential (Figure 1-2B). Mutations associated with inherited Long QT Syndrome may affect the pore forming subunits of ion channels (LQT1, LQT2, LQT3, LQT7, LQT8), accessory subunits of ion channels (LQT5, LQT6, LQT10) and proteins that regulate/localize ion channels (LQT4, LQT9, LQT11, LQT12). A net reduction of repolarizing current may result from decrease K_V activity (I_{Ks}, I_{Kr}, I_{K1}) or an increase in Na_V (I_{Na}) and Ca_V (I_{Ca}) activity. Table 1-1 summarizes the different types of inherited Long QT Syndrome.

A long QT interval indicates a prolonged action potential plateau (phase 2) that constitutes primarily inward Ca^{2+} and outward K^+. The balance of between Ca_V channels and K_V channels propagates the plateau phase of the action potential. An early question arose as to how much current is required to maintain the action potential plateau. Experiments designed to answer this question injected a small amount of hyperpolarizing current into myocytes and found the greatest changes in membrane potential during the action potential plateau [109, 110]. Using Ohm's law (Membrane Potential = Current x Membrane Resistance),

Table 1-1: Inherited Long-QT Syndrome (LQTS)

LQTS	Protein	Gene	Current	Chromosome	Mechanism	Notes
LQT1	$K_V7.1$ (K_VLQT1)	KCNQ1	I_{Ks}	11p15.5	Loss of function	Pore forming α subunit
LQT2	$K_V11.1$ (HERG)	KCNH2	I_{Kr}	7q35-36	Loss of function	Pore forming α subunit
LQT3	$Na_V1.5$	SCN5A	I_{Na}	3p21-24	Gain of function	Pore forming α subunit
LQT4	Ankyrin-B	ANK2		4q25-27	Loss of function	Miss-localization of NCX1, NKA and $InsP_3R$ causes increased Ca^{2+} transients
LQT5	MinK	KCNE1	I_{Ks}	21q22	Loss of function	Accessory β subunit to $K_V7.1$
LQT6	MiRP1	KCNE2	I_{Kr}	21q22	Loss of function	Accessory β subunit to $K_V7.1$
LQT7	$K_{ir}2.1$	KCJN2	I_{K1}	17q23.1-q24.2	Loss of function	Andersen-Tawil Syndrome, pore forming subunit
LQT8	$Ca_V1.2$ (α_{1c})	CACNA1C	I_{Ca}	12p13.3	Gain of function	Timothy Syndrome, pore forming α subunit
LQT9	Caveolin 3	CAV3	I_{Na}	3p25	Gain of function	Mutations increased late I_{Na} of $Na_V1.5$
LQT10	$Na_V\beta_4$	SCN4B	I_{Na}	11q23	Gain of function	Accessory β subunit to $Na_V1.5$
LQT11	A-kinase anchor protein-9	AKAP9	I_{Ks}	7q21-q22	Loss of function	Mutation reduces phosphorylation of $K_V7.1$ and decreases I_{Ks}
LQT12	alpha-syntrophin	SNTA1	I_{Na}	20q11.2	Gain of function	Mutation leads to S-nitrosylation of SCN5A, which increase late I_{Na}

the action potential plateau is found to have very high resistance, meaning that small changes in current during the action potential plateau will have dramatic effects on membrane potential. The changes in membrane potential caused by the changes in current during the action potential plateau allow for additional action potential defects called afterdepolarizations. Afterdepolarizations may trigger ventricular tachycardia or Torsades de Pointes [87, 119, 125], which can lead to sudden death (Figure 1-2A).

Two main types of afterdepolarizations have been characterized based upon where they occur during the action potential. Early afterdepolarizations (EADs) occur during the action potential plateau phase [115] and delayed afterdepolarizations (DADs) occur after the action potential plateau [1, 116] (Figure 1-2B). EADs and DADs occur from separate molecular mechanism. EADs are believed to be caused by enhanced Ca^{2+} channel activity [115], whereas DADs are initiated by inward Na^{+} ions through the Na^{+}/Ca^{2+} exchanger (NCX) [1, 116]. The molecular mechanisms that lead to afterdepolarizations need to be better understood because failing hearts with LV hypertrophy exhibit afterdepolarizations and arrhythmias [119].

Excitation-contraction coupling and intracellular Ca^{2+} handling

As an action potential propagates across the heart, individual cardiomyocytes contract through a process called excitation-contraction coupling (ECC) [9, 10]. During the ventricular action potential (Figure 1-3, inset black) $Ca_V1.2$ opens and Ca^{2+} moves into the cell, triggering the release of Ca^{2+} through

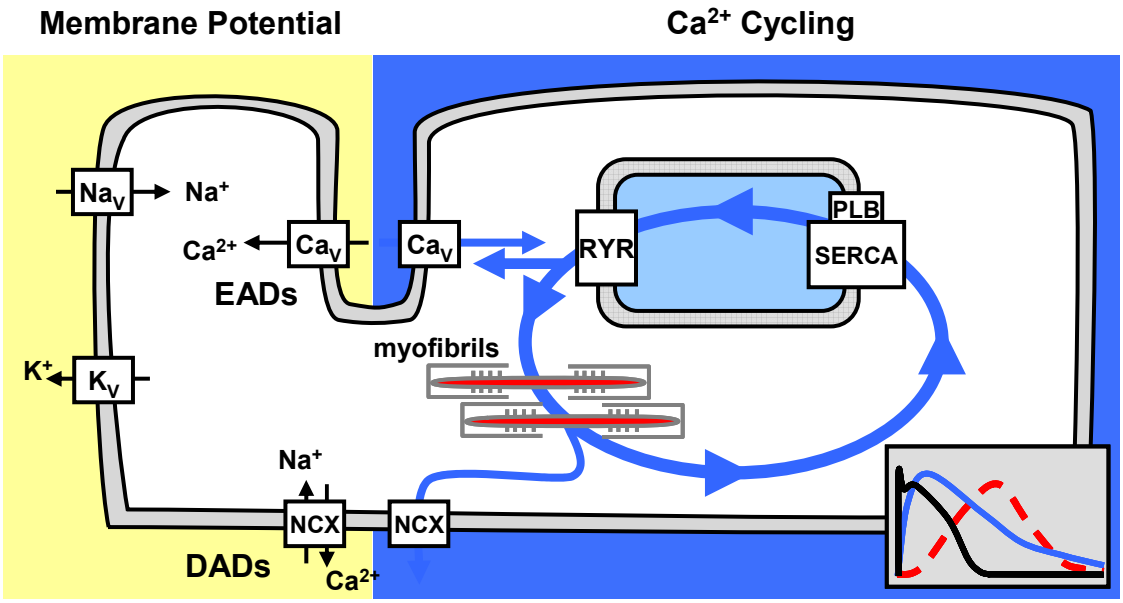

Figure 1-3: Excitation contraction coupling (ECC) highlighting key proteins; Na+ channels (Na_V), K^+ channels (K_V), Ca^{2+} channels (Ca_V), Ryanodine receptor (RYR), Phospholamben (PLB), Sarcoplasmic Reticulum Ca^{2+} ATPase (SERCA), Na^+/Ca^{2+} exchanger (NCX). During an action potential Na^+ and Ca^{2+} depolarize the cell and K^+ repolarizes the cell. The direction of NCX is dictated by the concentration gradient of intracellular Ca^{2+}. Ca^{2+} (blue arrows) enters the myocyte through Ca_V and induces SR Ca^{2+} release through RYR. SR Ca^{2+} regulates the Ca_V and causes contraction at the myofibrils. Ca^{2+} is cycled out of the myocyte through NCX or returned to the SR through SERCA. **Inset:** Depicts relationship between action potential (solid black), Ca^{2+} wave (solid blue) and contraction (dashed red).

ryanodine receptors (figure 1-3, RYR) by Ca^{2+}-induced Ca^{2+} release (figure 1-3, inset blue) [9]. The SR Ca^{2+} release initiates myocyte contraction (figure 1-3, inset red) [9]. The process resets, as Ca^{2+} is recycled back into the SR through the sarcoplasmic reticulum Ca^{2+} ATPase (figure 1-3, SERCA) and out of the cell through the Na^{+}/Ca^{2+} exchanger (Figure 1-3, NCX) [9].

The importance of $Ca_V1.2$ during ECC is in converting the electrical signal of the action potential (membrane depolarization) into a second messenger signal (Ca^{2+}) that helps to initiate and grade contraction (Figure 1-3). Furthermore, because $Ca_V1.2$ is the primary entry point of Ca^{2+} into a cardiomyocyte, the amount of available Ca^{2+} in the SR is related to $Ca_V1.2$ activity [27].

β-adrenergic receptor activation initiates a signaling cascade that leads to phosphorylation of several ECC protein targets, including $Ca_V1.2$ [124], the RYR [75] and phospholamban (PLB) [96]. Protein kinase A (PKA) is known to phosphorylate the pore forming α_{1c} subunit (Ser 1928) [23, 40] and the β subunit (Ser 478/9, Ser 459) [41] of $Ca_V1.2$. PKA phosphorylation increases $Ca_V1.2$ activity [124]. Experiments expressing an α_{1c} with a Ser 1928 Ala mutation retained an adrenergic response [38]. A truncation of the α_{1c} subunit that eliminates an AKAP binding site prevented the $Ca_V1.2$ adrenergic response [38]. PKA phosphorylation of RYR (Ser2809, Ser 2814) results in an increased sensitivity to Ca^{2+} and an increase in opening probability (Po) [75]. PLB binds to SERCA and attenuates its activity. Phosphorylation of PLB by PKA at Ser 16 results in a dissociation of PLB from SERCA [68, 107], thereby relieving inhibition of SERCA activity [103]. This

adrenergic signaling enhances several aspects of ECC by causing increases $Ca_V1.2$ activity, greater SR Ca^{2+} release through RYR and faster cycling of Ca^{2+} through SERCA [9].

Cycling of Ca^{2+} is a fundamental aspect of ECC and these oscillations of Ca^{2+} regulate the multifunctional Ca^{2+}/CaM dependent kinase II (CaMKII). CaMKII phosphorylates several of the same protein proteins involved in ECC that PKA phosphorylates, including $Ca_V1.2$, PLB and RYR. The role of CaMKII in ECC is complicated by the fact that the SR is also a critical source of Ca^{2+} for activating CaMKII, which in turn increases I_{Ca} [113, 114] and phosphorylates RYR [1, 108]. CaMKII phosphorylates the $Ca_V1.2$ β_{2a} subunit at residue Thr498 and increases the channel's activity [43]. PLB may be phosphorylated at residue Thr 17 [96] and causes a dissociation between PLB and SERCA. Thr 17 phosphorylation allows for frequency dependent acceleration of relaxation (FDAR) [8, 48] and allows the heart to adapt to changes in rate [8, 48]. However, PLB phosphorylation is not the only factor in FDAR because it has been shown that FDAR still occurs in PLB genetic knock-out mice [28]. CaMKII is known to phosphorylate RYR at residues Ser 2809 and Ser 2815 [108, 111]. Phosphorylation of RYR by CaMKII has been shown to increase and decrease spontaneous SR Ca^{2+} release [73, 108, 120]. Despite this controversy, failing hearts have been shown to have hyperphosphorylated RYR with increased spontaneous SR Ca^{2+} release [1, 75]. The role of CaMKII in regulating ECC is a fundamental process in myocytes adapting to heart rate frequency changes. The exact mechanisms of CaMKII

regulating ECC are still being investigated, but it is clear that mis-regulation of Ca^{2+} handling proteins allow for action potential defects like EADs and DADs.

DADs are favored by increased and spontaneous SR Ca^{2+} during diastole [1, 116]. The excess intracellular Ca^{2+} is partly removed by the Na^{+}/Ca^{2+} exchanger, where 3 Na^{+} ions are moved into the cell and one Ca^{2+} ion is moved out of the cell. This movement of ions has a net inward current, which depolarizes the membrane potential manifesting as a DAD. The net inward current through the exchanger may even trigger a full action potential if the threshold potential for Na_V is crossed. EADs occur due to reopening of $Ca_V1.2$ during the action potential plateau phase and EADs correspond with secondary increases of intracellular Ca^{2+} [21]. Secondary increases of Ca^{2+} associated with EADs are synchronous throughout the entire myocyte [21]. The synchronous increase of intracellular Ca^{2+} supports the idea of $Ca_V1.2$ reopening and triggering SR Ca^{2+} release [21]. The increase of intracellular Ca^{2+} may trigger an arrhythmia, which would magnify the increase of intracellular Ca^{2+}, thereby creating a self-perpetuating mechanism of arrhythmia for Torsades de Pointes and ventricular tachycardia [104].

CaMKII structure and function

CaMKII is a Ser/Thr kinase that often recognizes the general consensus site of RXXS/T on substrates and phosphorylates the S/T of the substrate [17, 85]. The CaMKII monomer consists of three domains, the catalytic (kinase) domain, a regulatory domain and an association domain (Figure 1-4A). Together these

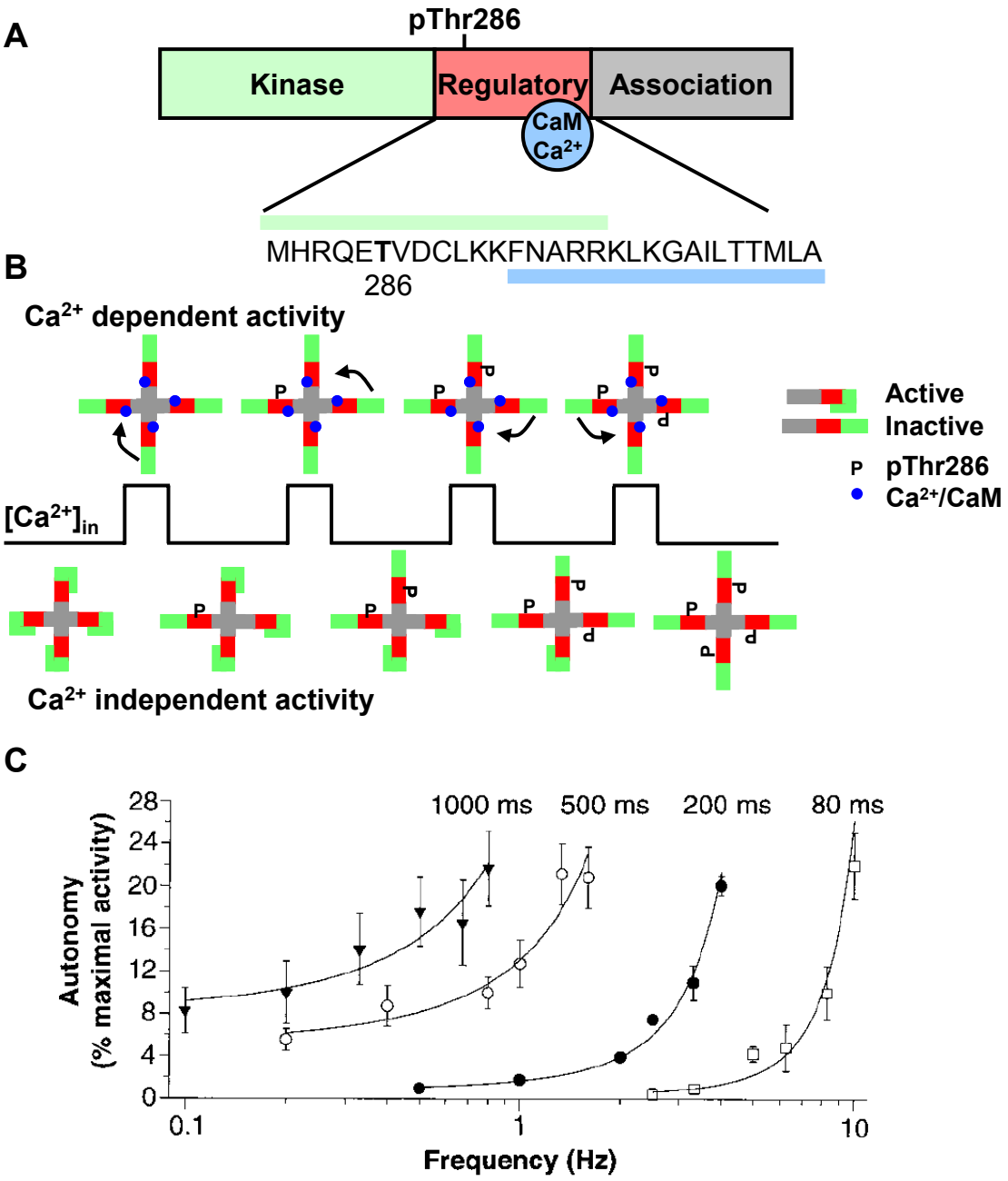

Figure 1-4: A) Ca^{2+} and CaM dependent protein kinase II (CaMKII) domains (Kinase, Inhibitory, Association). The regulatory sequences highlighted inlcuding the Thr 286 auto-phosphorylation site (pThr286), Kinase binding domain on the Inhibitory domain (green line over sequence) and the CaM binding domain (blue line under sequence). **B)** Diagram depicting how the holoenzyme structure of CaMKII allows the kinase to respond to oscillations of intracellular Ca^{2+} ($[Ca^{2+}]_{in}$) and remain active under Ca^{2+} independent conditions. **C)** CaMKII Ca^{2+} independent activity following different frequencies and pulse durations of Ca^{2+} (reproduced from De Koninck *et. al.*).

domains interact to provide CaMKII the unique ability to undergo Ca^{2+} dependent activation [11], Ca^{2+} independent activity [65, 71, 94] and respond to intracellular Ca^{2+} transient frequencies and duration [25] in the absence of Ca^{2+}/CaM or autophosphorylated Thr286.

The kinase domain of CaMKII is similar to known Ser/Thr kinases, such as PKA and PKC. The catalytic activity requires the kinase domain to bind Mg^{2+} to stabilize ATP during phosphorylation of a substrate [17]. The inhibitory domain binds the kinase domain (Figure 1-4A) and prevents phosphorylation of substrates [18-20].

Portions of the inhibitory domain regulate kinase activation by allowing the inhibitory domain to release the kinase domain in the presence of Ca^{2+} bound CaM (Figure 1-4A) [50, 81]. This process results in Ca^{2+} dependent activity (Figure 1-4B). Upon the removal of Ca^{2+}, CaM will no longer interact with the inhibitory domain and the kinase domain will once again become bound to the inhibitory region of the regulatory domain unless autophosphorylation or Met oxidation has occurred [32]. During Ca^{2+} dependent activity the kinase domain may auto-phosphorylate Thr286 within the inhibitory domain [93] (Figure 1-4A), which increases the binding affinity for CaM [79] and allows for Ca^{2+} independent activity [65, 71, 94] (Figure 1-4B). With Thr286 phosphorylated the inhibitory domain will not bind the kinase domain even in the absence of Ca^{2+} and CaM. Oxidation of paired methionines within the regulatory region also results in Ca^{2+} independent activity [32]. Ca^{2+} independent activity from phosphorylation may be reversed by phosphatase activity de-phosphorylating pThr286 [37, 95]. The reversibility of

oxidation Ca^{2+} independent activity is thought to occur by methionine sulfoxide reductase [32].

The association domain of CaMKII allows multiple monomers (6-12 subunits) to form larger holoenzymes [56, 63, 64] that can collectively respond to frequencies and pulse durations of Ca^{2+} [25] (Figure 1-4B). The proximity of each monomer to its neighbor allows for autophosphorylation during Ca^{2+} dependent activation by Ca^{2+}/CaM. If the intracellular Ca^{2+} transients are frequent or prolonged enough [25] and a majority of the holoenzyme reaches an auto-phosphorylated state, then the entire holoenzyme will remain active during the absence of Ca^{2+} [25] (Figure 1-4C). Longer (1000ms) Ca^{2+} transients achieve maximal Ca^{2+} independent activity at low frequencies, whereas shorter durations (80ms) of Ca^{2+} require higher frequencies (10Hz) to achieve the same Ca^{2+} independent activity (Figure 1-4C). The ability of CaMKII to respond to both frequency and duration of Ca^{2+} transients increases the dynamic range that CaMKII can respond to intracellular Ca^{2+} oscillations.

Patients and animals with cardiac hypertrophy and failure have increased CaMKII activity and expression [47, 55]. Our laboratory established a link between increased cardiac CaMKII activity, increased $Ca_V1.2$ openings, EADs and arrhythmias, in a mouse model of cardiac hypertrophy [117]. These cellular phenotypes were reversed by cellular dialysis of the CaMKII inhibitory peptide (AC3I), while a non-peptide CaMKII inhibitor (KN-93) reduced arrhythmias *in vivo* [117].

$Ca_V1.2$ structure and function

Ca^{2+} enters ventricular myocytes with each heart beat. The predominant pathway for this Ca^{2+} entry is through voltage-gated, L-type Ca^{2+} channels. The cardiac L-type Ca^{2+} channel consists of a pore forming α_{1c} subunit ($Ca_V1.2$), a β subunit (β_2 is the most common heart isoform [45]) and an $\alpha_2\delta$ subunit (Figure 1-5A). $Ca_V1.2$ is one of many voltage gated Ca^{2+} channels important for human physiology (Table 1-2). The pore forming $Ca_V1.2$ subunit is comprised of four domains with six transmembrane helices. Within each domain is a pore loop, which is selective for Ca^{2+}, over other physiological cations (but not Ba^{2+}, for example) and a voltage sensor (S4) that senses depolarization of the membrane through a lysine rich sequence. The β subunit acts as both a chaperone and modulator of $Ca_V1.2$ [26, 86]. The $\alpha_2\delta$ subunit supports the interaction between $Ca_V1.2$ and β subunits. The C-terminus of $Ca_V1.2$ contains many regulatory elements including three calmodulin (CaM) binding domains, A, CB IQ [97, 127, 128], an AKAP binding domain [40] and a serine residue phosphorylated by PKA [23, 89] (Figure 1-5A). The separate domains (I-IV) of the α_{1c} subunit orientate to form a selective pore for Ca^{2+} ions (Figure 1-5B).

Single channel recordings of $Ca_V1.2$ have revealed three types (gating modes) of activity (Figure 1-5C). An inactive state where current is not moving through the channel is called mode 0. Upon depolarization $Ca_V1.2$ may leave the inactive state (mode 0) and enter either a brief opening high activity state (mode 1) or a long opening high activity state (mode 2) [53]. Mode 1 activity is associated with brief openings (~1ms), whereas mode 2 is associated with long openings

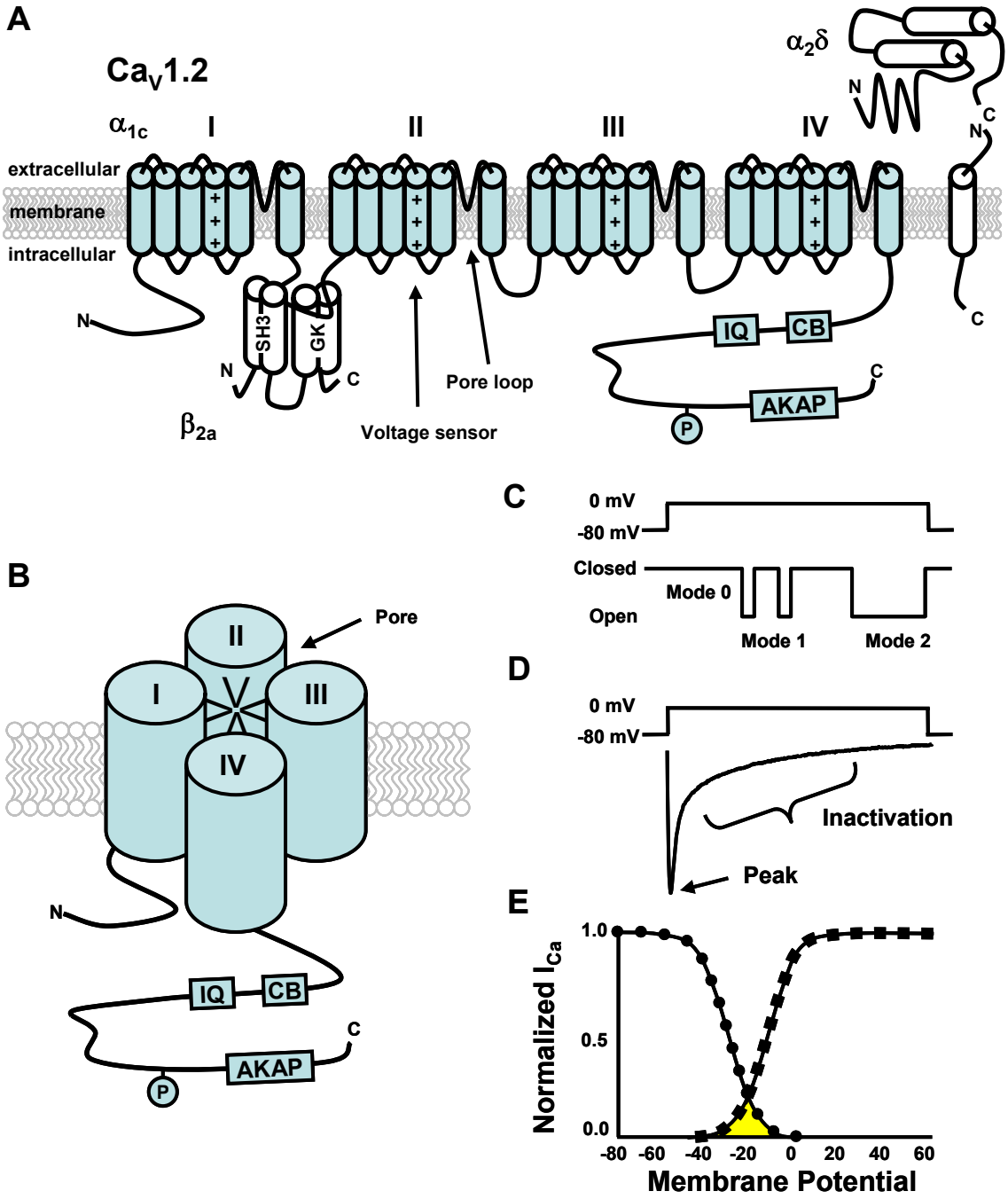

Figure 1-5: A) $Ca_V1.2$ pore forming α_{1c} subunit with accessory subunits β_{2a} and $\alpha_2\delta$. **B)** $Ca_V1.2$ α_{1c} domains I-IV orientate to form pore for Ca^{2+} entry into cell. **C)** Example of single channel $Ca_V1.2$ recording depicting the 'Open' and 'Closed' channel states and highlighting $Ca_V1.2$ modal gating (Mode 0 = closed, Mode 1 = low activity state, Mode 2 = high activity state). **D)** Example of inward Ca^{2+} current (I_{Ca}) from -80mV to 0mV voltage step. E) Steady state inactivation (squares) and steady state activation (circles) with overlap indicating window current (yellow).

(>10ms) [53]. A shift of $Ca_V1.2$ activity from mode 1 to mode 2 will also increase the channel Po. A $Ca_V1.2$ dihydropyridine antagonist, such as nifedipine, shifts $Ca_V1.2$ activity into mode 0 and $Ca_V1.2$ dihydropyridine agonists, such as Bay-K 8644, shift $Ca_V1.2$ activity towards mode 2 [53]. $Ca_V1.2$ is more likely to re-open during prolonged action potentials [5, 62] and these reopening events are thought to cause afterdepolarizations by directly depolarizing the cell membrane during the action potential plateau (EADs) or by contributing to SR Ca2+ overload, a condition that favors DADs [117].

Failing hearts have been shown to exhibit increased $Ca_V1.2$ Po.[49, 91]. Phosphorylation by PKA [21, 88] or CaMKII [30] appears to be an important regulatory step that favors mode 2 activity and increasing Po. Constitutively active CaMKII shifts $Ca_V1.2$ activity from mode 1 to mode 2 [30]. The β_{2a} subunit is critical for increasing the Po [43] and that this increase in Po depends on CaMKII phosphorylation of the β_{2a} subunit at residue Thr498 [43].

Macroscopic or whole cell $Ca_V1.2$ currents (I_{Ca}) show that a depolarization of the cellular membrane causes $Ca_V1.2$ to open (activate) and conduct Ca^{2+} ions into the cell (Figure 1-5D) and then close (inactivate) over time. Steady state I_{Ca} inactivation and activation may be plotted as a function of voltage to normalized current and the resulting plots overlap yielding a “window” current (Figure 1-5E) [78]. This window current indicates that a small percentage of I_{Ca} will remain active within the membrane voltages associated with the overlap of the two plots [78]. The window current helps explain how $Ca_V1.2$ may reopen during

Table 1-2: Voltage gated Ca^{2+} channel family

Family	α subunit	Gene	Tissue
L-type	$Ca_V1.1$ $Ca_V1.2$ $Ca_V1.3$ $Ca_V1.4$	CACNA1S CACNA1C CACNA1D CACNA1F	Skeletal muscle, heart, brain
P/Q-type	$Ca_V2.1$	CACNA1A	Brain
N-type	$Ca_V2.2$	CACNA1B	Brain
R-type	$Ca_V2.3$	CACNA1E	Brain
T-type	$Ca_V3.1$ $Ca_V3.3$ $Ca_V3.3$	CACNA1G CACNA1H CACNA1I	Brain, heart, bone

prolonged action potentials. Inactivation of $Ca_V1.2$ is an important aspect of the window current and it is controlled by several different factors.

I_{Ca} peaks and then undergoes a process of inactivation. Where, despite the membrane being depolarized, channels stop conducting Ca^{2+} (Figure 1-5D). The process of inactivation is dictated by both Ca^{2+} [12] and voltage [82]. The voltage dependent component of inactivation (VDI) is an intrinsic property of $Ca_V1.2$ and does not require ions to move through the channel [46], whereas the Ca^{2+} dependent inactivation (CDI) component requires Ca^{2+} entering the cell to interact with CaM [127, 128]. CaM mutations on N-terminus lobe (N) and C-terminus lobe (C) eliminate Ca^{2+} binding [77]. Introducing CaM with C lobe or N and C lobes mutated prevents CDI [83]. CaM with only the N lobe mutated has no effect on CDI [83]. The mechanistic structural bases for VDI and CDI are still unknown, [36]. However, CDI and VDI may share a final molecular determinants to achieve inactivation [36]. A comparison between α_{1a} and α_{1c} examining CDI and VDI with different β subunits found that both CDI and VDI were altered [15]. In the $Ca_V1.2$ α_{1c} genetic disease Timothy Syndrome a single mutation causes a loss of VDI [100, 101]. This mutation favors $Ca_V1.2$ entering a higher activity state because of the defect within VDI [33]. Interestingly, the Timothy Syndrome mutation may not only decrease VDI but also enhance CDI [6]. Cav1.2 inactivation, CDI and VDI, are fundamental processes for normal heart rhythm where changes lead to human disease.

CHAPTER II

CARDIOMYOCYTE CAV1.2 EXOGENOUS EXPRESSION

Introduction

The majority of the work on $Ca_V1.2$ function relies on expression within heterologous cells, which provide a reliable model to study channel function directly. Heterologous cell studies of $Ca_V1.2$ have revealed important biophysical features such as $Ca_V1.2$ regulation by the β subunit [26, 86], regulation by PKA [40] and Ca^{2+} dependent inactivation [83, 128]. However, the function of $Ca_V1.2$ is integrated into the context of physiological properties where $Ca_V1.2$ is endogenously expressed. For cardiovascular $Ca_V1.2$ function, this includes the ultra-structure of ventricular myocytes, which involves specialized structures like T-tubules [13] and the tight coupling of the extracellular membrane with the SR [9]. These features of ventricular myocytes are critical to the function of $Ca_V1.2$. Heterologous cells do not contain the ultra-structure found within ventricular myocytes and therefore do not provide a sufficient model for studying $Ca_V1.2$ function in the context of cardiovascular biology. Furthermore, $Ca_V1.2$ participates in physiological events, such as action potentials and intracellular Ca^{2+} handling, which do not occur within heterologous cells. Using heterologous cells helps in predicting how the action potential and Ca^{2+} handling may change in ventricular myocytes, but only experiments that use ventricular myocytes will test those hypotheses.

The advantage of using heterologous cells over ventricular myocytes is the ease that mutated $Ca_V1.2$ may be expressed within heterologous cells and the ease that heterologous cell may be cultured. Advances in expressing mutated $Ca_V1.2$ in primary cells have allowed for studying $Ca_V1.2$ function within neurons [29] and ventricular myocytes [38, 39]. These studies rely on silencing the endogenous $Ca_V1.2$ with a dihydropyridine $Ca_V1.2$ antagonist while the exogenous $Ca_V1.2$ remains functional due to a dihydropyridine insensitivity mutation [52, 92].

The work with adult ventricular myocytes has only examined mutated $Ca_V1.2$ whole cell currents [38] and not integrated events such as action potentials and Ca^{2+} handling. An important and uninvestigated area is how over-expression of $Ca_V1.2$ and dihydropyridine silencing may affect integrated ventricular myocyte features. A genetic mouse model of $Ca_V1.2$ over-expression [98] indicates increased I_{Ca} and greater Ca^{2+} transient amplitude, but not changes in SR Ca^{2+} content or spontaneous SR Ca^{2+} release. ***I hypothesized that exogenous expression of dihydropyridine resistant $Ca_V1.2$ in adult ventricular myocytes will not affect cardiomyocyte physiology after pharmacological inhibition of endogenous $Ca_V1.2$.*** To test this hypothesis I will use a lenti virus carrying a dihydropyridine resistant $Ca_V1.2$ and introduce this virus to cultured adult rat ventricular myocytes. I will focus on assessing integrated ventricular myocyte events, including the $Ca_V1.2$ inward current properties, action potentials and intracellular Ca^{2+} handling.

Results

Heterologous expression of a modified $Ca_V1.2$

$Ca_V1.2$ was marked by the addition of an extracellular hemaglutanin (HA) epitope [2] (Figure 2-1A, B, green circle) and introduced a validated dihydropyridine-insensitivity mutation [52, 92] (Figure 2-1A, B, black circle). This DHP insensitivity mutation has been used to study L-type Ca^{2+} channel signaling not only in neurons [29] but also in cultured adult cardiomyocytes [38, 39]. The dihydropyridine-insensitivity mutation (DHP^R) allows the virally introduced $Ca_V1.2$ to remain functional while using nifedipine to inhibit endogenous $Ca_V1.2$ [29].

Exogenous $Ca_V1.2$ expression was confirmed by immunoblot (Figure 2-1C) and immunofluorescence (Figure 2-2A) in transduced HEK293T cells. The functions of $Ca_V1.2$ wild type (WT) and TS were confirmed by recording I_{Ca} using whole cell voltage clamp in HEK293T cells. Whole cell voltage clamp recordings were consistent with $Ca_V1.2$ I_{Ca} (Figure 2-2B) [101]. The current and voltage (IV) relationship (Figure 2-2C) and the voltage dependence of inactivation (VDI) (Figure 2-2D) were as expected [101].

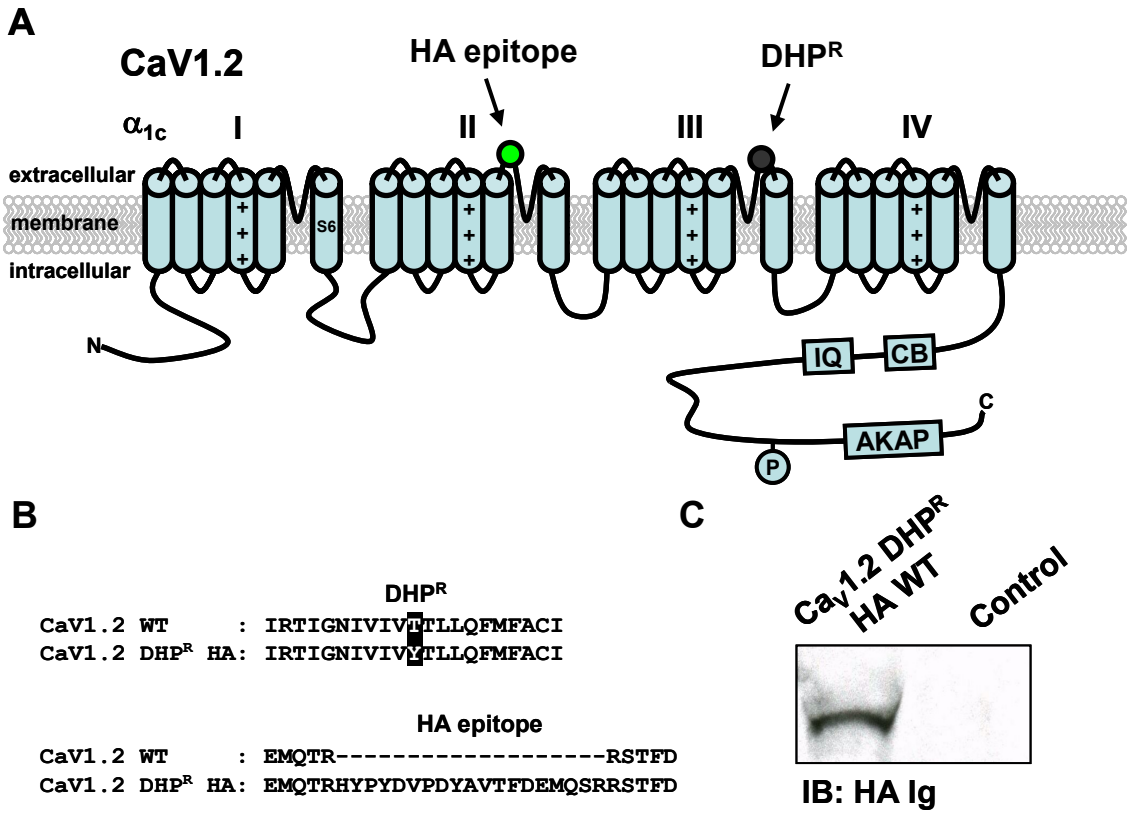

Figure 2-1: Modifications to $Ca_V1.2$ for expression within adult ventricular myocytes. **A)** Schematic of $Ca_V1.2$ depicting location of HA epitope and dihydropyridine resistance mutation (DHP^R). **B)** Sequence alignments of changes made to $Ca_V1.2$ open reading frame to include the DHPR mutation and HA epitope. C) Immuno-blot (HA-Ig) of modified $Ca_V1.2$ expressed in HEK293T cells.

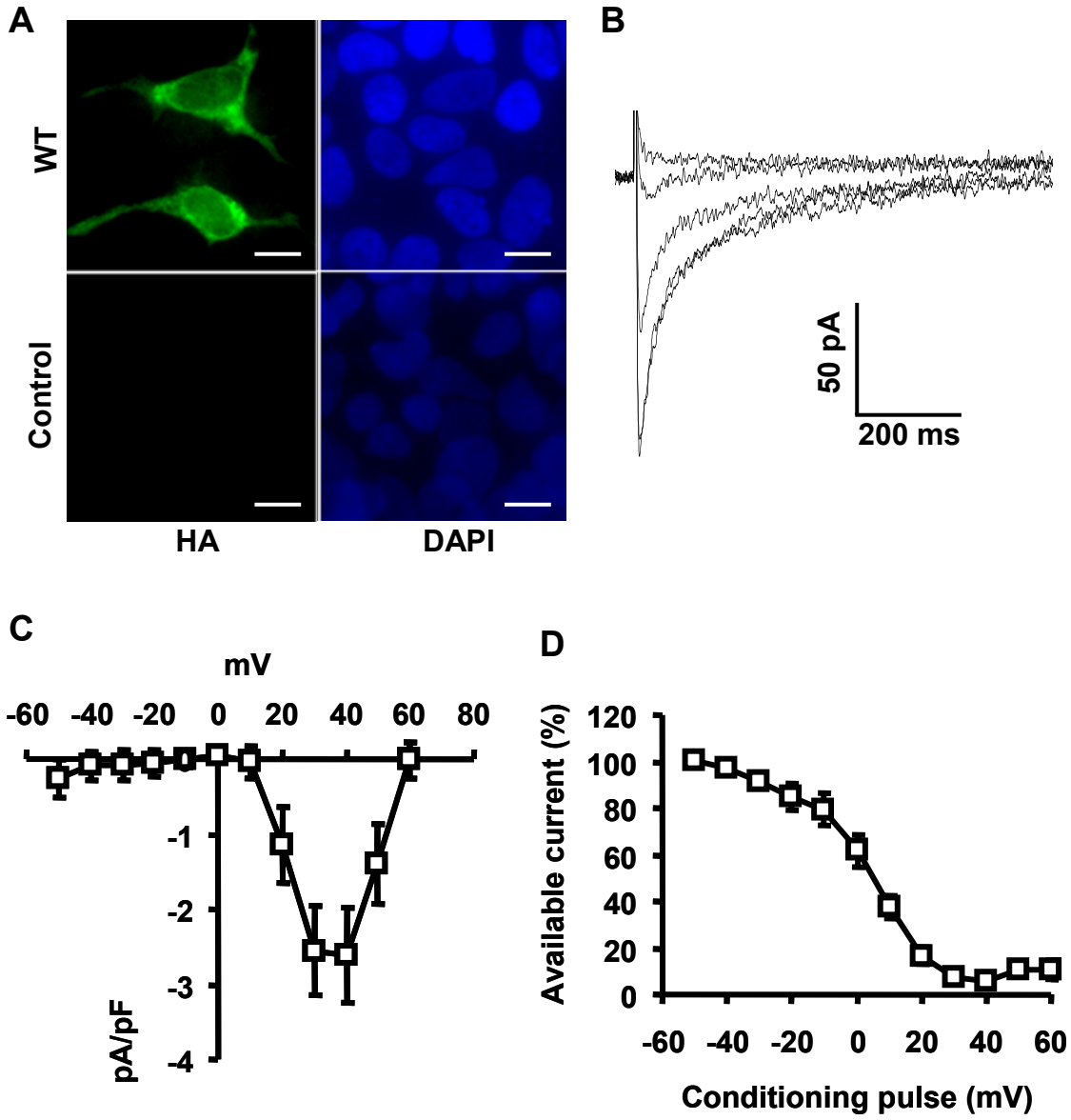

Figure 2-2: A) FITC immunofluorescence (HA Ig) of HEk293T cells expressing the modified $Ca_V1.2$ with corresponding nuclear stain by DAPI (Scale bar, 10μm) **B)** Example inward I_{Ca} (IV protocol) from HEK293T cells expressing the modified CaV1.2. **C)** Current voltage relationship and **D)** voltage dependence of inactivation.

Modifications to lenti virus plasmid

The initial viral construct to deliver $Ca_V1.2$ into cardiomyocytes yielded inadequate viral titers (Figure 2-3D). Titers were determined by immuno-fluorescence detecting the HA epitope of $Ca_V1.2$ (Figure 2-3C). For each given dilution of virus (10^{-2}, 10^{-3}, 10^{-4}, 10^{-5}, 10^{-6}) the number of cells were counted that indicated specific HA staining. The viral titer was determined by averaging the number of cells counted after correcting for the dilution factor and volume of virus used for each dilution (i.e. 1mL used for each well and 60 cells counted for the 10^{-5} dilution and 7 cells counted for the 10^{-6} dilution equals a $6.5x10^6$ TU/mL viral titer). The low titer was a result of the $Ca_V1.2$ (6.5kb) ORF exceeding the recommended packaging for lenti virus (6.0kb). To alleviate the packaging problem the lenti virus plasmid was modified.

The original plasmid, pLenti6, contained a blasticidin resistance gene with corresponding mammalian and bacterial promoters (Figure 2-3A). The utility of the blasticidin gene is to allow the generation of stable transductions and for bacterial antibiotic selection in addition to the ampicillin resistance gene. Neither of these functions of the blasticidin gene are necessary to virally infect adult ventricular myocytes. Therefore, the blasticidin gene and promoters were removed to create pLentiNB (Figure 2-3B). Upon removal of the blasticidin gene and promoters (869bp) the effective packaging was reduced from 6.5kb to 5.6kb. This reduction in the amount of DNA for packaging increased the viral titer dramatically (Figure 2-3D).

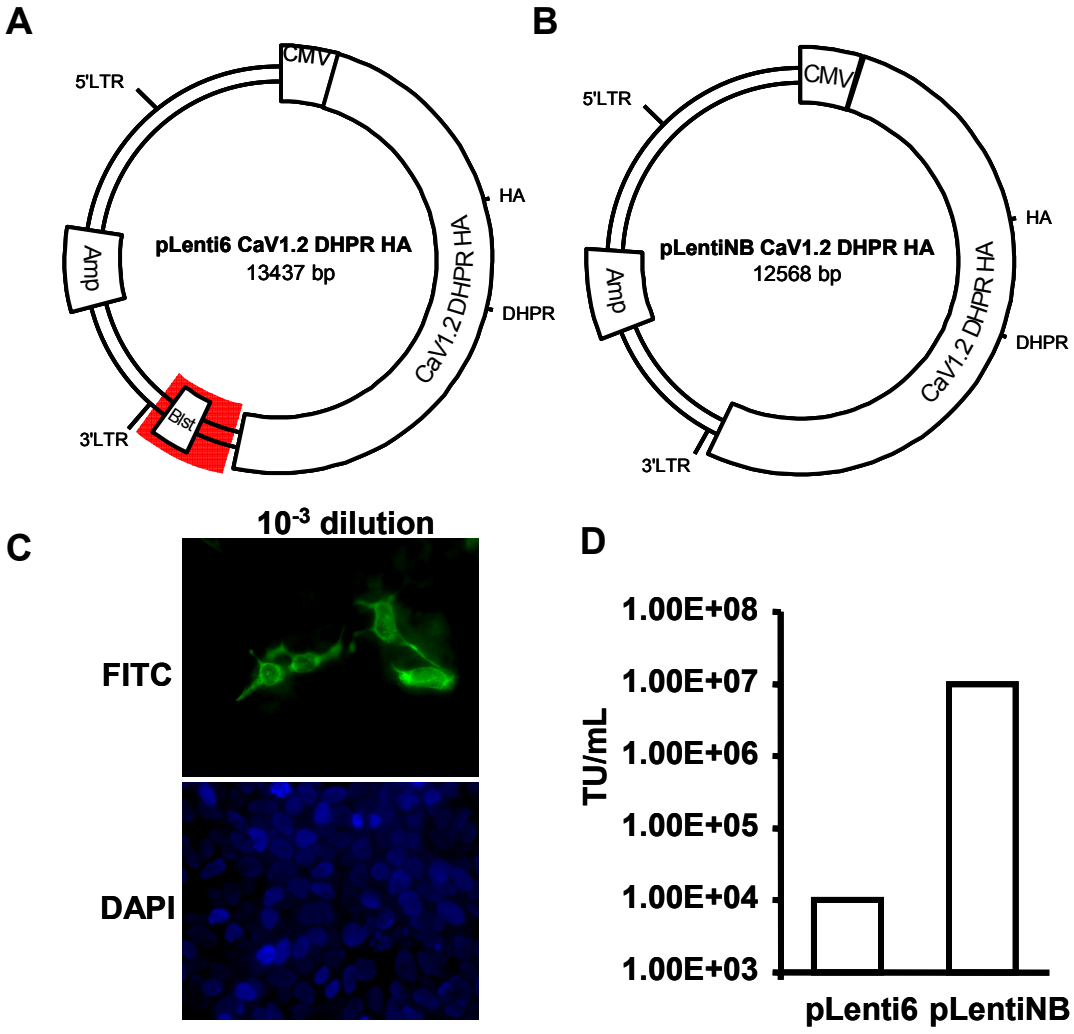

Figure 2-3: Removal of blasticidin resistance gene from pLent6 plasmid significantly improves titer of CaV1.2 virus. **A)** Plasmid map of pLenti6 with $Ca_V1.2$ highlighting the region of the blasticidin resistance gene (Blst) and promoters (896bp). Sequence between 5'-LTR and 3'-LTR packaged into virus is 6.5kB. Additional regions of interest include the ampicillan resistance gene (Amp), cytomeglovirus promoter (CMV), HA epitope (HA) and dihyrdopyridine resistance mutation (DHPR). **B)** Modified pLentiNB (*N*o *B*lasticidin resistance) with $Ca_V1.2$ plasmid map with reduced sequence for packaging (5.6kB). C. FITC immunofluorescence of HA epitope (HA Ig) of HEK293T after serial dilution of virus to determine viral titer. **D)** pLentiNB yielded a significantly improved viral titer (transducing units per mL, TU/mL) as compared to the pLenti6 plasmid.

Expression of modified $Ca_V1.2$ in ventricular myocytes

Expression of exogenous $Ca_V1.2$ in cultured adult ventricular myocytes was confirmed by confocal imaging of immunolabeled HA Ig (Figure 2-4A, B). Exogenous $Ca_V1.2$ was properly targeted to the transverse-tubule (T-tubule) network, based on the punctuate appearance and 1.8 μm spacing of the HA immunofluorescence, consistent with known distances between T-tubules in a resting sarcomere [10]. No HA immunostaining was detected in uninfected cardiomyocytes (Figure 2-4B).

Peak I_{Ca} in WT $Ca_V1.2$ infected cells was significantly resistant to nifedipine, as expected based upon the dihydropyridine-resistant mutation [29], compared to mock infected cells (Figure 2-4C). Nifedipine (single arrow, 10nM) resulted in peak I_{Ca} in WT infected myocytes that was similar to peak I_{Ca} measured in non-infected myocytes in the absence of nifedipine. This (10nM) nifedipine-titrated balance of endogenous and exogenous $Ca_V1.2$ allowed for the determination of the effects of the exogenously expressed $Ca_V1.2$ on cardiac electrophysiology independent of over-expression induced changes in peak I_{Ca}. The dose response (Figure 2-4C) also indicates that high concentration of nifedipine (double arrow, 1μM) will overcome the dihydropyridine resistance and block the majority of I_{Ca}.

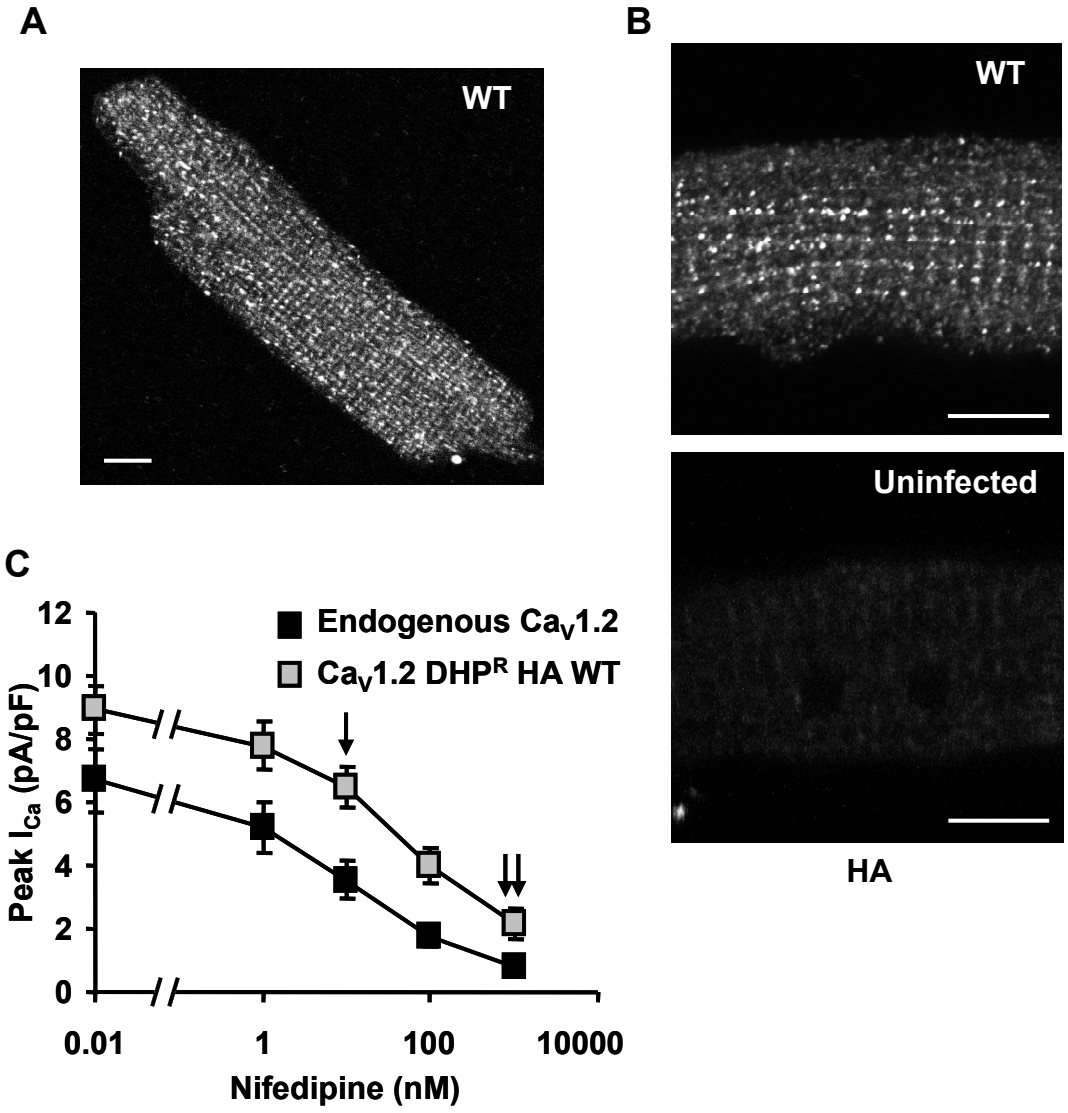

Figure 2-4: A) Exogenous $Ca_V1.2$ are expressed in regularly distributed punctae across cardiomyocytes as shown by HA immunostaining as compared to **B)** uninfected ventricular myocytes (Scale bar, 10μm). **C)** Preserved ICa during exposure to nifedipine. The single arrow indicates the nifedipine concentration (10nM) used to study the cellular consequences of the TS mutation, and the double arrow indicates the nifedipine concentration (1mM) to overcome dihydropyridine resistance and block the majority of ICa (N=5-8 cells/point, $P<0.05$ at each nifedipine concentration).

Voltage clamp properties of ventricular myocytes with exogenous $Ca_V1.2$

Over-expression of exogenous $Ca_V1.2$ should only increase the peak inward current peak amplitude (Figure 2-4C) [98]. The addition of 10nM nifedipine rectifies the difference in peak inward current in ventricular myocytes (figure 2-4C, single arrow). I compared the current and voltage (IV) relationship of ventricular myocytes expressing WT $Ca_V1.2$ under 10nM nifedipine to uninfected ventricular myocytes in the absence of nifedipine. The IV protocol involves a single voltage step that changes with each sweep. Data from the IV protocol is plotted to compare the peak current amplitude elicited by each voltage step. The current voltage relationship with Ca^{2+} as the charge carrier showed no significant differences between WT $Ca_V1.2$ and uninfected ventricular myocytes (Figure 2-5A, B).

Using the same conditions I examined two inactivation properties, voltage dependence and time dependence of inactivation. Voltage dependence of inactivation (VDI) results from $Ca_V1.2$ closing because of the voltage associated with a depolarization. VDI was examined with a two step protocol. The first voltage step is a long depolarization (conditioning) that allows the population of $Ca_V1.2$ to reach an inactivation steady state. The conditioning voltage step changes with each sweep. The second step (test) is the same for all sweeps and allows the comparison of available channels to open after the conditioning voltage step. Normalized (% of largest current) peak current from each test pulse is plotted against the corresponding conditioning voltage step. Ventricular myocytes expressing WT $Ca_V1.2$ inactivated with increasing depolarization voltages exactly like uninfected ventricular myocytes (Figure 2-5C). Time

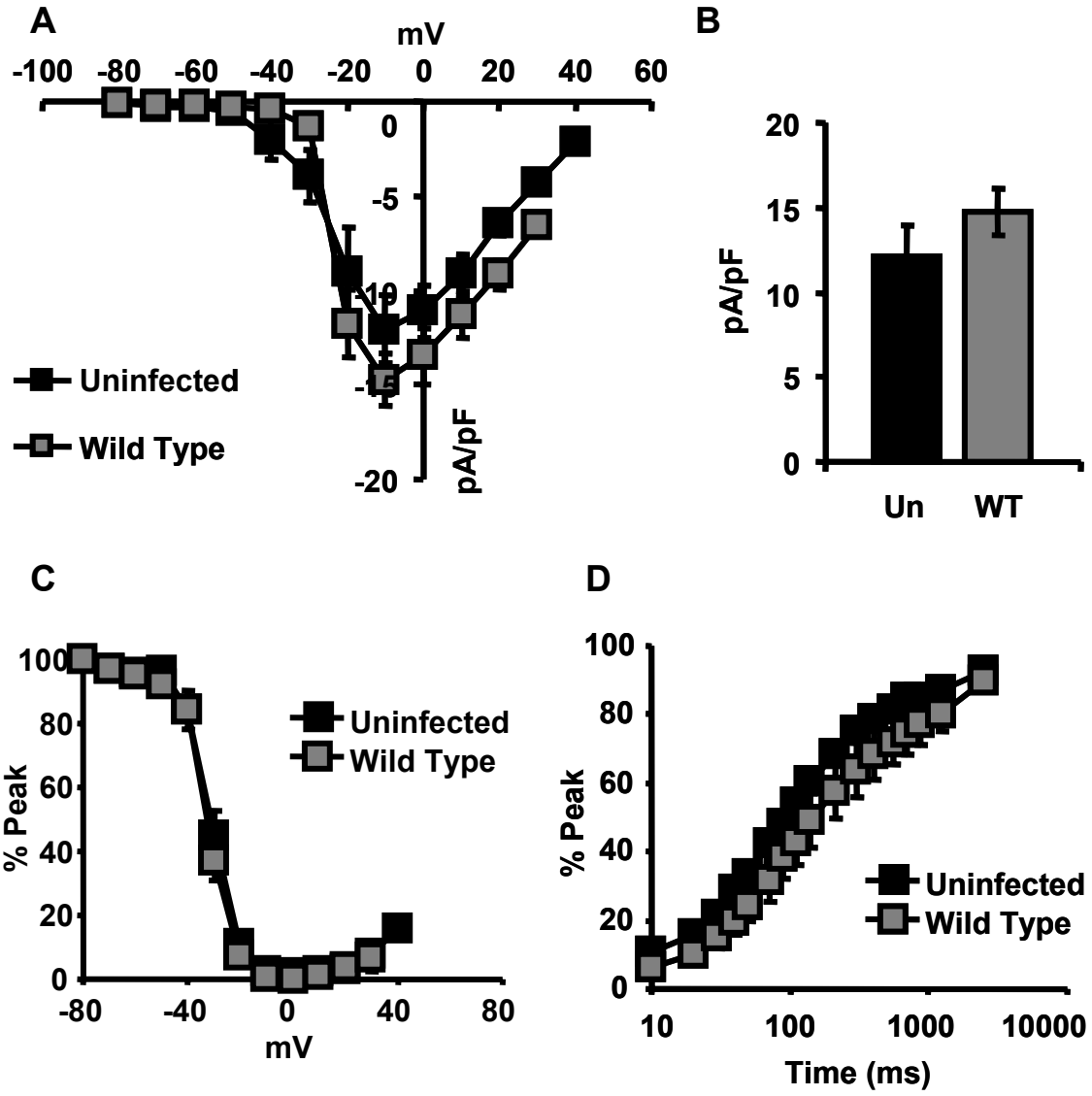

Figure 2-5: Voltage clamp I_{Ca} (Ca^{2+} charge carrier) data from WT $Ca_V1.2$ (10nM nifedipine) and uninfected (no nifedipine) ventricular myocytes. **A)** Current voltage relationship. **B)** Peak I_{Ca} from current voltage data. **C)** Voltage dependence of inactivation. **D)** Time dependence of inactivation.

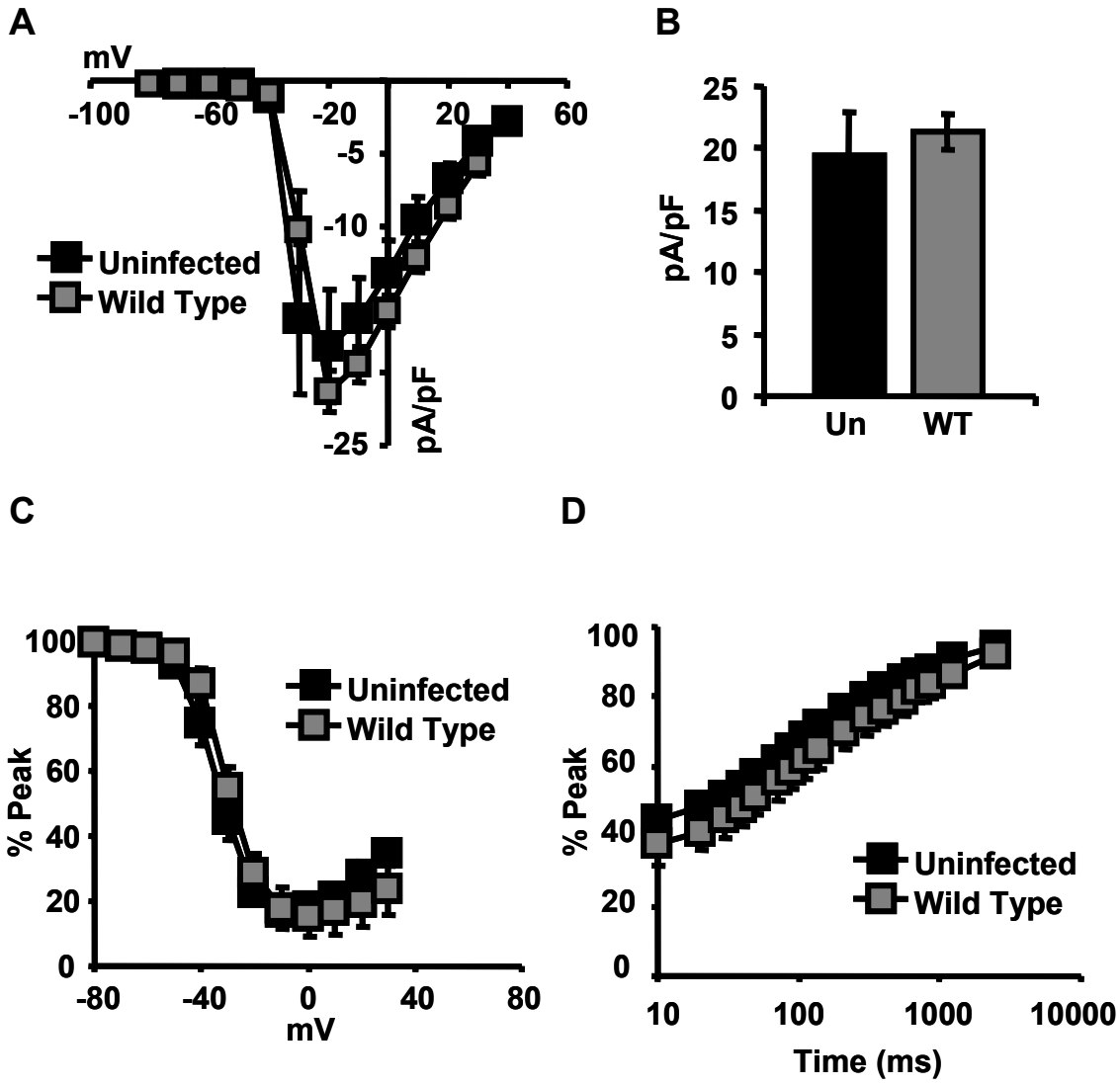

Figure 2-6: Voltage clamp I_{Ba} (Ba^{2+} charge carrier, 20mM BAPTA pipette solution) data from WT $Ca_V1.2$ (10nM nifedipine) and uninfected (no nifedipine) ventricular myocytes. **A)** Current voltage relationship. **B)** Peak I_{Ba} from current voltage data. **C)** Voltage dependence of inactivation. **D)** Time dependence of inactivation.

dependence of inactivation (TDI) results from more $Ca_V1.2$ inactivation with longer depolarizations. The TDI protocol examines the recovery from time dependent inactivation by using a two step protocol. Both voltage steps are to the same voltage for the same duration but the time between the steps is increased with each sweep. With increasing time between the first and second voltage steps the peak amplitude of the second voltage step gradually increases to that observed in the first voltage step. The normalized (% of first voltage step) peak current from the second voltage step is plotted against the time between the two voltage steps. Ventricular myocytes over-expressing WT $Ca_V1.2$ showed no changes in recovery from TDI as compared to uninfected ventricular myocytes (Figure 2-5D).

Many properties of $Ca_V1.2$ are dependent on Ca^{2+}. To fully eliminate Ca^{2+} dependent properties all Ca^{2+} must be sequestered from the channel. Extracellular Ca^{2+} is replaced with Ba^{2+}, which has the unique ability to move through $Ca_V1.2$ better than Ca^{2+} [54] but not interact well with Ca^{2+} binding proteins [80]. Intracellular Ca^{2+} is tightly buffered by the addition of a fast Ca^{2+} chealator BAPTA within the pipette solution [115]. Together, Ba^{2+} and BAPTA eliminate $Ca_V1.2$ Ca^{2+} dependent properties. Repeating the IV, VDI and TDI protocols under Ca^{2+} free conditions found no significant differences between WT $Ca_V1.2$ expressing ventricular myocytes (10nM nifedipine) and uninfected ventricular myocytes (no nifedipine).

Current clamp properties of ventricular myocytes with exogenous $Ca_V1.2$

Stimulated action potentials (Figure 2-7A) were recorded from $Ca_V1.2$ WT expressing and uninfected ventricular myocytes (Figure 2-7B) under increasing concentrations of nifedipine. Exogenous expression of $Ca_V1.2$, recorded under 10nM nifedipine, did not affect action potential duration compared to measurements in uninfected cardiomyocytes recorded in the absence of nifedipine (Figure 2-7C, D). No action potential recordings from uninfected, without nifedipine, and $Ca_V1.2$ over-expressing myocytes yielded afterdepolarizations (Figure 2-7E).

The low concentration of nifedipine (<1nM) used with $Ca_V1.2$ WT expressing cardiomyocytes yielded an increased action potential duration as compared to uninfected without nifedipine (Figure 2-7C, D). Despite increasing action potential duration, low concentrations of nifedipine did not allow for the generation of afterdepolarizations from cardiomyocytes with exogenous Cav1.2 expression (Figure 2-7E). Ventricular myocytes over-expressing $Ca_V1.2$ and uninfected cardiomyocytes showed no changes in either peak amplitude (Figure 2-8A, B) of the action potential or the resting membrane potential (Figure 2-8C, D).

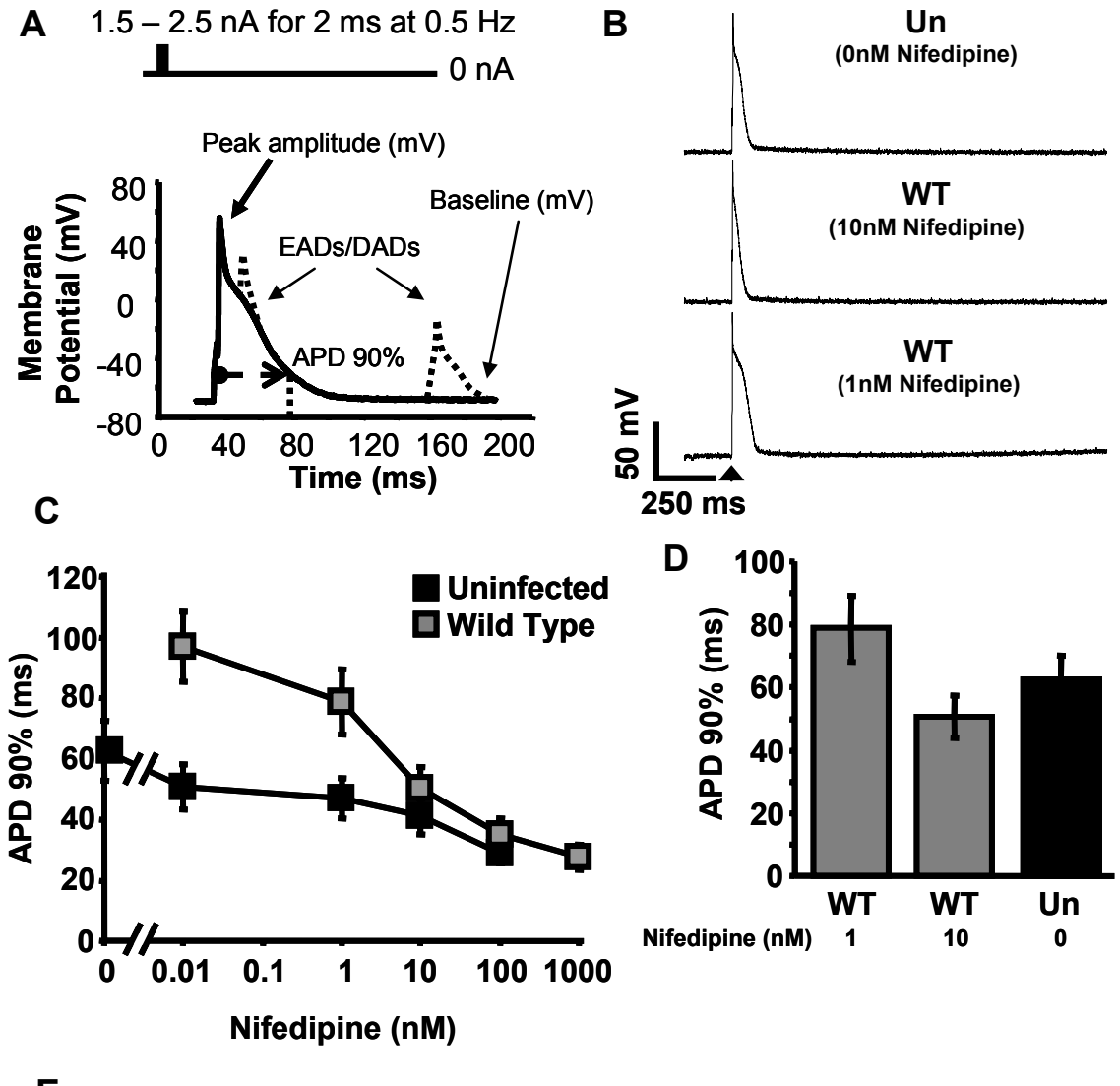

E

Nifedipine (nM)	0	0.01	1	10	100	1000
WT		0/6	0/6	0/10	0/5	0/5
Un	0/15	0/11	0/16	0/13	0/13	

Figure 2-7: A) Action potential stimulation protocol (top) with example action potential (bottom) with parameters measured. **B)** Example data from uninfected, WT $Ca_V1.2$ with 10nM and 1nM nifedipine. **C)** Action potential duration 90% (APD 90%) nifedipine dose response for WT $Ca_V1.2$ and uninfected ventricular myocytes. **D)** APD90% summary data. **E)** Afterdepolarization summary data for each nifedipine concentration. Numeral indicate fraction of cells with afterdepolarizaitons.

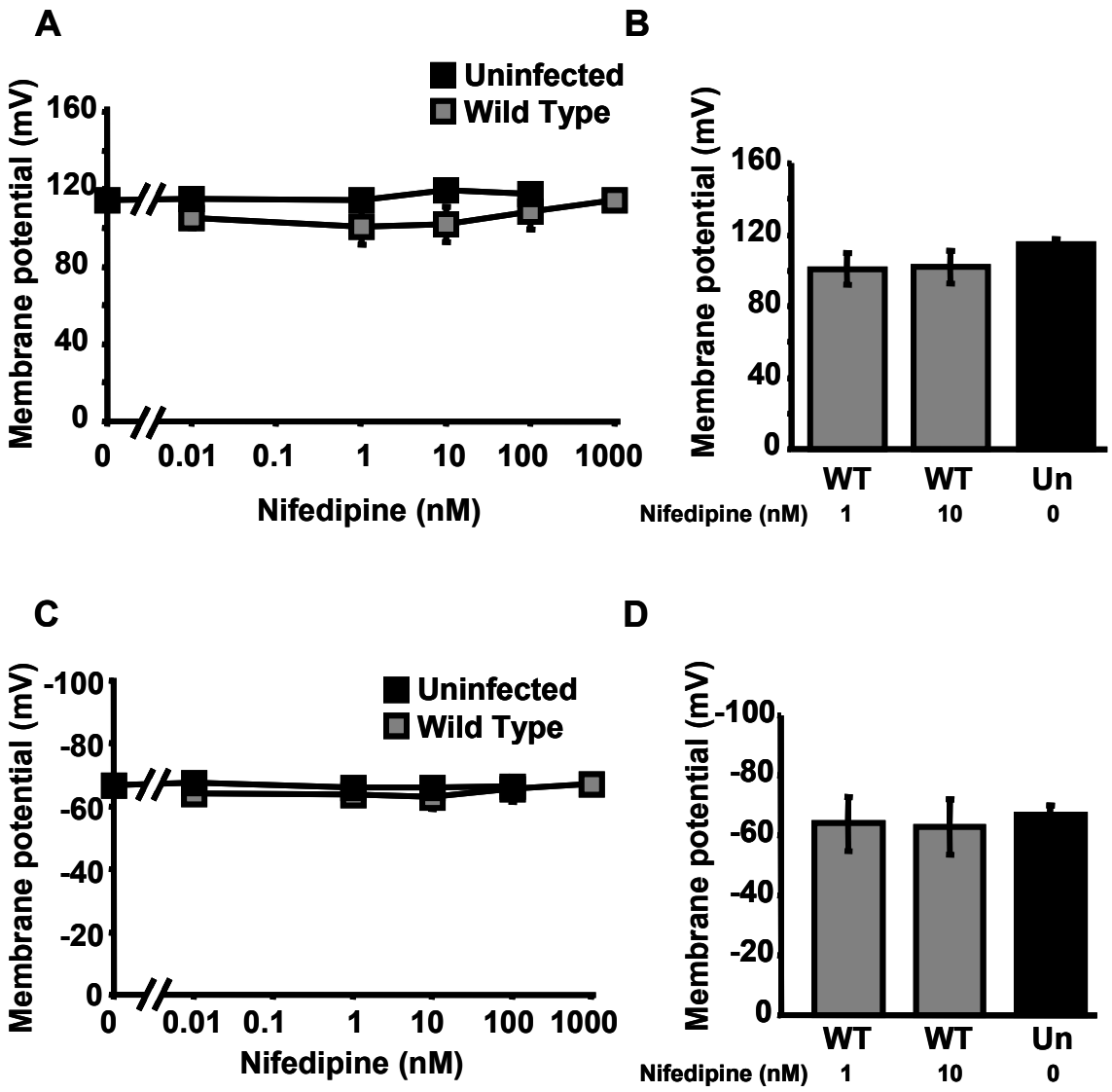

Figure 2-8: A) Action potential peak membrane depolarization amplitude nifedipine dose response for WT $Ca_V1.2$ and uninfected ventricular myocytes. **B)** Peak membrane depolarization amplitude summary data comparing WT CaV1.2 1nM and 10nM nifedipine to uninfected ventricular myocytes without nifedipine. **C)** Resting membrane potential nifedipine dose response for WT CaV1.2 and uninfected ventricular myocytes. D) Resting membrane potential summary data comparing WT CaV1.2 1nM and 10nM nifedipine to unifected ventricular myocytes without nifedipine.

Intracellular Ca^{2+} handling

Intracellular Ca^{2+} handling (Figure 1-3) is a fundamental aspect of cardiovascular physiology at the cellular level. A transgenic mouse model of WT $Ca_V1.2$ over-expression has been shown to increase the amplitude but not affect the decay time of the Ca^{2+} transient [98]. My model is different from the transgenic mouse $Ca_V1.2$ over-expression in having less over-expression of $Ca_V1.2$ and my model represents an acute over-expression of $Ca_V1.2$ rather than a chronic over-expression of $Ca_V1.2$. It is important to characterize the Ca^{2+} handling of this model for proper application in future studies utilizing this model.

Stimulated (1Hz) Ca^{2+} waves were measured using a fluorescent Ca^{2+} indicator (fluo-3 AM) to measure global changes in Ca^{2+} handling [99]. Both WT $Ca_V1.2$ over-expressing and uninfected ventricular myocytes were assessed. The Ca^{2+} wave was examined for changes in peak amplitude (Figure 2-9A) and decay time (Figure 2-9B). The peak amplitude of the Ca^{2+} wave signifies the maximum amount of Ca^{2+} released by the RYR from the SR Ca^{2+} stores (Figure 1-3). Whereas, the decay time represents the ability of SERCA and NCX to cycle Ca^{2+} back into the SR or out of the cell (Figure 1-3). No significant differences were observed between WT $Ca_V1.2$ ventricular myocytes and uninfected ventricular myocytes (Figure 2-9A, B). After recording steady-state Ca^{2+} transients the SR Ca^{2+} stores were fully released by the addition of caffeine (10mM). The caffeine induced SR release of Ca^{2+} showed no significant differences between WT $Ca_V1.2$ and uninfected ventricular myocytes (Figure 2-9C).

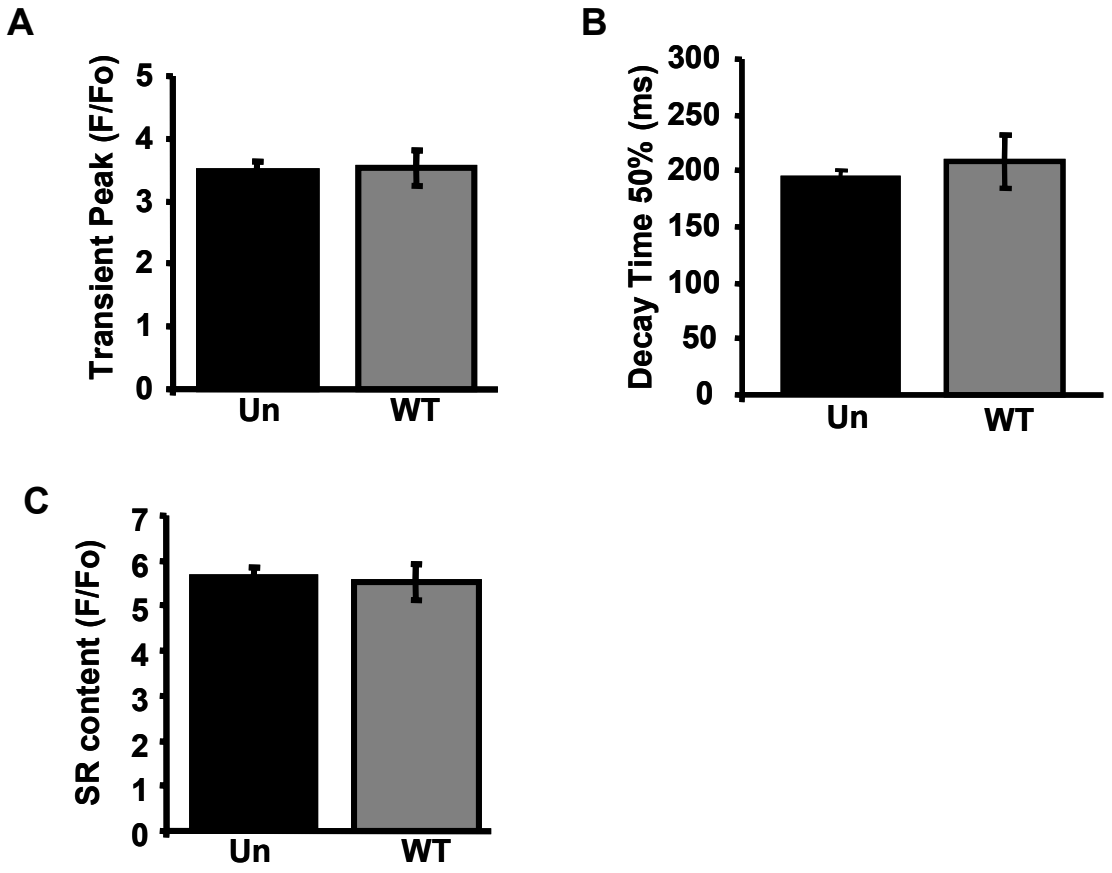

Figure 2-9: Stimulated Ca^{2+} transients from WT $Ca_V1.2$ ventricular myocytes and uninfected ventricular myocytes. **A)** Peak Ca^{2+} transient amplitude. **B)** Decay time to 50% peak amplitude. **C)** Peak SR Ca^{2+} release by caffeine (10mM).

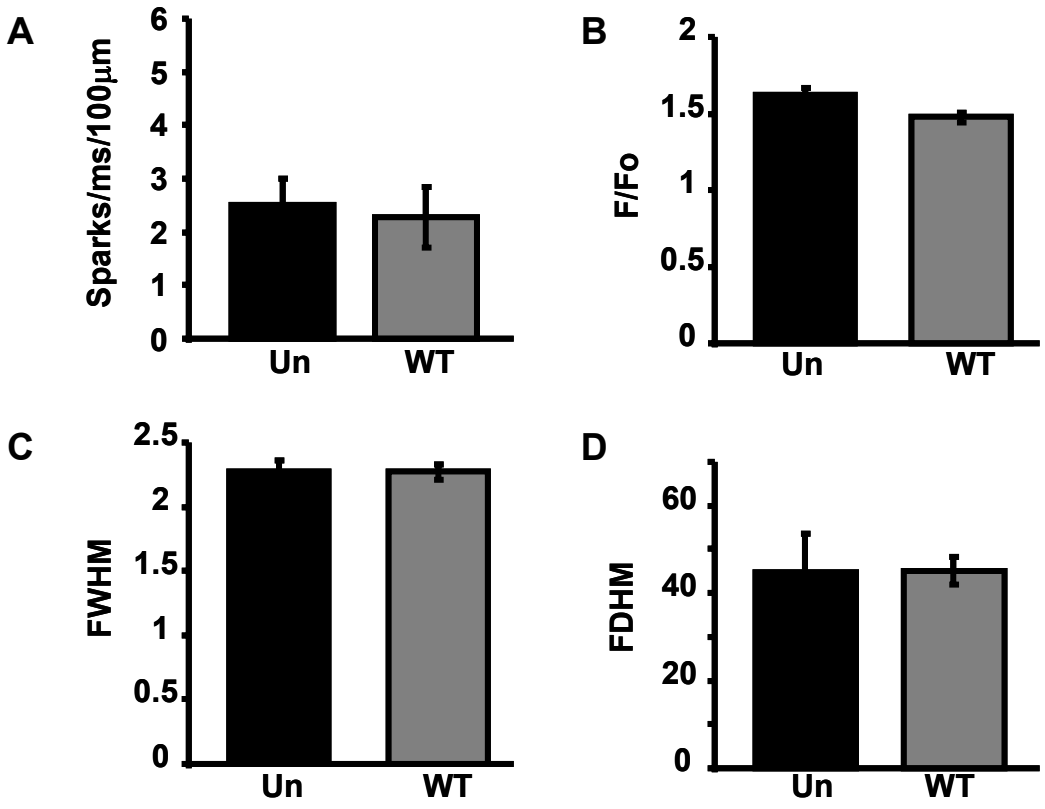

Figure 2-10: Spontaneous RYR SR Ca^{2+} spark from WT $Ca_V1.2$ ventricular myocytes and uninfected ventricular myocytes. Ca^{2+} sparks assesed for **A)** frequency, **B)** peak amplitude, **C)** width and **D)** duration.

An important aspect of ventricular myocyte Ca^{2+} handling is the propensity of RYR to release SR Ca^{2+} stores. The ability of RYR to release SR Ca^{2+} stores is regulated by phosphoyrlation and by Ca^{2+} [9]. The transgenic mouse model of $Ca_V1.2$ over-expression found no changes in RYR release of SR Ca^{2+} [98]. Spontaneous release of SR Ca^{2+} by RYR can be measured as Ca^{2+} sparks using fluorescent Ca^{2+} indicators. Ca^{2+} sparks may be examined for changes in frequency (Figure 2-10A), peak amplitude (Figure 2-10B), width (Figure 2-10C) and duration (Figure 2-10D). The Ca^{2+} spark profile between WT $Ca_V1.2$ and uninfected ventricular myocytes showed no significant differences.

Discussion

Importance for studying $Ca_V1.2$ in primary cells

Many of the most important discoveries on $Ca_V1.2$ function were discovered in heterologous cells and heterologous cell will remain a fundamental tool for investigating $Ca_V1.2$ properties. Studying $Ca_V1.2$ within primary cells is an important but underutilized experimental direction to fully understand how $Ca_V1.2$ activity relates to the greater context of the cells that endogenously express $Ca_V1.2$. In neurons, mutating the CaM binding IQ motif on the $Ca_V1.2$ C-terminus, and not the ligand gated NMDA receptor Ca^{2+} channel [29],.was found to be critical for MAPK signaling This finding provide insight into Ca^{2+} signaling in neurons in that what Ca^{2+} signaling pathway activated depends on where the Ca^{2+} originated and not just global intracellular Ca^{2+} concentration. In ventricular myocytes, mutating the $Ca_V1.2$ C-terminus the PKA phosphorylation site serine 1928 to an alanine had no effect on adrenergic signaling enhancement of I_{Ca} [38]. However, deleting the $Ca_V1.2$ distal C-terminus prevented adrenergic signaling increase of I_{Ca} [38]. These findings are contrary to the long-standing importance of serine 1928 for $Ca_V1.2$ adrenergic signaling. Rather, this work suggests that localization of PKA, via AKAP79 binding the $Ca_V1.2$ C-terminus [40], is more critical than serine 1928 phosphorylation during adrenergic signaling. These findings in neurons and ventricular myocytes depended on studying a $Ca_V1.2$ within the context of a primary cell and have provided profound insight into the mechanisms of cellular physiology that $Ca_V1.2$ partakes.

The previous work conducted in ventricular myocytes did not examine integrated events such as action potentials and intracellular Ca^{2+} handling, both of which are fundamental in understanding cardiovascular disease. My work has taken what others have done to study $Ca_V1.2$ mutations and increased its utility within ventricular myocytes. I have shown that $Ca_V1.2$ may be exogenously expressed within ventricular myocytes without affecting the action potential or intracellular Ca^{2+} handling, which provides the framework to study how mutations within $Ca_V1.2$ affect ventricular myocytes physiology.

Methods

Cloning

The open reading frame of $Ca_V1.2$ α1c subunit (NCBI X15539) was amplified by PCR and ligated into a modified pLenti6 plasmid (Invitrogen), pLentiNB, which had the blasticidin resistance gene and promoters of the pLenti6 plasmid removed to facilitate viral packaging. An extracellular hemaglutanin epitope was added to $Ca_V1.2$ by methods previously published[2]. The dihydropyridine resistance mutation (DHP^R, T1066Y) was introduced by using the PCR method Quikchange (Stratagene) as per manufacturer's protocol.

Lenti virus

The transgene plasmid pLentiNB carrying the modified $Ca_V1.2$ was transfected (Qiagen, Effectene) with the Lenti viral packaging plasmids (Invitrogen's pLP1, pLP2 and pVSVG) into HEK293FT cells (Invitrogen). Media was collected and replaced at 24, 48 and 72 hours post-transfection. The viral containing media was concentrated by either ultrafiltration (Millipore Centricon Plus-70 30kDa) or ultacentrifugation. Viral titer (transducing units per mL, TU/mL) was determined by serial dilution (10^{-3}, 10^{-4}, 10^{-5}, 10^{-6}, 10^{-7}, no virus) on HEK293 cells followed by immuno-staining (see Immunoflourescence methods) for the $Ca_V1.2$ HA epitope (anti-HA conjugated Alexa 488 Ig) and counting positively stained cells within each dilution. Viral titers achieved were between 10^5 and 10^7

TU/mL. Extracts from HEK293 cells used to produce virus were analyzed by SDS-PAGE and immunoblotting with an affinity-purified HA Ig.

Ventricular myocyte isolation, culturing and viral transduction

Adult male Sprague-Dawley rats (250-300g) were anesthetized by Avertin (2.5%) with Heparin (55 units/mL) through IP injection (0.2mL/10g). Hearts were excised, perfused retro-aortically (Langendorff, Figure 3-11) and enzymatically digested with a mixture of Collogenase (Worthington, 250units/mL), Hyaluronidase (Sigma, 0.01%) and Protease Type XIV (Sigma, 0.0025%) in a modified tyrodes solution (0.1mM $CaCl_2$, 10mM BDM). Dissociated cardiomyocytes (Figure 2-12A) were washed three times in Joklik MEM (Sigma M0518) with 1% Pen/Strep and 1X ITS with increasing Ca^{2+} (0.25mM, 0.5mM, 0.75mM). Ventricular myocytes were plated on glass coverslips coated with Geltrex (Invitrogen) and allowed to attach for 1 hour. Cells were washed with a culture media consisting of a 50:50 mix of DMEM and F10 media with 1% Pen/Strep and 1X ITS. Attached cardiomyocytes (Figure 2-12B) were counted and the cell density was calculated (Figure 2-13). Lenti virus was added to the cells at a multiplicity of infection (MOI) of 1-3 (Figure 2-13), and cells cultures were maintained for 24-36 hours (Figure 2-12C,D).

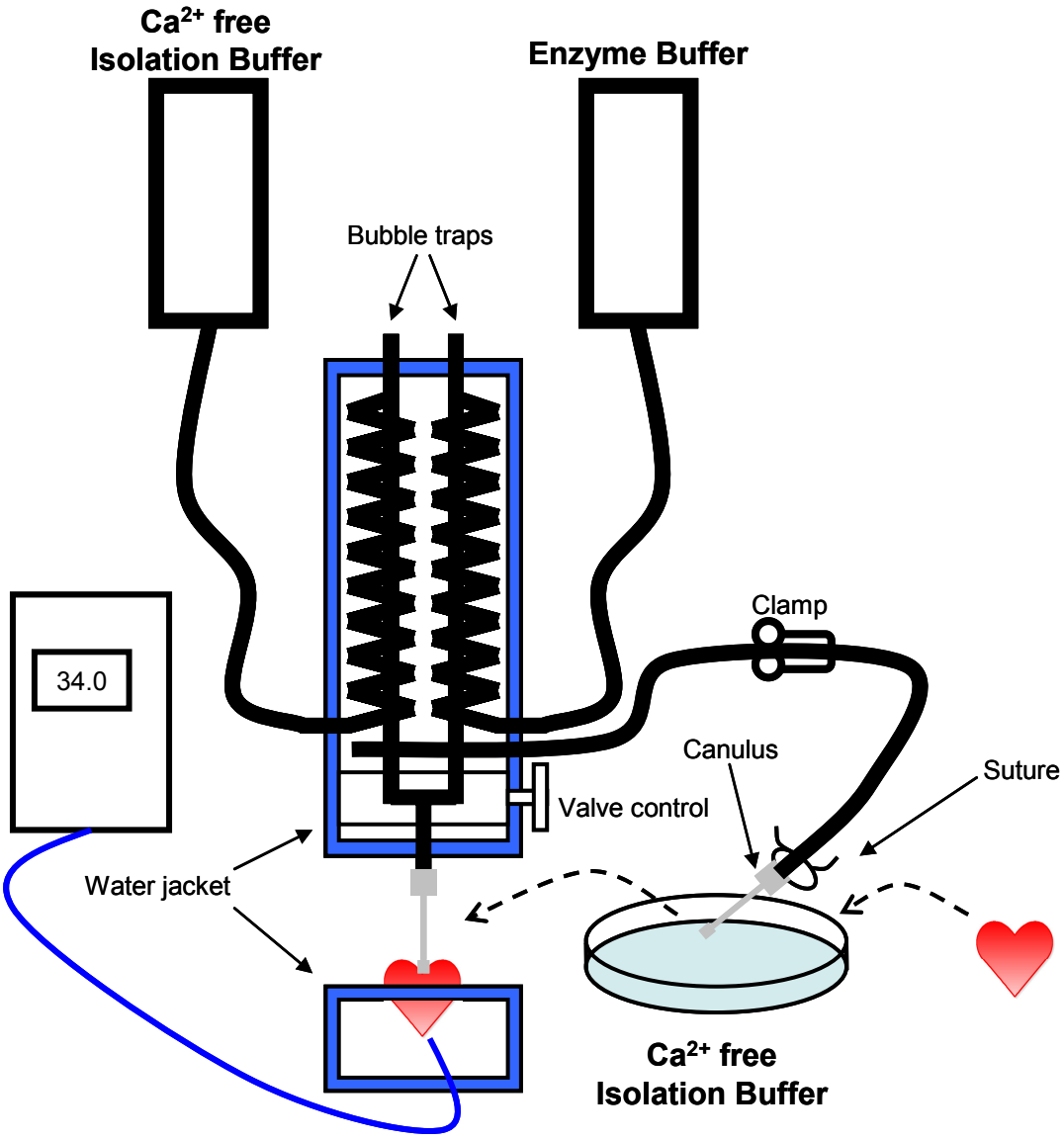

Figure 2-11: Schematic of Langendorff used to isolate ventricular myocytes. Isolation buffer and enzyme buffer are heated by the water jacket to 34C and introduced to the heart by retrograde perfusion.

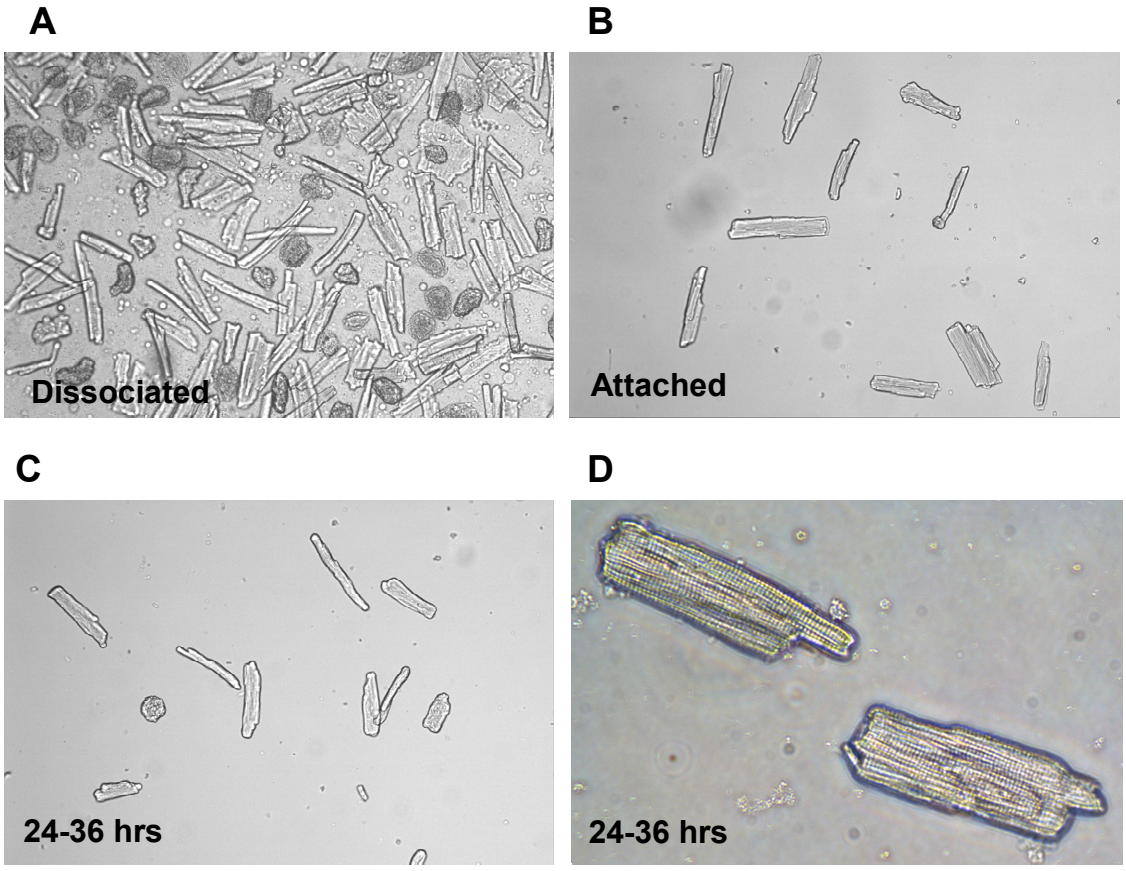

Figure 2-12: A) Ventricular myocytes dissociated from ventricular tissue after enzymatic digestion by retrograde perfusion. **B)** Ventricular myocytes allowed to attach to glass coverslips coated with an extracellular matrix. **C)** Ventricular myocytes after 24-36 hours in culture. **D)** 40x view of 24-36 hour cultured ventricular myocytes.

Hemocytometer Square = $0.04mm^2$

Culture Well = 24mm x 67mm = $1608mm^2$

MOI = Multiplicity of Infection, ratio of virus particles to each cell

TU/mL = viral titer, determined experimentally

$$\text{Cell \# / Well} = \frac{\text{Average Cell \# at 20x}}{\text{19.2 Hemocytometer Squares}} \times \frac{1608mm^2}{0.04mm^2}$$

$$\mu\text{L Virus} = \frac{\text{MOI} \times \text{Cell \# / Well}}{\frac{\text{TU/mL}}{1000}}$$

Figure 2-13: Equations used to determine the multiplicity of infection (MOI) for attached ventricular myocytes to be cultured with virus.

Electrophysiology

For both voltage clamp and current clamp, microelectrode tips were pulled (Sutter Instruments, P-97) from (Fisherbrand, 22-362-574) to between 2.0MΩ and 3.0MΩ. Recordings were accomplished using an Axopatch 200b amplifier (Axon Instruments) and pClamp 9.

HEK293 I_{Ca} recordings for voltage dependence of inactivation (VDI) used a two step voltage clamp protocol (repeated 0.1 Hz, resting -80mV, 25°C) with an initial conditioning step (0.8s, -50mV to +60mV, ∆10mV) followed by a test pulse (300ms, +30mV). Bath solution (Table 2-1) was in mM; 130 NMDG, 10 HEPES, 5 KCl, 15 $CaCl_2$. Pipette solution (Table 2-2) was in mM; 120 Cs methanesulfonate, 5 $CaCl_2$, 1 $MgCl_2$, 2 MgATP, 10 HEPES, 10 EGTA. Available current observed each test pulse after a given conditioning pulse was accessed a percent of the maximum current observed.

Ventricular myocyte voltage clamp used two sets of bath solutions and pipette solutions for conditions with Ca^{2+} or without Ca^{2+}. To prevent Ca^{2+} dependent inactivation, Ca^{2+} was tightly buffered through the use of Ba^{2+} as the charge carrier in the bath solution and BAPTA with no Ca^{2+} in the pipette solution. Bath solution (Table 2-3) was in mM; 137 NMDG, 10 HEPES, 10 Glucose, 1.8 $BaCl_2$, 0.5 $MgCl_2$, 25 CsCl. Pipette solution (Table 2-4) was in mM; 120 CsCl, 10 TEA, 1 MgATP, 1 NaGTP, 5 phosphocreatine, 10 HEPES, 20 BAPTA. Ca2+ containing conditions used a bath solution (Table 2-5) with in mM, 137 NMDG, 10 HEPES, 10 Glucose, 1.8 $CaCl_2$, 0.5 $MgCl_2$, 25 CsCl. Pipette solution (Table 2-6) was in mM; 120 CsCl, 10 TEA, 1 MgATP, 1 NaGTP, 5 phosphocreatine, 10 HEPES, 10 EGTA.

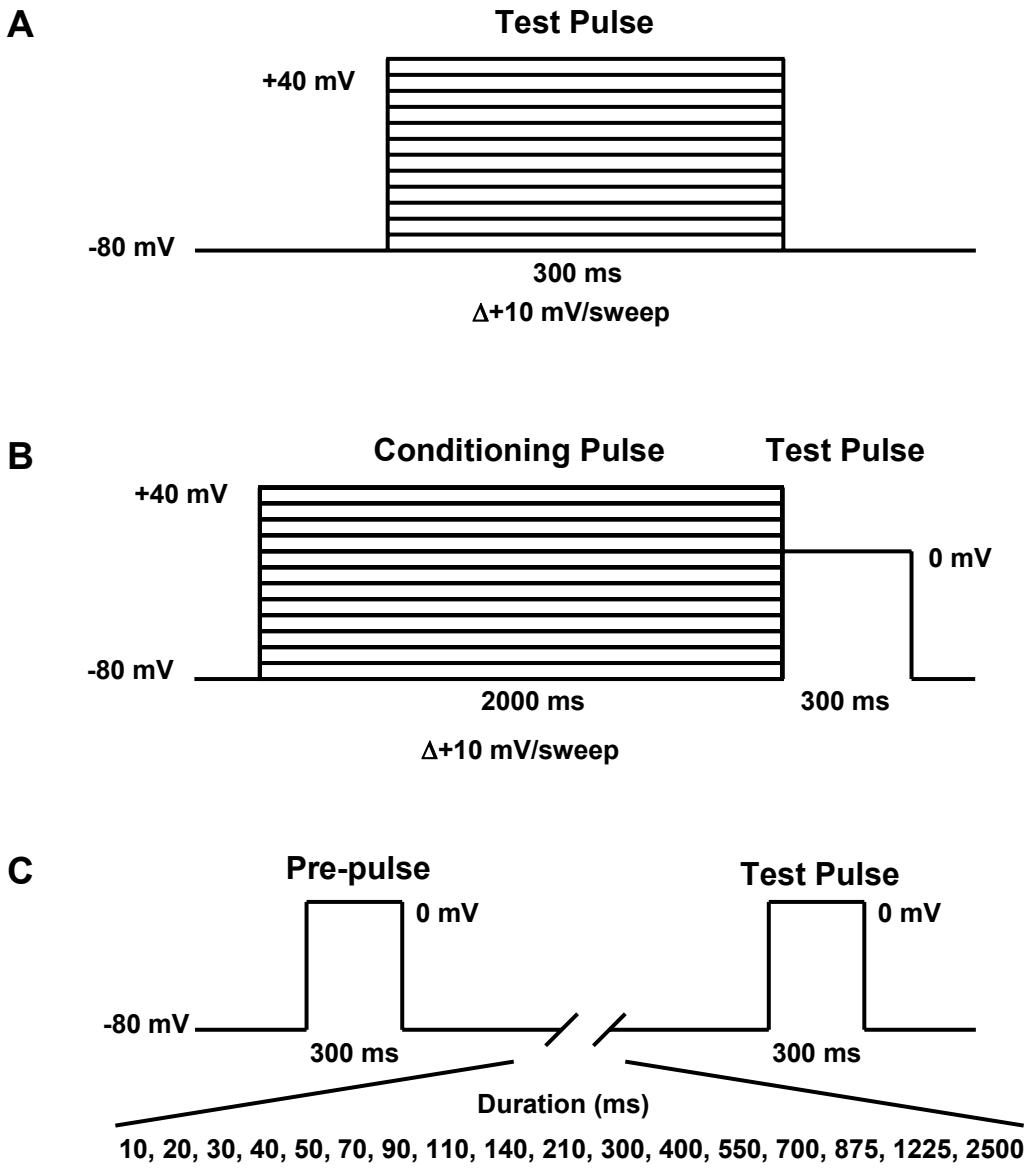

Figure 2-14: Schematics of voltage clamp protocols. A) Current voltage (IV) relationship protocol. B) Voltage dependence of inactivation (VDI) protocol. C) Time dependence of inactivation (TDI) protocol.

Ventricular myocyte current voltage relationship (IV) (Figure 2-14A) used a single step protocol (300ms, -80mv to +40mV, ∆10mV, repeated 0.5Hz, resting -80mV, 25°C). The peak current each sweep elicited was plotted against the voltage step. Cardiomoycte I_{Ba} recordings for VDI (Figure 3-14A) used a two step voltage clamp protocol (repeated 0.1 Hz, resting -80mV, 25°C) with an initial conditioning pulse (2.0s, -80mV to +30mV, ∆10mV) followed by a test pulse (300ms, 0mV). Available current observed each test pulse after a given conditioning pulse was accessed as a percent of the maximum current observed. Time dependence of inactivation (TDI) was recorded using a two step protocol (Figure 2-14B) with an initial pre-pulse (0mV, 200ms) followed by a test pulse (0mV, 200ms). The time between the two pulses was gradually increases to allow more recovery from inactivation (duration (ms): 10, 20, 30, 40, 50, 70, 90, 110, 140, 210, 300, 400, 550, 700, 875, 1225, 2500). The current elicited by the test pulse was plotted as a percentage of the current from the pre-pulse and plotted against the duration time between the pre-pulse and the test pulse..

Cardiomyoycte action potentials (AP) were stimulated (2ms, 1.5-2.5nA) in current clamp mode (0.5Hz, 25°C). Bath solution (Table 2-7) was in mM; 140 NaCl, 4 HEPES, 10 Glucose, 5.4 KCl, 1.8 $CaCl_2$, 1 $MgCl_2$. Pipette solution (Table 2-8) was in mM; 120 K aspartate, 5 HEPES, 25 KCl, 4 Na_2ATP, 1 $MgCl_2$, 10 EGTA, 2 Na_2 phosphocreatine, 1 $CaCl_2$, 2 NaGTP. Recorded APs were analyzed using ClampFit's (Axon Instruments) event detection algorithm and statistics decay time (ms) algorithm.

The equilibrium potential was determined for each ion (Table 2-9) using the Nernst equation (Table 2-10). For the Nernst equation, the extracellular ion concentrations were determined base upon the bath solution (Table 2-8) and the intracellular ion concentrations were calculated (Table 2-11) from the program MaxChealator (WEBMAXC, http://www.stanford.edu/~cpatton/downloads.htm) using the pipette solution (Table 2-8) components.

Table 2-1: HEK293 I_{Ca} Bath Solution

Bath Solution

Chemical	F.W.	mmol/L	Wt.g/L
NMDG	195.2	130	**25.376**
HEPES	238.3	10	**2.383**
KCl	74.56	5	**0.373**
CaCl2	147.02	15	2.205
Titrate to pH 7.4 with 12.1N HCl			

Table 2-2: HEK293 ICa Pipette Solution

Internal Perfusion Solution

Chemical	F.W.	mmol/L	Wt.g/L	Wt. g/100mL
Cs methanesulfonate	228	120	27.360	**2.736**
CaCl2	147.02	5	0.735	**0.074**
MgCl2	203.31	1	0.203	**0.020**
MgATP	507.2	2	1.014	**0.101**
HEPES	238.3	10	2.383	**0.238**
EGTA	380.04	10	3.800	**0.380**
Titrate to pH 7.2 with 1N CsOH				

Table 2-3: Ventricular Myocyte I_{Ba} Bath Solution

Bath Solution

Chemical	F.W.	mmol/L	Wt.g/L	Stock (mM)	mL/L
NMDG	195.2	137	**26.742**		
HEPES	238.3	10	**2.383**		
Glucose	180.2	10	**1.802**		
$BaCl_2$	244.3	1.8	0.440	1000	**1.8**
$MgCl_2$	203.31	0.5	0.102	40	**12.5**
CsCl	168.4	25	**4.210**		
Titrate to pH 7.4 with 12.1N HCl					

Table 2-4: Ventricular Myocyte I_{Ba} Pipette Solution

Internal Perfusion Solution with BAPTA

Chemical	F.W.	mmol/L	Wt.g/L	Wt. g/100mL
CsCl	168.4	120	20.208	**2.021**
CaCl2	147.02	3	0.441	**0.044**
TEA	165.7	10	1.657	**0.166**
Mg ATP	507.2	1	0.507	**0.051**
NaGTP	523.2	1	0.523	**0.052**
phosphocreatine	255.1	5	1.276	**0.128**
HEPES	238.3	10	2.383	**0.238**
BAPTA	476.43	20	9.529	**0.953**
Titrate to pH 7.2 with 1N CsOH				

Table 2-5: Ventricular Myocyte I_{Ca} Bath Solution

Bath Solution

Chemical	F.W.	mmol/L	Wt.g/L	Stock (mM)	mL/L
NMDG	195.2	137	**26.742**		
HEPES	238.3	10	**2.383**		
Glucose	180.2	10	**1.802**		
$CaCl_2$	147.02	1.8	0.265	100	**18**
$MgCl_2$	203.31	0.5	0.102	40	**12.5**
CsCl	168.4	25	**4.210**		
Titrate to pH 7.4 with 12.1N HCl					

Table 2-6: Ventricular Myocyte I_{Ca} Pipette Solution

Internal Perfusion Solution

Chemical	F.W.	mmol/L	Wt.g/L	Wt. g/100mL
CsCl	168.4	120	20.208	**2.021**
$CaCl_2$	147.02	3	0.441	**0.044**
TEA	165.7	10	1.657	**0.166**
Mg ATP	507.2	1	0.507	**0.051**
NaGTP	523.2	1	0.523	**0.052**
phosphocreatine	255.1	5	1.276	**0.128**
HEPES	238.3	10	2.383	**0.238**
EGTA	380.04	10	3.800	**0.380**
Titrate to pH 7.2 with 1N CsOH				

Table 2-7: Ventricular Myocyte AP Bath Solution

Bath Solution

Chemical	F.W.	mM	Wt.g/L	Stock (mM)	mL/L
NaCl	58.44	140	**8.182**		
HEPES	238.3	4	**0.953**		
Glucose	180.2	10	**1.802**		
KCl	74.56	5.4	**0.403**	100	**54**
$CaCl_2$	147.02	1.8	**0.265**	100	**18**
$MgCl_2$	203.31	1	**0.203**	40	**25**
Titrate to pH 7.4 with 4 mmol NaOH (FW 40.0, 0.016g/100mL)					

Table 2-8: Ventricular Myocyte AP Pipette Solution

Internal Perfusion Solution

Chemical	F.W.	mM	Wt.g/L	Wt. g/100mL
K aspartate	171.2	120	20.544	**2.054**
HEPES	238.3	5	1.192	**0.119**
KCl	74.56	25	1.864	**0.186**
Na_2ATP	551.1	4	2.204	**0.220**
$MgCl_2$	203.31	1	0.203	**0.020**
EGTA	380.04	10	3.800	**0.380**
Na_2 phosphocreatine	255.1	2	0.510	**0.051**
$CaCl_2$	147.02	1	0.147	**0.015**
Na GTP	523.2	2	1.046	**0.105**
Titrate to pH 7.2 with 10mmol KOH (F.W. 56.11, .05611g/100mL)				

Table 2-9: Equlibrium Membrane Potential (Nernst Equation) Based upon Ventricular Myocyte AP Bath and Pipette Solutions

Ion	Extracellular (mM)	Intracellular (mM)	$[Ion]_{out}/[Ion]_{in}$	Equil. Potential (mV)
Ca^{2+}	1.8	1.58E-05	114285.7143	149.64
Mg^{2+}	1	0.0252	39.6825	47.29
K	5.4	145	0.0372	-84.55
Na	140	14	10.0000	59.17
Cl	151	29	5.2069	-42.40

Table 2-10: Nernst Equation Calculations Based upon Ventricular Myocyte AP Bath and Pipette Solutions

Gas Constant R	Temperature Celsius	Kelvin	Faraday Const. F
8.315	25	298.16	9.65E+04

RT/F (mV)	RT/2F (mV)	RT/-F (mV)
25.70	12.85	-25.70

Table 2-11: Intracellular Divalent Ion Concentrations from MaxChealator using Ventricular Myocyte Bath and Pipette Solutions

Max Chelator		
pH = 7.2 25 C 0.1 N Ionic contribution [ABS] 0.0257070 N		
Name	Free (M)	Total (M)
Ca^{2+}	1.58E-08	0.001
Mg^{2+}	0.0000252	0.001
ATP	0.0030395	0.004
EGTA	0.0089856	0.01

Immunoflourescence

Either cardiomyocytes or HEK293 cells, cultured on coverslips (glass #1), were gently washed with PBS and fixed for 20 minutes in 2% paraformaldyhyde (25°C). Fixed cells were permeabilized for 10 minutes with PBS with 0.1% Triton X-100, 2 mg/mL BSA and 2% fish gelatin. Permeabilized cells were blocked with PBS with 2 mg/mL BSA and 2% fish gelatin. Cells were incubated overnight (4°C) in either anti-HA conjugated Alexa 488 Ig or an affinity-purified HA Ig and washed. The cells incubated with HA Ig were then incubated in donkey anti-mouse Alexa 488 Ig (Molecular Probes) at 4°C. Cardiomyocytes were mounted with glass coverslips and Vectashield (with or without DAPI; Vector Laboratories).

Cardiomyocyte images were collected on a Zeiss 510 Meta confocal microscope (Carl Zeiss), under 40x magnification (oil, 1.30 NA lens), with a pinhole of 1.0 airy disc (Carl Zeiss), using the Zeiss image acquisition software. HEK293 images were taken at 40x magnification using both the FITC filter and DAPI filter. All images were exported to Photoshop (Adobe) for cropping and linear adjustment of contrast.

Statistics

Data are presented as means with SEM. Sigma Stat was used to compare two groups with a Student T-test and multiple groups with an ANOVA. Significance was set at a p value < 0.05. Categorical data between two groups was compared using a 2-tailed Fisher Exact Test with significance set at $P<0.05$.

CHAPTER III

PROARRHYTHMIC DEFECTS IN TIMOTHY SYNDROME REQUIRE CALMODULIN KINASE II

Introduction

Timothy Syndrome (TS) is an autosomal genetic disease of the primary cardiac Ca^{2+} channel ($Ca_V1.2$) consisting of a missense mutation, G406R, in the pore forming α_{1c} subunit protein (Figure 3-1C) [100]. The TS mutation leads to a multisystem disease associated with syndactaly, autism, cognitive disorders, hypoglycemia, immune defects, arrhythmias and structural heart disease [100, 101]. In fact, TS patients have an average life expectancy of only 2.5 years due to severe cardiac disease. TS is also known as long QT syndrome 8 (LQT8) and the prolonged QT intervals in TS patients (Figure 3-1B) are thought to cause cardiac arrhythmias and sudden death. TS disease phenotypes are apparently initiated by excessive Ca^{2+} entry, at least in part, due to impaired voltage dependence of inactivation (VDI) of $Ca_V1.2$ current (I_{Ca}) [100, 101]. The loss of VDI is independent of accessory β subunits and Ca^{2+} dependent inactivation [6]. Mathematical modeling predicts that intracellular Ca^{2+} overload and action potential prolongation stimulate afterdepolarizations that are the cellular mechanism underlying the arrhythmias in TS [100, 101].

In cardiomyocytes multiple signaling pathways are activated by increased intracellular Ca^{2+} entry, including the multifunctional Ca^{2+} and calmodulin

dependent kinase II (CaMKII) [114], a procardiomyopathic and proarrhythmic signaling molecule [126]. Increased CaMKII activity causes AP prolongation and arrhythmias, similar to observed phenotypes in TS patients, in part by increasing sarcoplasmic reticulum (SR) Ca^{2+} leak and I_{Ca} facilitation [73, 117]. On the other hand, CaMKII inhibition restores normal intracellular Ca^{2+} homeostasis and suppresses arrhythmias [117, 126]. ***Based upon these concepts, I hypothesized that the increased Ca^{2+} entry in TS cardiomyocytes enhances CaMKII actions and that CaMKII activity is important for the proarrhythmic cellular phenotype in TS.*** To test this hypothesis I created an adult ventricular myocyte model of TS by viral infection of a dihydropyridine-resistant $Ca_V1.2$ α_{1c} subunit [29] harboring the TS mutation. My studies found that $Ca_V1.2$ G406R requires CaMKII activity to cause the proarrhythmic phenotypes in adult ventricular myocytes.

Timothy Syndrome introduction and phenotype

The initial documentation of Timothy Syndrome, in 1995, investigated a correlation between a long QT arrhythmia and syndactaly (webbed fingers and toes) (Figure 3-1A, B) [74]. Almost ten years later, mutations within domain I helix S6 (DI/S6) of $Ca_V1.2$ were identified from these patients (Figure 3-1C). The mutations (Figure 3-1D) were found either on exon 8a, TS type 1 (TS1) [101], or on exon 8, TS type 2 (TS2) [100]. TS1 stems from a Gly 406 to Arg missense mutation (G1216A transition) on exon 8a. TS2 originates from either a Gly 406 to Arg

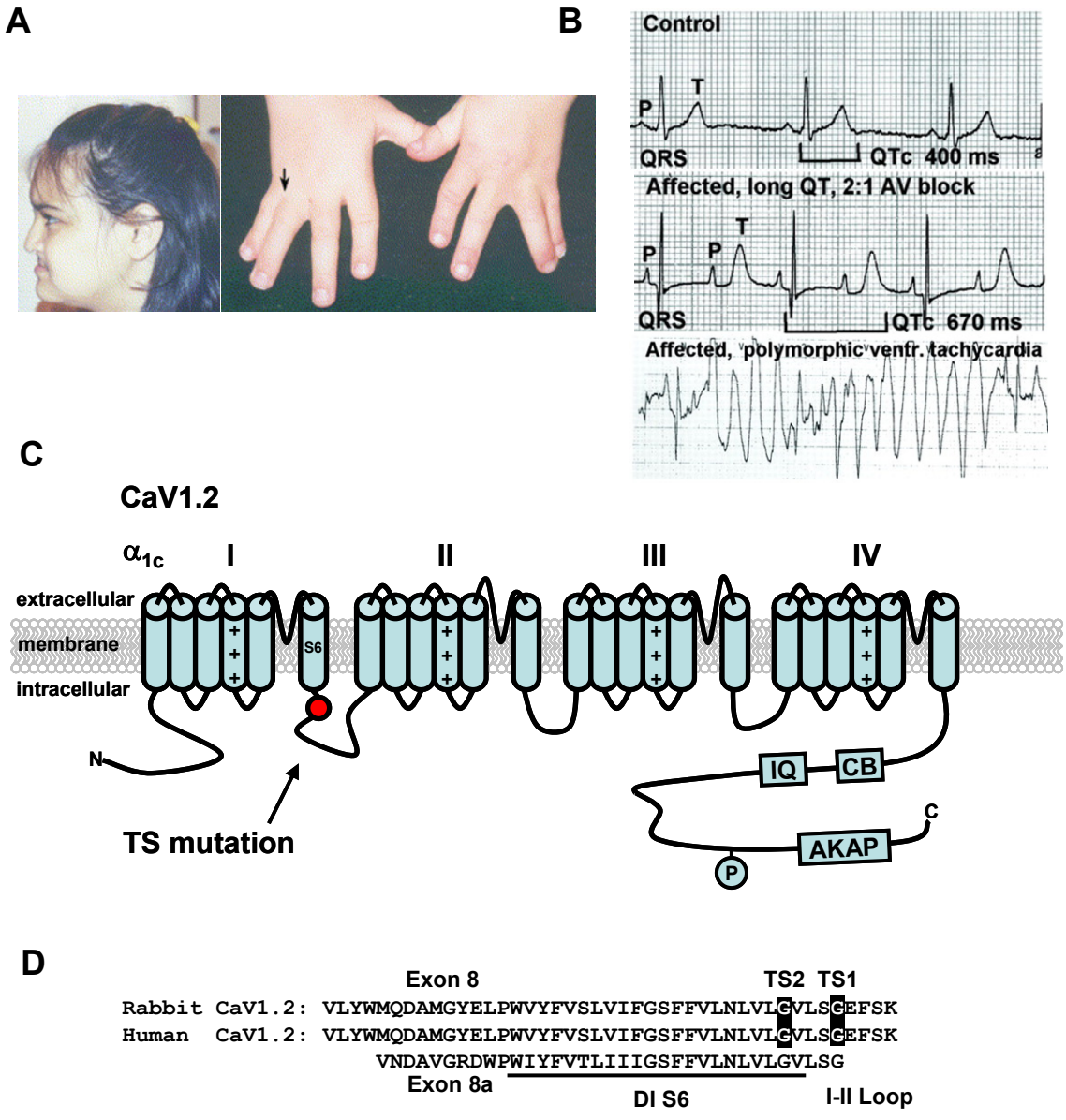

Figure 3-1: Timothy Syndrome (TS) **A)** TS patients exhibit dysmorphic facial feature and syndactyly (reprinted from Splawski *et. al.* Cell 2004). **B)** TS patients have significantly prolonged QT intervals and have episodes of ventricular tachycardia (reprinted from Splawski *et. al.* PNAS 2005). **C)** TS is caused by a missense mutation on the I-II loop of $Ca_V1.2$ α subunit. **D)** Multiple sequence alignment highlighting the location of TS mutations (TS1 = Gly 406 Arg, TS2 = Gly 402 Ser).

(G1216A transition) or a Gly 402 to Ser (G1204A transition) mutation on exon 8.

The manifestation of Timothy Syndrome, type 1 and type 2, mutations may be categorized into three major groups; physical, cognitive and cardiac. The most common physical features of TS include syndactaly, myopia, small teeth and baldness at birth [100, 101]. Cognitive defects include developmental delays in language and motor skills, and a few cases of diagnosed autism [100-102]. The most life-threatening manifestations of TS occur in the heart. ECGs from TS patients reveal not only an increased QT interval but also several arrhythmias, such as AV block (atria contraction not always followed by ventricular contraction), bradycardia (slow rhythm), ventricular tachycardia (fast rhythm) and ventricular fibrillation (uncoordinated rhythm) [100, 101]. Treatments for TS patients focus on managing the arrhythmias, which are the main cause of death [61, 100, 101].

Expression of $Ca_V1.2$ and the distribution of exon 8a/8

To understand how a single mutation of a Ca^{2+} channel can have such a widespread effect on multiple tissues, initial studies on TS examined $Ca_V1.2$ expression throughout human and mouse. Northern and mRNA dot blot analysis against $Ca_V1.2$ reveal expression of the Ca^{2+} channel in many different tissues, including predominately the brain and the heart but also stomach, bladder, prostate and uterus [101]. Areas of the heart expressing $Ca_V1.2$ included the aorta, atria (left and right), ventricles (left and right), septum and apex [101]. *In situ* hybridization of mouse tissue for $Ca_V1.2$ (anti sense probe) was used to better quantify $Ca_V1.2$ distribution. Expression was found throughout the heart and

within specific areas of the brain (cortex, hippocampus, thalamus, hypothalamus, caudate putamen and amygdale) [101]. Congruent with additional TS phenotypes, $Ca_V1.2$ was found in the eye (retina and sclera), developing digits and tooth papilla [101].

Not only is it important to understand where $Ca_V1.2$ is expressed but also what percent of $Ca_V1.2$ carry the TS mutation. Despite Timothy Syndrome being a heterozygous disease, the TS mutation is not found in half of all $Ca_V1.2$ because of splice variants between exon 8a and exon 8. A cloning and PCR screen of human cDNA was used to ascertain the actual distribution of $Ca_V1.2$ exon 8 and exon 8a. Exon 8a was found to be within 22.8% of total $Ca_V1.2$ in heart and 23.2% of total $Ca_V1.2$ in brain [101]. Whereas, exon 8 was found to be 77.2% and 76.8% in heart and brain respectively [101]. Because of these splice variations and heterozygosity of TS, TS1 (exon 8a) is found in 11-12% of total $Ca_V1.2$ [101] and the TS2 mutations (exon 8) are found in 38-39% of total $Ca_V1.2$ [100].

Understanding that $Ca_V1.2$ is widely expressed in many tissues helps to elucidate how so many different pheontypes arise from a single mutation within a Ca^{2+} channel. Surprisingly, the percent of channels necessary to drastically affect physiology may be as little as 11-12%. In accordance with this observation, the longest surviving TS patients, currently in their twenties, are mosaics for the TS mutation [61, 100].

Biophysics of TS mutation

To date, the biophysics of the TS mutations have been studied in a heterologous cell system using Chinese Hamster Ovarian cells (CHO) and *Xenopus* oocytes [100, 101]. The TS mutations were collectively found to eliminate the voltage dependence of inactivation.

Data on TS $Ca_V1.2$ (reconstituted from β_{2a} and $\alpha_2\delta$ subunit co-expression) collected from experiments with CHO cells was obtained using whole cell voltage clamp to record Ca^{2+} currents (I_{Ca}) under 15 mM Ca^{2+}. Various biophysical properties were studied, such as the current and voltage relationship (IV plot), the steady state of activation and the voltage dependence of inactivation (VDI). No changes were observed with the IV plot or activation [100, 101]. TS mutation causes $Ca_V1.2$ to only partially inactivate after 300 ms depolarization, whereas wild type $Ca_V1.2$ inactivation has almost completed during the same duration [101]. Furthermore, a VDI plot reveals a minimum I_{Ca} availability (56%) at potentials +30mV and above [101]. However, wild type $Ca_V1.2$ has almost no I_{Ca} availability for the potentials +20mV and above [101]. Moreover, I_{Ca} availability increases again for the TS mutation $Ca_V1.2$, not for wild type $Ca_V1.2$, at potentials +50 mV and higher because of a recovery from Ca^{2+} dependent inactivation (CDI) [35, 101]. TS mutation $Ca_V1.2$ inactivation time constant (τ, ms) plotted against voltage is U-shaped, τ is fastest at 0 mV (from CDI) and slows with increasing voltage, unlike wild type $Ca_V1.2$ where τ becomes faster with voltage (from both CDI and VDI) [35, 101].

Interpreting the impact of the TS mutations on inactivation kinetics from the CHO cell Ca^{2+} current experiments is complicated by the Ca^{2+} dependent component of inactivation. CDI can be eliminated by substituting Ba^{2+} for Ca^{2+}. Additional experiments expressed the TS mutation $Ca_V1.2$ within *Xenopus* oocytes and whole cell Ba2+ currents (I_{Ba}) were recorded with 40 mM Ba^{2+}. In the absence of CDI, a +30 mV depolarizing potential inactivated <20% TS $Ca_V1.2$, whereas the same potential inactivated >90% wild type $Ca_V1.2$ [100, 101].

Experiments from CHO cells and *Xenopus* oocytes reveal not only a loss of VDI but also and overall increase in Ca^{2+} conducted into a cell. Therefore, TS mutations are a gain of function by attenuating the Ca^{2+} channel's ability to "turn off" after the cellular membrane has depolarized.

Computational models of TS

Predictions were made on how the $Ca_V1.2$ carrying the TS mutation would affect the action potential (AP) and trigger arrhythmias. The Luo-Rudy mammalian ventricular cell model, with 11.5% TS1 $Ca_V1.2$ or 38% TS2 $Ca_V1.2$, predicts an elongation in the action potential [35, 100]. Despite the TS $Ca_V1.2$ causing a small overall effect on $Ca_V1.2$ inactivation, this small change is enough to increase AP duration and thereby increase the QT interval of TS patient ECGs. Modeling a 3Hz train of APs followed by a pause indicates that the TS $Ca_V1.2$ leads to SR Ca^{2+} overload and pro-arrhythmic delayed afterdepolarizations[100].

Modeling of I_{Ca} during the elongated action potential shows that TS $Ca_V1.2$ causes a larger peak I_{Ca}, because the loss of VDI allows fewer $Ca_V1.2$ to be inactivated during the peak depolarization of the AP [35]. Furthermore, TS $Ca_V1.2$ I_{Ca} modeling indicates an increase in I_{Ca} during the late phase of the AP, due to a recovery from CDI from the decrease in intracellular Ca^{2+} [35].

Treatment for TS

Treatment for TS centers on managing the Long QT arrhythmia. Therefore, any therapy would need to prevent the AP elongation and DAD initiation. Modeling has helped guide treatment by indicating that a 35% reduction of I_{Ca} would rescue the AP duration and thereby prevent arrhythmia inducing events like DADs [101]. Ca^{2+} channel antagonists are suitable for reducing I_{Ca}. Reducing I_{Ca} by directly blocking $Ca_V1.2$ has complications. First of all, TS $Ca_V1.2$ have a reduced sensitivity for the dihydropyridine Ca^{2+} channel antagonists. Nisoldipine was shown, in heterologous cells, to have a 50% inhibitory concentration (IC50) of 267+/-5 nM for TS rather than the IC50 of 74+/-7 nM observed with wild type [101]. Secondly, direct Ca^{2+} channel antagonism may cause excessive vasodilation and bradycardia [51]. The Ca^{2+} channel antagonist, verapamil (not a dihydropyridine), has been shown to successfully treat one TS patient [61]. More likely a TS patient will receive an implanted cardioverter-defibrillator (ICD) to control cardiac rhythm and lethal arrhythmias, such as ventricular tachycardia and ventricular fibrillation. The addition of verapamil decreased the number of ICD events, but not all ICD events were eliminated [61].

Results

An adult ventricular myocyte TS model

I marked exogenous $Ca_V1.2$ by the addition of an extracellular hemaglutanin (HA) epitope [2] (Figure 3-2A, green circle) and introduced a validated dihydropyridine-insensitivity mutation [29] (Figure 3-2A, black circle). The dihydropyridine-insensitivity mutation allows the virally introduced $Ca_V1.2$ to remain functional while using nifedipine to inhibit endogenous $Ca_V1.2$ [29]. Exogenous $Ca_V1.2$ expression was confirmed by immunoblot (Figure 3-2B) and immunofluorescence (Figure 3-2C) in transduced HEK293T cells. The function of $Ca_V1.2$ wild type (WT) and TS (G406R exon 8) were confirmed by recording I_{Ca} using whole cell voltage clamp in HEK293T cells. I_{Ca} recorded from TS expressing HEK293T cells exhibited a significant loss of VDI (Figure 2-2D), as previously published [6, 100, 101].

Over-expression of $Ca_V1.2$ in ventricular myocytes yielded 33.7% increase in peak I_{Ca} (Figure 3-3A, B) and an average 31.9% increase in total $Ca_V1.2$ protein (Figure 3-3C). Due to the dihydropyridine-resistance mutation [29], peak I_{Ca} in $Ca_V1.2$ infected ventricular myocytes was significantly resistant to nifedipine, as compared to uninfected cells (Figure 3-3A, B). In TS and WT infected ventricular myocytes 10nM nifedipine resulted in a peak I_{Ca} (WT 6.6±0.7 pA/pF N=5, TS 6.9±0.7 pA/pF N=6) that was similar to the peak I_{Ca} (6.7±1.0 pA/pF N=8) measured in non-infected myocytes recorded without nifedipine (Figure 3-3A, B). This nifedipine engineered balance of endogenous and exogenous $Ca_V1.2$

allowed me to determine the effects of the TS mutation on cardiac electrophysiology independent of over-expression induced changes in peak I_{Ca}.

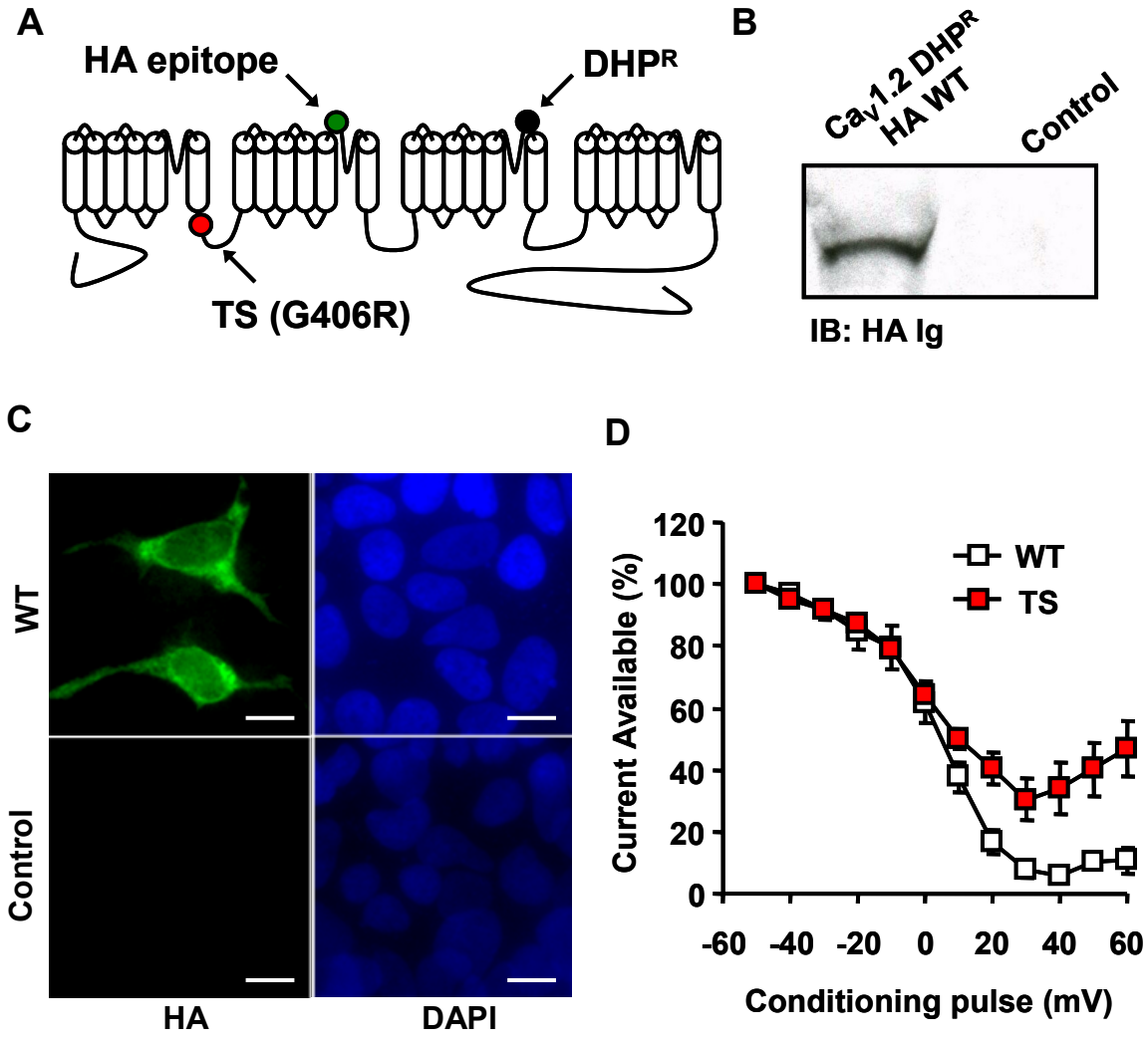

Figure 3-2: Dihydropyridine-resistant $Ca_V1.2$ α subunit Timothy Syndrome (TS) model. **A)** A topology diagram of $Ca_V1.2$ depicting dihydropyridine resistance mutation (DHP^R, black circle), extracellular hemaglutanin epitope (HA, green circle) and the TS mutation (G406R, red circle) on the I-II intracellular loop. **B)** Immunoblot (HA Ig) of HEK293T cells expressing the modified $Ca_V1.2$ or empty vector control. **C)** FITC immunofluorescence (HA Ig) of HEK293T cells expressing the modified $Ca_V1.2$ with corresponding nuclear stain by DAPI (Scale bar, 10μm). **D)** $Ca_V1.2$ TS expressing HEK293T cells show a reduction in VDI as compared to HEK293T cells transfected with $Ca_V1.2$ WT (N=5 cells/point).

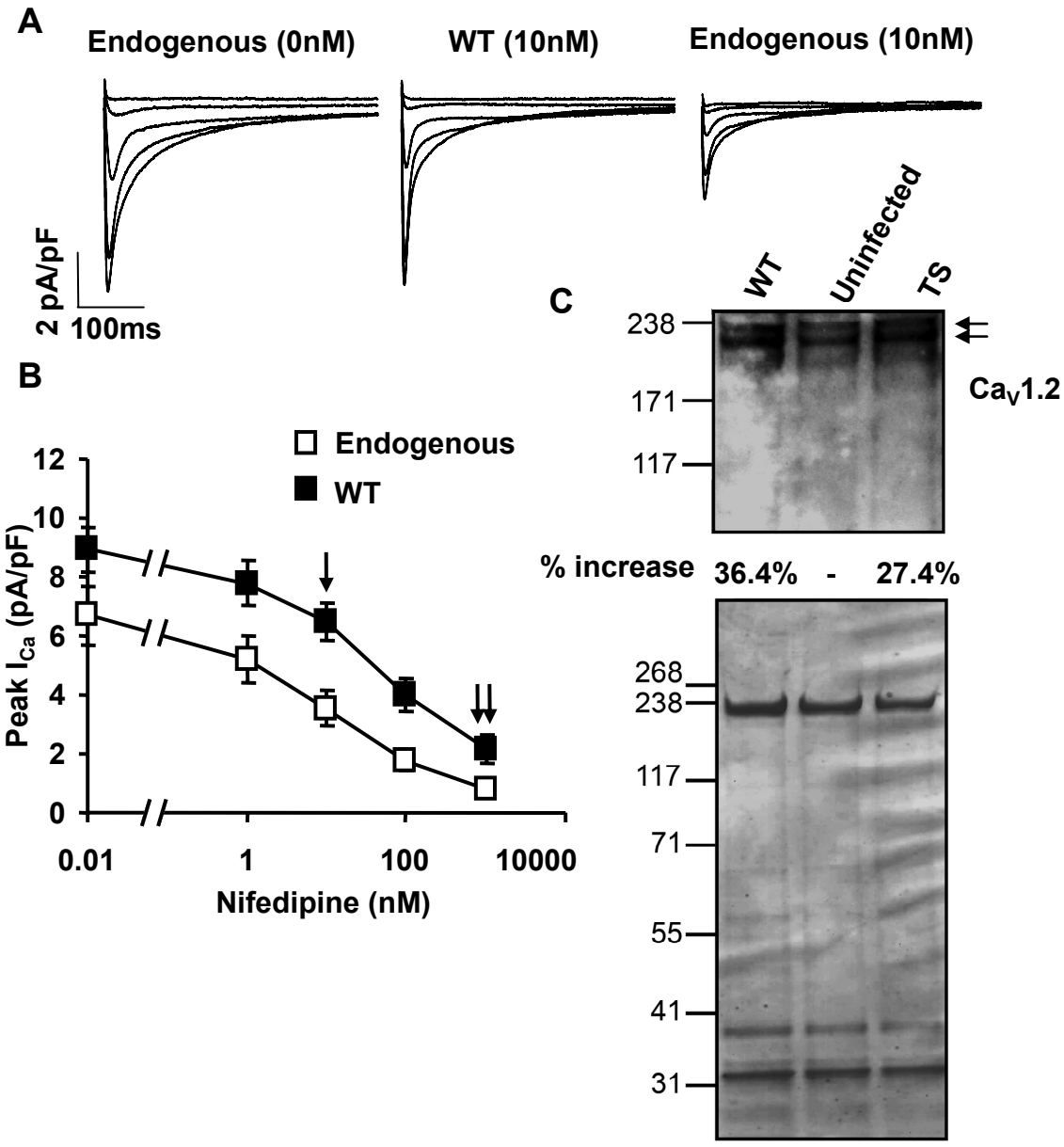

Figure 3-3: $Ca_V1.2$ dihyrdropyridine resistance mutation. **A)** Raw current traces showing WT DHP^R and endogenous I_{Ca}. **B)** Preserved I_{Ca} during exposure to nifedipine. The single arrow indicates the nifedipine concentration (10nM) used to study the cellular consequences of the TS mutation, and the double arrow indicates the nifedipine concentration (1mM) to overcome dihydropyridine resistance and block the majority of I_{Ca} (N=5-8 cells/point, $P<0.05$ at each nifedipine concentration). **(C top)** Immunoblot for total $Ca_V1.2$ protein and from ventricular myocytes infected with $Ca_V1.2$ WT **(lane 1)**, $Ca_V1.2$ TS **(lane 3)** or uninfected **(lane 2)** as a control. The average increase in WT and TS $Ca_V1.2$ protein relative to uninfected was 31.9% (WT=36.4%, TS=27.4%) after correcting for total protein loading observed in the **(C bottom)** Coomassie stained lanes.

TS ventricular myocytes exhibit increased CaMKII autophosphorylation

I confirmed expression of exogenous $Ca_V1.2$ in cultured adult ventricular myocytes by immuno-staining for the HA epitope (Figure 3-4D,G). Virally introduced $Ca_V1.2$ was properly targeted to the transverse-tubule (T-tubule) network, based upon the punctate appearance and 1.8 μm spacing of the HA immunofluorescence that is consistent with known distances between T-tubules in a resting sarcomere [10]. No HA immuno-staining was detected in uninfected ventricular myocytes (Figure 3-4A).

Ventricular myocytes were immuno-stained for the CaMKII autophosphorylation site, Thr 286, which is a marker of CaMKII activation [71]. TS ventricular myocytes (Figure 3-4H,I) exhibited greater levels of CaMKII autophosphorylation compared to both WT (Figure 3-4E, F) and uninfected ventricular myocytes (Figure 3-4B, C). Total CaMKII immuno-staining revealed no changes in CaMKII protein levels between WT, TS and uninfected ventricular myocytes (Figure 3-5E, H). These data show that activated CaMKII is recruited in TS $Ca_V1.2$ expressing ventricular myocytes and suggest that CaMKII activity may contribute to the cellular arrhythmia phenotypes in TS.

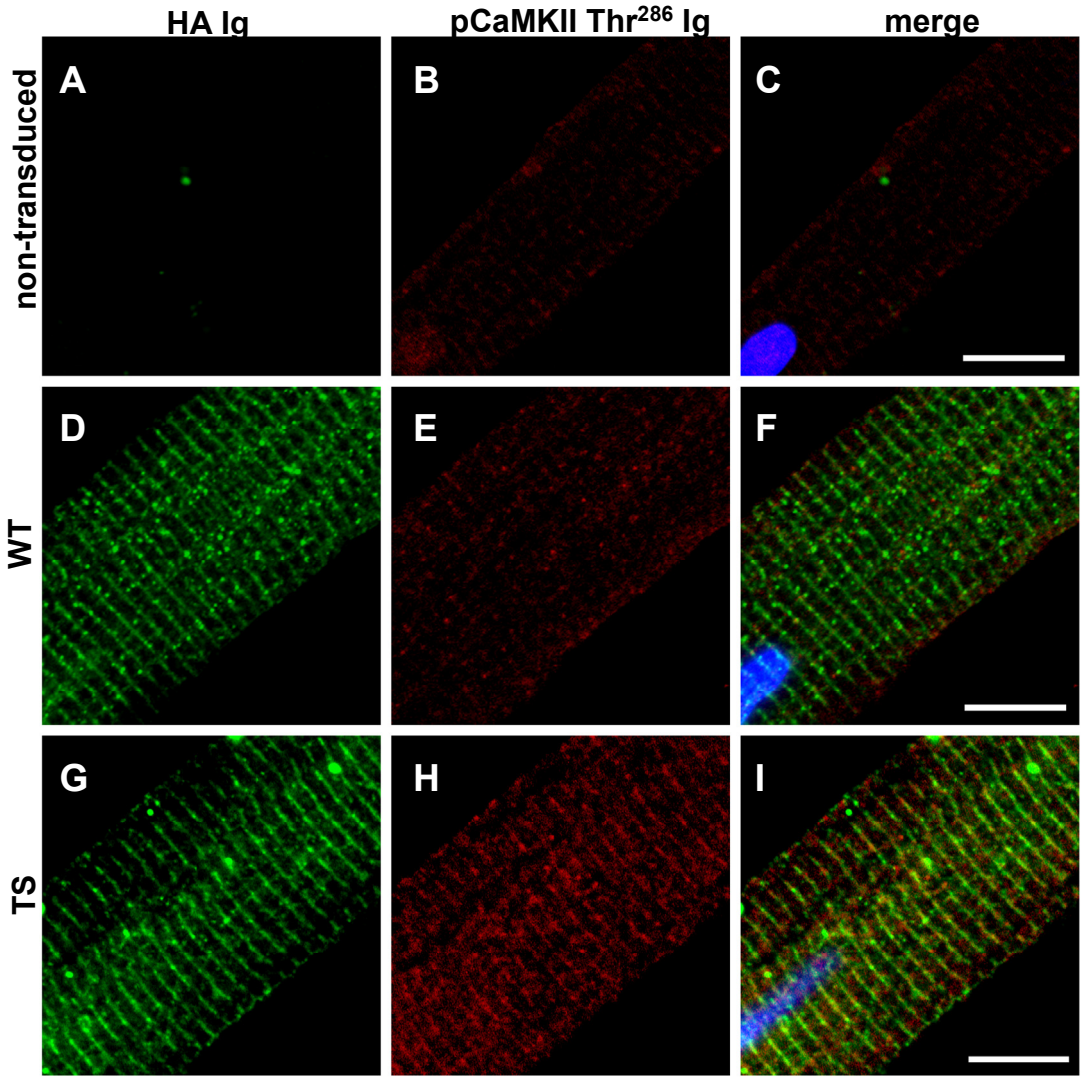

Figure 3-4: CaMKII recruitment in the TS adult ventricular myocyte model. **(A-C)** Non-transduced, **(D-F)** WT and **(G-I)** TS adult ventricular myocytes. **(A,D,G)** Exogenous $Ca_V1.2$ channels are expressed in regularly distributed punctae across ventricular myocytes as shown by HA immunostaining. Both WT and TS $Ca_V1.2$ show spacing consistent with T-tubule network localization. HA immunofluorescence section of $Ca_V1.2$ WT, TS mutation, and uninfected negative control. **(H)** More activated CaMKII (pCaMKII Thr286) immuno-stained with **(I)** TS ventricular myocytes as compared to WT **(E and F)** and non-transduced **(B and C)** ventricular myocytes. (Scale bar, 10μm)

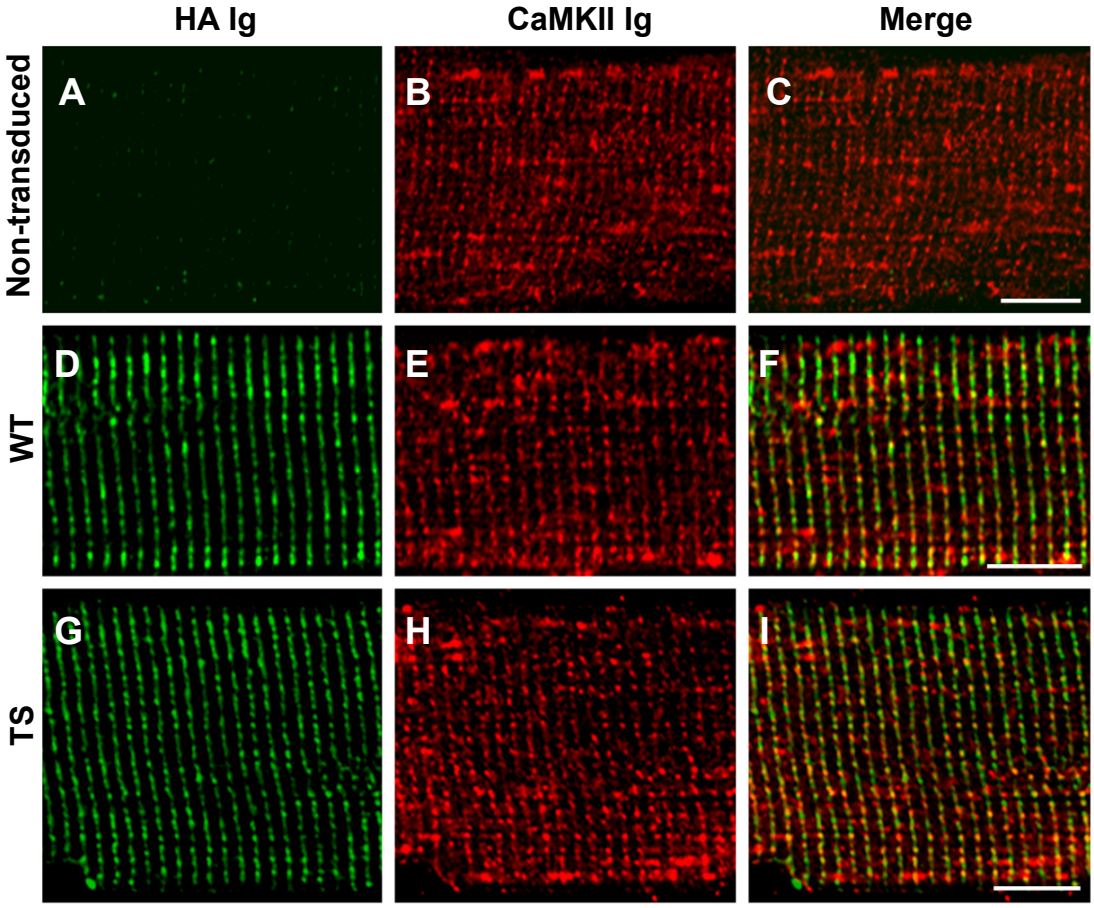

Figure 3-5: Adult ventricular myocytes **(A,B,C)** non-transduced, infected with **(D,E,F)** WT $Ca_V1.2$ virus or infected with **(G,H,I)** TS $Ca_V1.2$ virus (scale bar 10μm). TS and WT infected ventricular myocytes show overexpressed $Ca_V1.2$ **(D,G)** by HA immuno-staining, but no changes in total CaMKII protein **(E,H)** as compared to non-transduced ventricular myocytes **(B)**.

Action potential prolongation in TS ventricular myocytes is reversed by CaMKII inhibition

Stimulated action potentials (arrow head, Figure 3-6A) were recorded in nifedipine treated (10 nM) WT and TS ventricular myocytes. Compared to WT, the TS mutation significantly prolonged the action potential duration (Figure 3-6A, B) as determined by the time to 90% repolarization (APD90%). Excessive action potential prolongation favors the generation of afterdepolarizations [90]. I observed afterdepolarizations from TS ventricular myocytes (5 out of 10 cells, Figure 3-6A, C), whereas none were observed in any of the WT cells (0 out of 10 cells, Figure 3-6A, C). Most afterdepolarizations were delayed afterdepolarizations (DADs), but early afterdepolarizations (EADs) were also recorded from TS ventricular myocytes. DADs are favored by increased diastolic Ca^{2+} leak from the sarcoplasmic reticulum (SR) [1, 116] and EADs are caused by increased I_{Ca} facilitation [115]. The action potential prolongation and the tendency for afterdepolarizations in TS ventricular myocytes are consistent with predictions from computational modeling [100, 101].

Action potential durations from WT and TS ventricular myocytes in 1 μM nifedipine were reduced to equivalent times and neither WT nor TS ventricular myocytes exhibited afterdepolarizations under these conditions (Figure 3-6B, C). The 1 μM nifedipine bath solution overcomes the dihydropyridine resistance mutation and inhibited the total peak I_{Ca} by >50% (Figure 3-3B, double arrows). These findings indicate that the observed TS phenotypes were initiated by increased I_{Ca}.

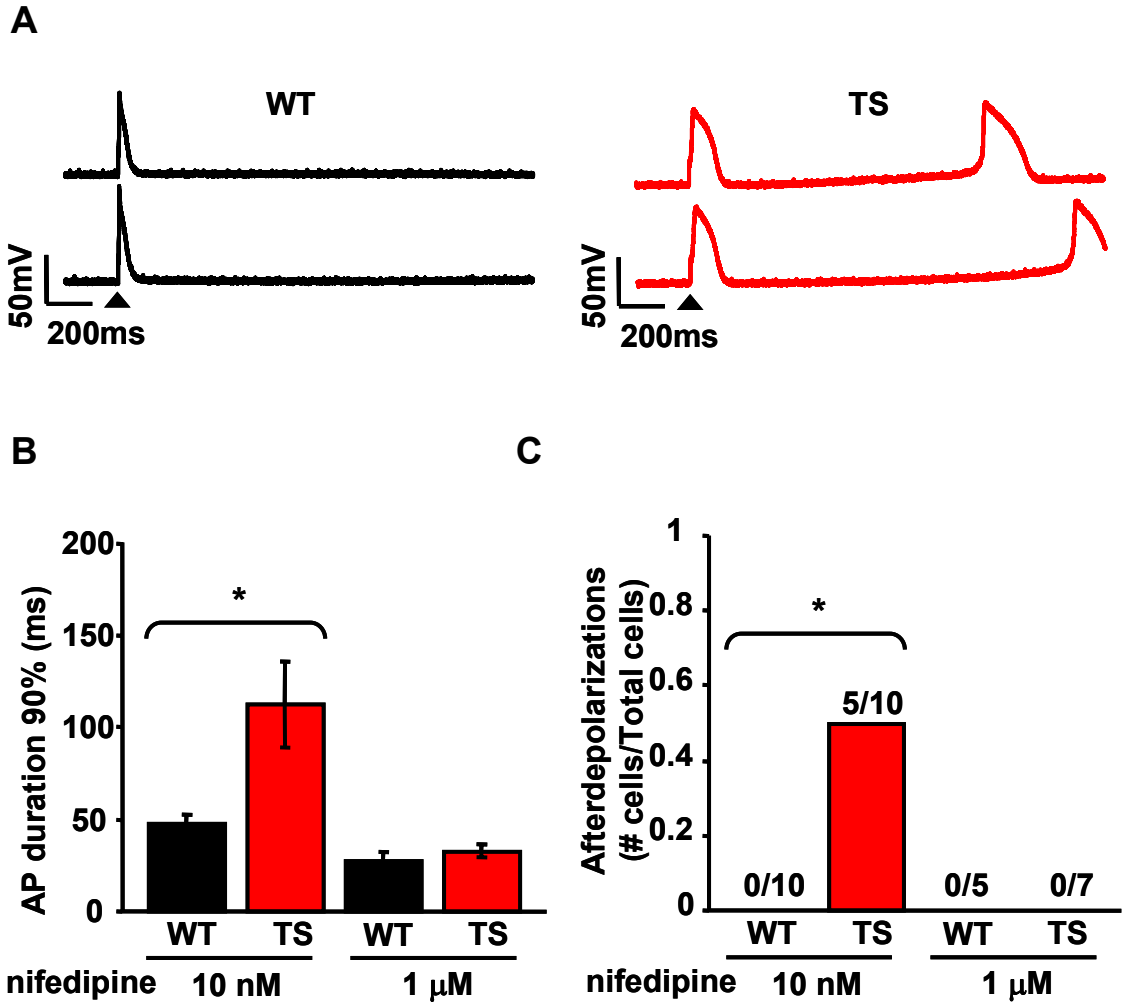

Figure 3-6: TS mutation causes action potential prolongation and afterdepolarizations. **A)** Action potential recordings from WT and TS ventricular myocytes. The first action potential for each sweep was initiated by injected current (arrow head), but the subsequent action potentials in TS arose from spontaneous afterdepolarizations. **B)** $Ca_V1.2$ TS results in an increased action potential duration (N=5-10 cells/group, *P=0.018) and **C)** afterdepolarizations (N=5-10 cells/group, *P=0.033). Numerals indicate the fraction of cells studied with afterdepolarizations.

I tested the role of CaMKII activity in the observed proarrhythmic cellular phenotypes observed from TS ventricular myocytes by dialysis of AC3-I, a selective CaMKII inhibitory peptide [112, 126]. AC3-I normalized the action potential duration in TS to WT levels (P=0.40, Figure 3-7A, B). The inactive control peptide, AC3-C [112, 126], had no effect, suggesting that CaMKII-dependent increases in I_{Ca} contributed to action potential prolongation in TS. The CaMKII inhibitory peptide also eliminated afterdepolarizations in TS ventricular myocytes (P=1.0, Figure 3-7A, C), whereas AC3-C did not (P=0.04, Figure 3-7A, C). These data support the concept that CaMKII activity is required for the proarrhythmic electrophysiological phenotypes in TS ventricular myocytes.

In WT ventricular myocytes the CaMKII inhibitory peptide, AC3-I, resulted in a non-significant (P=0.28) shortening of the action potential duration (Figure 3-7B) compared to WT ventricular myocytes dialyzed with the control peptide, AC3-C. WT ventricular myocytes did not exhibit afterdepolarizations after dialysis with AC3-I or AC3-C (Figure 3-7C). I assessed additional action potential parameters, including resting cell membrane potential and peak cell membrane depolarization amplitude. Both TS and WT ventricular myocytes exhibited equivalent resting membrane potentials and peak action potential amplitudes (Table 3-1). Action potential parameters from WT ventricular myocytes, in the presence of 10nM nifedipine, were similar to uninfected ventricular myocytes, cultured for the same time period (24-36 hours) and recorded without nifedipine (Table 3-1). These controls suggest that viral expression of $Ca_V1.2$ does not alter the action potential when peak I_{Ca} is adjusted to normal levels (by 10nM

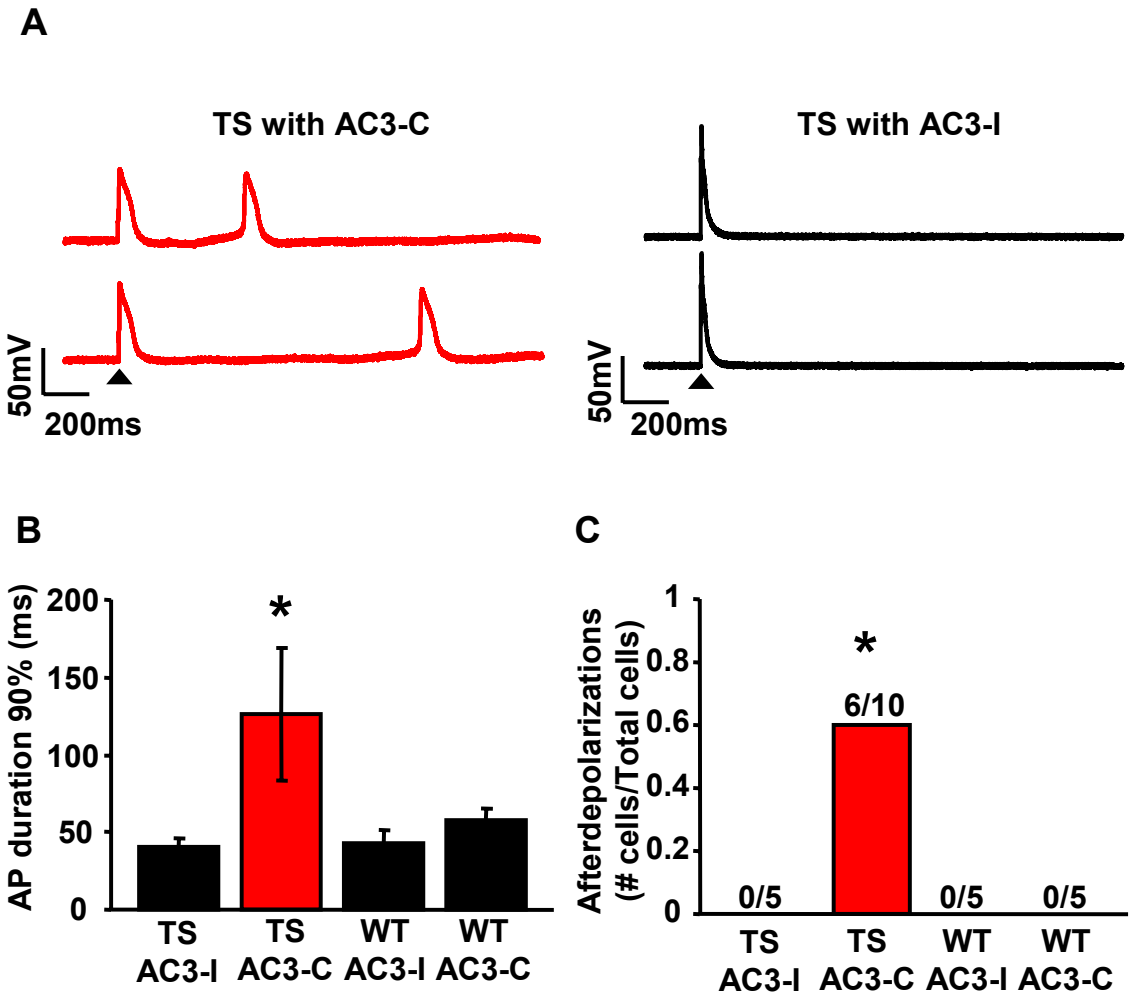

Figure 3-7: CaMKII inhibition reverses TS ventricular myocyte action potential (AP) prolongation and afterdepolarizations. **A)** Action potential recordings from TS ventricular myocytes with either the CaMKII inhibitory peptide, AC3-I, or a control peptide, AC3-C. **(B and C)** Dialyzing AC3-I restored action potential duration in TS to WT levels and prevented afterdepolarizations (N=5-10 cells/group, TS with AC3-I compared to WT: APD90% P=0.403, afterdepolarizations P=1.0). **(A-C)** Dialyzing the control peptide, AC3-C, did not alter the TS mutation affects on action potential duration or afterdepolarizations (N=5-10 cells/group, TS with AC3-C compared to TS with AC3-I: APD90% *P=0.017, afterdepolarizations *P=0.044).

nifedipine) and that the proarrhythmic phenotype observed in TS ventricular myocytes was due to the TS mutation.

Taken together, these findings are the first to demonstrate experimentally that the action potential phenotypes observed in TS ventricular myocytes were dependent upon increased Ca^{2+} entry through $Ca_V1.2$. These observations suggest that the TS VDI defect is insufficient, in the absence of increased CaMKII activity, to cause significant action potential prolongation in ventricular myocytes.

Table 3-1: AP Data and Statistics

				P value	
	WT	**TS**	**Uninfected**	**WT:TS**	**WT:Un**
Nifedipine (nM)	10	10	0		
Number of Cells (n)	10	10	12		
APD90% (ms)	46.35 ±8.02	112.00 ±23.47	68.04 ±12.54	**0.018**	0.17
Afterdepolarizations (#/Total)	0/10	5/10	0/11	**0.033**	1
Resting Potential (mV)	-62.60 ±3.69	-60.85 ±3.20	-67.10 ±1.02	0.497	0.966
Peak Amplitude (mV)	101.77 ±9.42	99.88 ±5.97	113.08 ±3.50	0.799	0.103

TS reduces VDI in ventricular myocytes independent of CaMKII activity

Expression of TS $Ca_V1.2$ in *Xenopus* oocytes [100, 101] and heterologous cells [6, 100, 101] (Figure 3-2D) showed a loss of $Ca_V1.2$ VDI. The *Xenopus ooctye* experiments [100, 101] included Ca^{2+} independent conditions that would not favor CaMKII activation because Ba^{2+} substituted Ca^{2+} as the charge carrier. To test the effect of the TS mutation on VDI in ventricular myocytes under conditions not permissive to CaMKII activation, I recorded I_{Ca} from TS and WT ventricular myocytes (10nM nifedipine) using Ba^{2+} (1.8mM) as the charge carrier and under high intracellular Ca^{2+} buffering (20mM BAPTA). TS ventricular myocytes exhibited a loss of VDI as a significant ($p = 0.008$, Figure 3-8A) rightward shift compared to WT. The TS $V_{1/2}$ (-30.7 mV) shifted to more positive potentials compared to WT $V_{1/2}$ (-35.8 mV). In contrast, the peak I_{Ca} elicited by the conditioning pulses showed no difference between WT and TS (Figure 3-8B), confirming equivalent expression of exogenous WT and TS $Ca_V1.2$. No differences were observed in peak I_{Ca} or VDI recorded from adult ventricular myocytes expressing WT dihydropyridine-resistant $Ca_V1.2$, with 10nM nifedipine, compared to uninfected adult ventricular myocytes, without nifedipine (Table 3-2). These findings show that TS causes a loss of $Ca_V1.2$ VDI in ventricular myocytes, establishing the initial requirement for increased cellular Ca^{2+} entry necessary to recruit CaMKII.

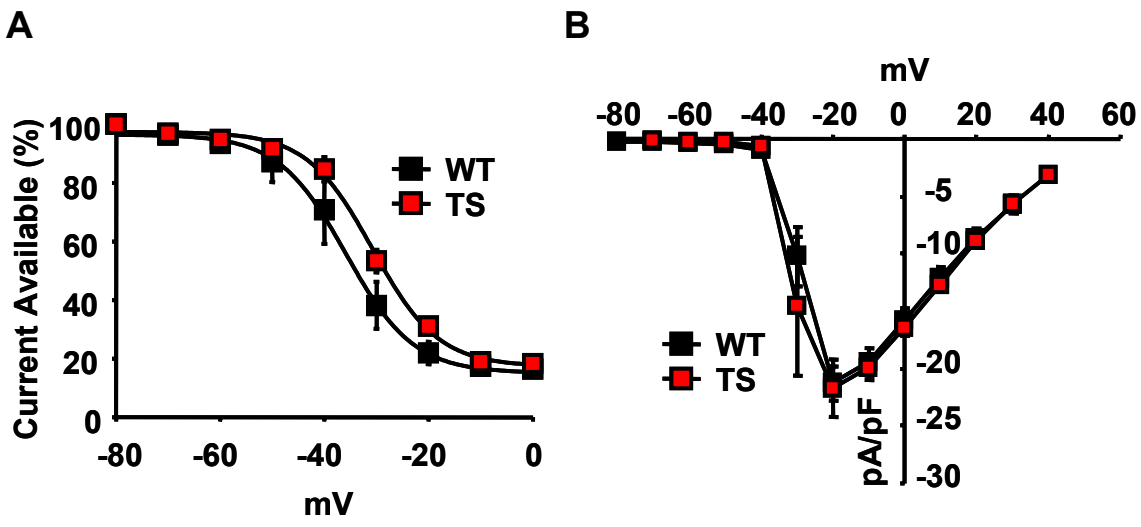

Figure 3-8: TS mutation shifts the VDI independent of Ca^{2+} signaling. **A)** The TS mutation shifts the $Ca_V1.2$ I_{Ba} VDI (N=5 cells/point, *P=0.008), **B)** without changing the current-voltage (IV) relationship (N=5 cells/group, P=0.88).

Table 3-2: VDI Data and Statistics

				P value	
	WT	**TS**	**Uninfected**	**WT:TS**	**WT:Un**
Nifedipine (nM)	10	10	0		
Number of Cells (n)	5	5	5		
VDI $V_{1/2}$ (mV)	-35.8	-30.7	-37.06	**0.008**	0.507
Peak (pA/pF)	21. 3 ±1.45	21. 7 ±2.48	19.40 ±3.56	0.880	0.583

CaMKII is required for TS effects on I_{Ca}

To test the importance of CaMKII for additional I_{Ca} changes other than VDI in our TS model, I measured CaMKII-dependent I_{Ca} facilitation [30, 115]. I_{Ca} facilitation consists of dynamic increases in peak I_{Ca} and slowing of inactivation with repetitive depolarizations [3, 123]. TS ventricular myocytes exhibited maximal peak I_{Ca} during the first depolarization, whereas WT attained peak I_{Ca} after the initial depolarization (Figure 3-9A, 3-10A). Subsequent depolarizations showed no difference in peak I_{Ca} between TS and WT (Figure 3-9A, Figure 3-10A). To measure the effects of I_{Ca} facilitation on cellular Ca^{2+} entry, I integrated total I_{Ca} during the voltage clamp command step. Integrated I_{Ca} was significantly greater in TS compared to WT during all depolarization steps (First step P=0.029, Remaining steps P<0.001, Figure 3-9B). I found the fast component of I_{Ca} inactivation (τ_{fast}) was slower in TS compared to WT (First step P=0.006, Remaining steps P<0.001, Figure 3-9C), consistent with increased I_{Ca} facilitation and augmented cellular Ca^{2+} entry in TS ventricular myocytes.

AC3-I restored the dynamic response characteristics of integrated I_{Ca} and τ_{fast} in TS to levels recorded from WT cells (integrated I_{Ca} P=0.522, τ_{fast} P=0.294, Figure 3-9D, E). In contrast, dialysis of AC3-C had no effect of τ_{fast} or integrated I_{Ca}. Dialysis of the CaMKII inhibitory peptide prevented I_{Ca} facilitation in WT ventricular myocytes (Figure 3-B, C), whereas the control peptide had no effect on WT ventricular myocyte I_{Ca} facilitation. These measurements show that CaMKII is a significant determinant of I_{Ca} from TS mutant channels, along with the previously reported shift in VDI.

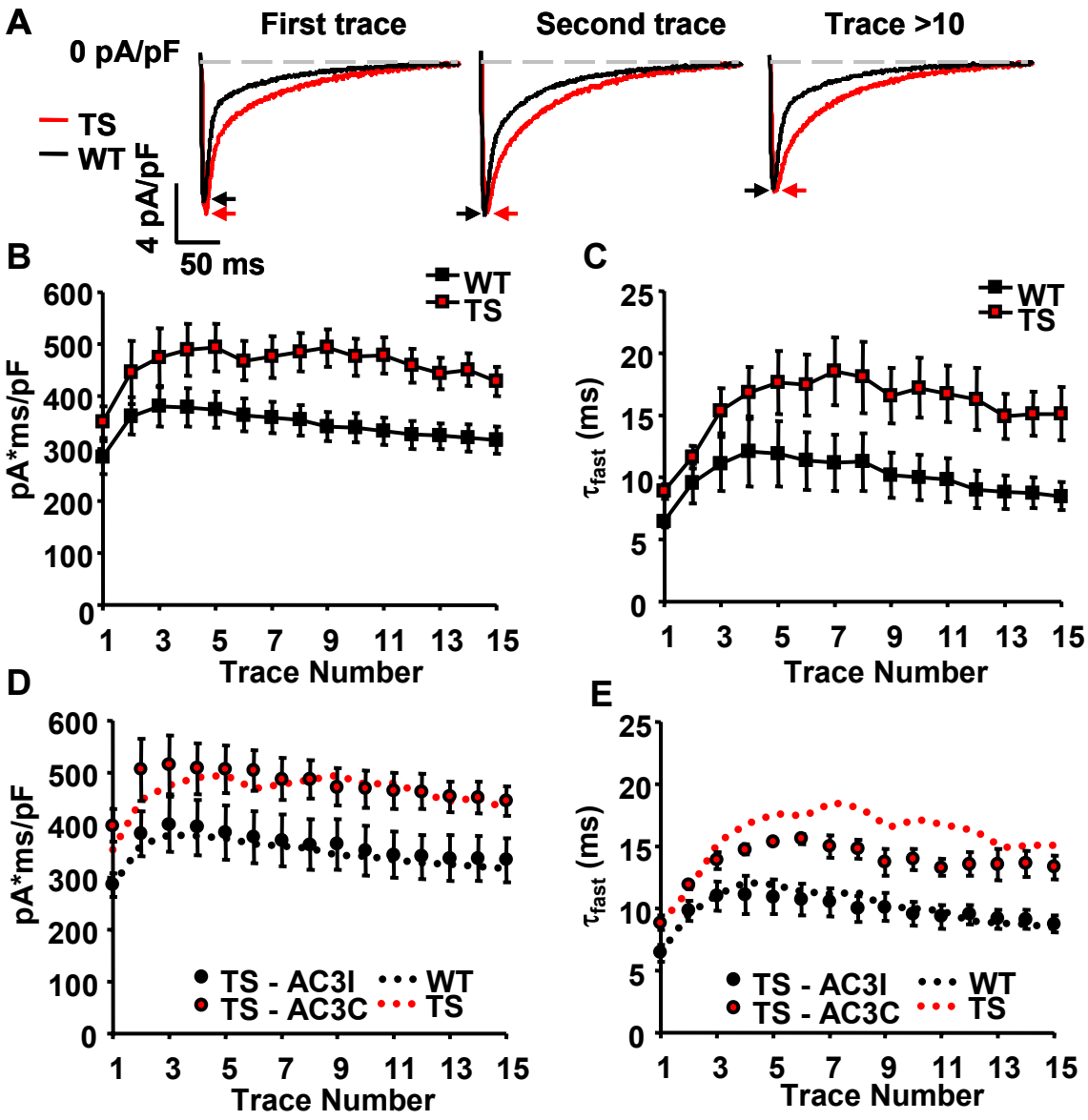

Figure 3-9: TS mutation enhances I_{Ca} facilitation. **A)** TS ventricular myocytes exhibit increased peak I_{Ca} (arrows) during the first depolarizing voltage clamp command step (-80mV to 0mV, 300ms, 0.5Hz) and slowing of inactivation during all depolarizing steps. **B)** Integrated I_{Ca} evoked by repetitive depolarizing voltage command steps (as in **A** above) is greater in TS mutation than WT (N=6-7 cells/point, First step P=0.029, Remaining steps P<0.001). **C)** The time constant of the fast component of I_{Ca} inactivation (τ_{fast}) is significantly slower in TS ventricular myocytes than WT (N=6-7 cells/point, first step P=0.006, remaining steps P<0.001). **(D and E)** Integrated ICa and τ_{fast} were restored to WT levels in TS ventricular myocytes dialyzed with the CaMKII inhibitory peptide, AC3-I (N=5-6 cells/point, TS with AC3-I compared to WT: integrated I_{Ca} P=0.522, τ_{fast} P=0.294). Dialyzing the control peptide, AC3-C, did not alter the TS mutation affects on I_{Ca} facilitation (N=5 cells/group, TS with AC3-C compared to TS with AC3-I: integrated I_{Ca} P<0.001, τ_{fast} P<0.001).

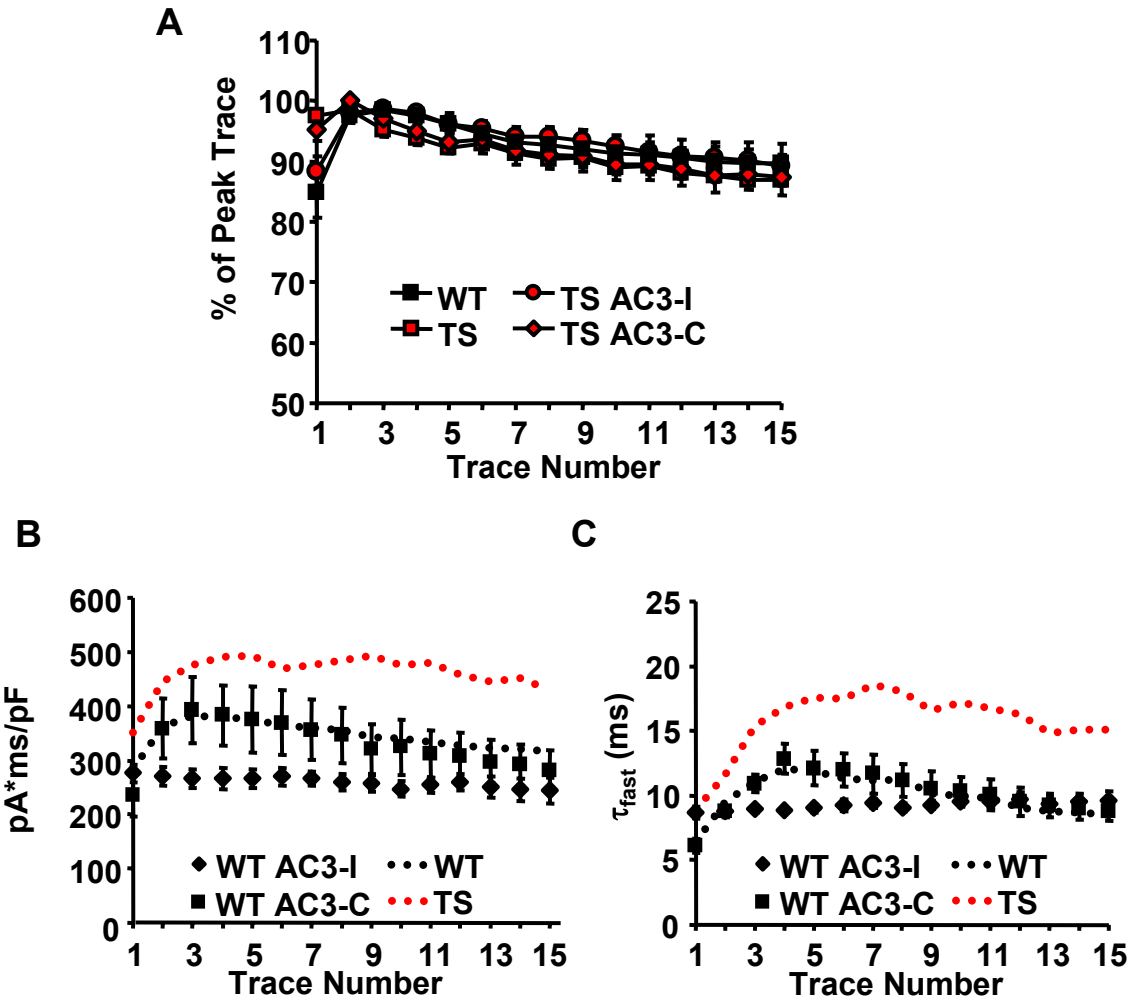

Figure 3-10: TS ventricular myocyte I_{Ca} facilitation **(A)** TS ventricular myocytes show increased peak I_{Ca} during the first depolarizing voltage clamp command step (-80mV to 0mV, 300ms, 0.5Hz) over WT ventricular myocytes (N=6-7 cells/point, P=0.02). With the second depolarizing step WT ventricular myocytes match the peak I_{Ca} observed with TS ventricular myocytes (N=6-7 cells/point, P=0.46). The CaMKII inhibitory peptide, AC3-I, restores normal I_{Ca} facilitation to TS ventricular myocytes (N=5-6, P vs. WT=0.469), but not the control peptide AC3-C (N=5-6 cells/point, P vs. WT=0.038). **(B)** WT cardiomyocytes dialyzed with the CaMKII inhibitory peptide, AC3-I, loose the dynamic increase of integrated I_{Ca} and **(C)** the dynamic change of the fast time constant (τ_{fast}) that are associated with facilitation (N=5 cells/point; integrated I_{Ca} WT AC3-C vs. WT AC3-I P<0.001 ; τ_{fast} WT AC3-C vs. WT AC3-I P<0.001). **(C and D)** The control peptide, AC3-C, has no effect on I_{Ca} facilitation (N=5 cells/point; integrated I_{Ca} WT AC3-C vs. WT P=0.675; τ_{fast} WT AC3-C vs. WT P=0.85).

TS augments intracellular Ca^{2+}

Mathematical modeling studies predicted alterations in intracellular Ca^{2+} handling in TS, including increased Ca^{2+} transient amplitude and increased SR Ca^{2+} content [100]. Ca^{2+} transients were recorded (Figure 3-11A) from WT and TS ventricular myocytes loaded with fluo-3 AM and field stimulated at 1Hz [99]. TS caused a significant increase in the peak Ca^{2+} transient compared to WT (P=0.04, Figure 3-11B), which is consistent with computer models [35, 99, 100]. Interestingly, the 50% decay time for Ca^{2+} transients in TS was significantly shortened over WT (P=0.02, Figure 3-11C). A faster decay time implicates increased SERCA activity [9], which was not predicted by modeling studies, but is associated with CaMKII signaling [8, 28, 48, 84]. These experimental data reveal that TS alters intracellular Ca^{2+} handling by increasing the peak Ca^{2+} transient amplitude and enhancing the decay of the intracellular Ca^{2+} transient.

Mathematical modeling also predicted increased SR Ca^{2+} content with TS, due to enhanced I_{Ca} from TS $Ca_V1.2$. Surprisingly, the TS SR Ca^{2+} content was not different than WT (P=0.55, Figure 3-11D). The increased SR Ca^{2+} leak in TS may balance faster SR Ca^{2+} uptake [9], thereby preventing a net increase in SR Ca^{2+} content compared to WT. Increased SR Ca^{2+} leak is implicated in CaMKII signaling [44, 73, 108] and in triggering DADs [1, 116], a prominent feature of the TS ventricular myocytes (Figure 3-6A,C). Diastolic SR Ca^{2+} leak was assessed by measuring spontaneous Ca^{2+} sparks from TS and WT ventricular myocytes (Figure 3-11E) [106]. The SR Ca^{2+} sparks were significantly increased in TS compared to WT (P=0.001, Figure 3-11E, F), indicating increased SR Ca^{2+} leak in TS. The spark amplitude for TS was significantly greater than WT (P=0.002,

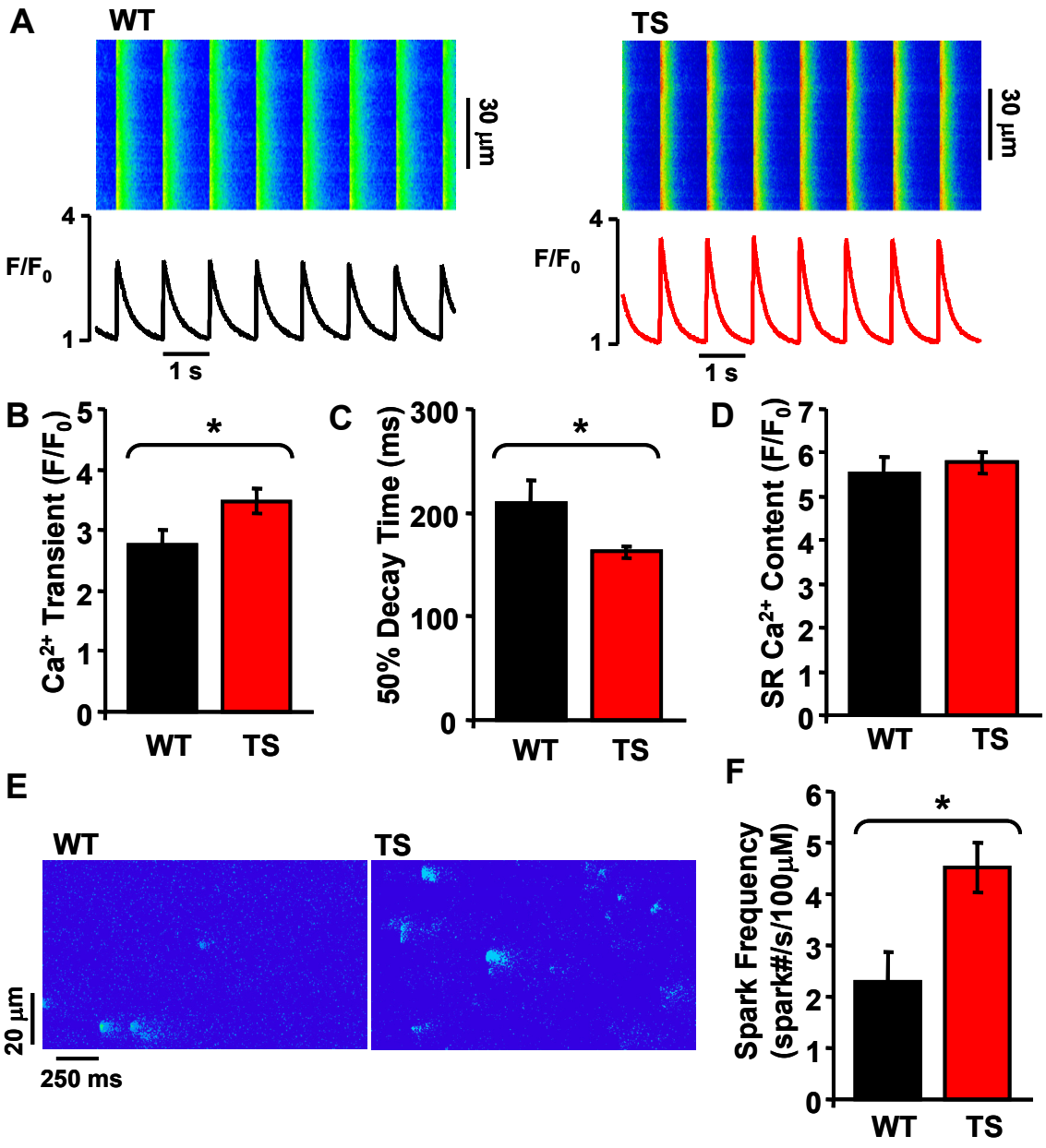

Figure 3-11: The TS mutation augments intracellular Ca^{2+} handling. **A)** Confocal Ca^{2+} transient recordings from WT and TS ventricular myocytes. **B)** Summary data showing TS mutation causes an increase in the peak Ca^{2+} transient during 1Hz stimulations (N=14-28 cells/group, *P=0.042). **C)** Summary data showing the 50% decay time of the whole cell Ca^{2+} transients were faster in TS ventricular myocytes (N=14-28 cells/group, *P=0.047). **D)** No difference was observed in SR Ca^{2+} content between TS and WT ventricular myocytes (N=14-28 cells/group, P=0.524). **E)** Ca^{2+} sparks recorded from WT and TS ventricular myocytes. **F)** Summary data showing TS infected ventricular myocytes exhibited an increased frequency of Ca^{2+} sparks during diastole (N=22-37 cells/group, *P=0.001).

Table 3-3), consistent with the increase in peak Ca^{2+} transient observed with TS. The effects of TS on intracellular Ca^{2+} handling had two unexpected results, first the faster decay time and second the increase in spark frequency. Taken together, these data suggest that SR Ca^{2+} cycling is enhanced in TS ventricular myocytes, resulting in significantly increased SR Ca^{2+} uptake and diastolic Ca^{2+} leak, but without a change in SR Ca^{2+} content.

In contrast to TS, WT exhibited no difference in the Ca^{2+} transient peak amplitude or decay time as compared to uninfected ventricular myocytes (Table 3-3). No significant changes were observed in the width or duration of the Ca^{2+} sparks (Table 3-3) between WT, TS and uninfected cells. The spark frequency and profile of individual sparks showed no difference between WT and uninfected ventricular myocytes (Table 3-3) [98].

Table 3-3: Intracellular Ca^{2+} Handling Data and Statistics

				P value	
	WT	**TS**	**Uninfected**	**WT:TS**	**WT:Un**
Number of Cells (n)	14	20	28		
Calcium Transient (F/F_0)	2.76 ±0.26	3.48 ±0.21	2.84 ±0.18	**0.042**	0.792
50% Decay Time (ms)	208.47 ±23.21	161.97 ±6.09	193.61 ±7.50	**0.047**	0.475
SR calcium content (F/F_0)	5.52 ±0.38	5.78 ±0.24	5.64 ±0.22	0.524	0.705
Spark Frequency (Sparks/ms/100 μm)	2.28 ±0.58	4.52 ±0.50	2.50 ±0.51	**0.001**	0.354
Spark Intensity (F/F_0)	1.47 ±0.03	1.75 ±0.06	1.62 ±0.05	**0.002**	0.138
Spark Duration (FDHM)	2.27 ±0.06	2.22 ±0.07	2.28± 0.08	0.121	0.056
Spark Width (FWHM)	45.02 ±3.13	53.56 ±3.80	44.81 ±8.79	0.457	0.474

Revised TS mathematical modeling

Several studies have modeled the impact of TS on myocardial electrophysiology by using a shift in $Ca_V1.2$ VDI estimated from measurements in non-myocytes[35, 100, 101]. Using data from our TS ventricular myocyte model, a new mathematical model of TS incorporating CaMKII signaling (Figure 3-12A) was created. As the basis for a new model of TS, the Luo-Rudy dynamic model (LRd) [34, 72] was used, because of its established utility in studying cardiac arrhythmia mechanisms.

Our model of TS incorporated three modifications to match the experimental observations. First, the $Ca_V1.2$ steady-state VDI was shifted in the LRd model to simulate the measured TS defect on channel gating. Second, the downstream CaMKII effect on $Ca_V1.2$ I_{Ca} facilitation associated with TS was simulated by slowing I_{Ca} inactivation to increase integrated I_{Ca} as measured experimentally (Figure 3-13A, B). Third, the CaMKII actions on intracellular Ca^{2+} handling associated with TS was simulated by increasing the mean open time of the ryanodine receptor SR Ca^{2+} release channels, decreasing the threshold for spontaneous SR Ca^{2+} release and increasing SR Ca^{2+} release. Consistent with the experimental measurements, the new model of TS predicted an increase in the intracellular Ca^{2+} transient amplitude without any change in SR Ca^{2+} load compared to WT (Figure 3-13C). The model also predicted an increase in action potential duration (Figure 3-12B) and afterdepolarizations (Figure 3-12C) during a pause after pacing. CaMKII inhibition was simulated using the TS LRd model by reversing the simulated downstream CaMKII effects, but leaving in place the shift in $Ca_V1.2$ VDI measured under conditions not permissive for CaMKII activity

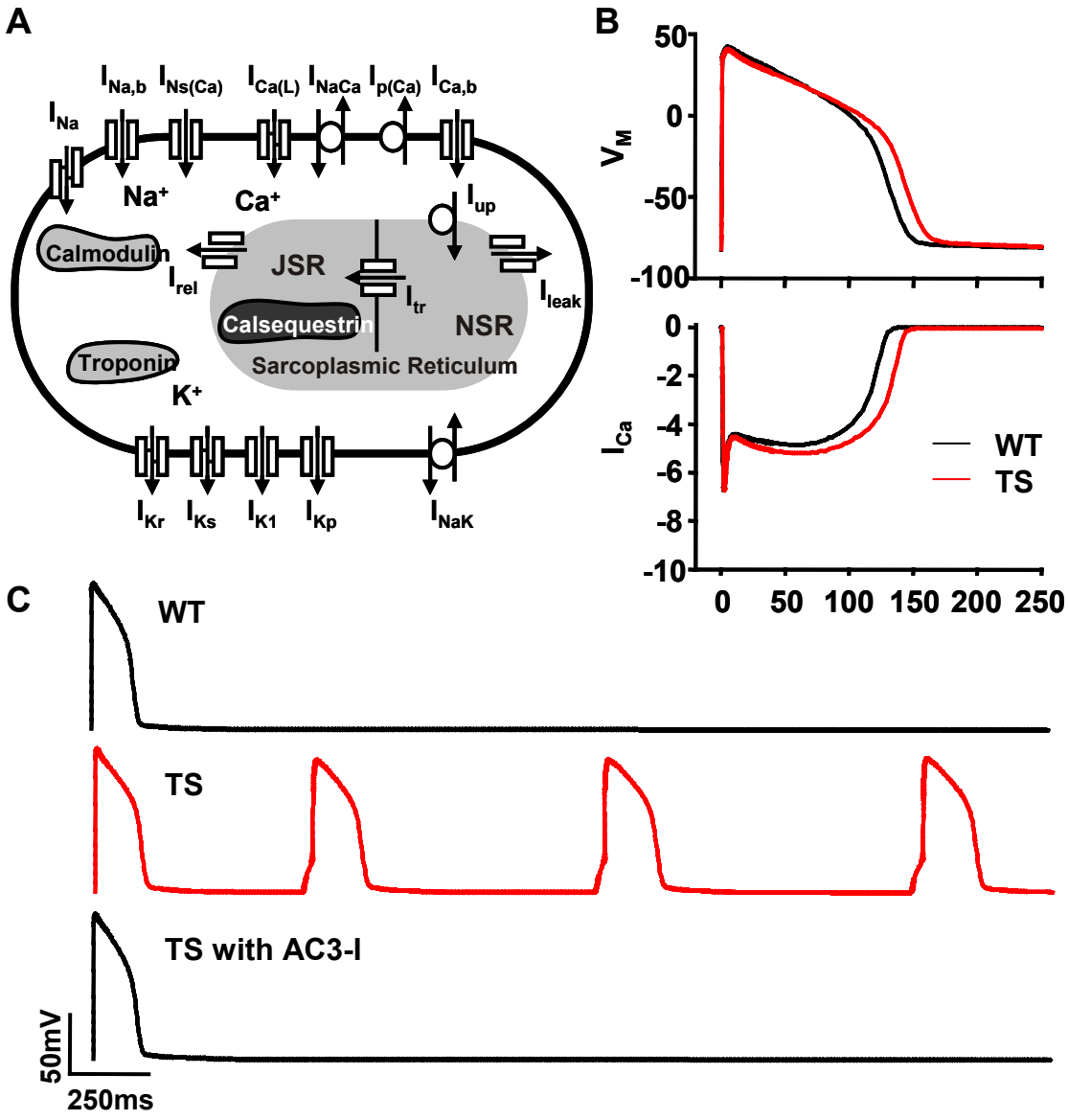

Figure 3-12: LRd modeling of WT, TS and TS with AC3-I based upon experimental data from ventricular myocytes. **A)** Schematic of LRd model. **B)** LRd model indicates CaMKII activation in TS causes increased I_{Ca} and action potential prolongation (CL = 700ms) and **C)** afterdepolarizations.

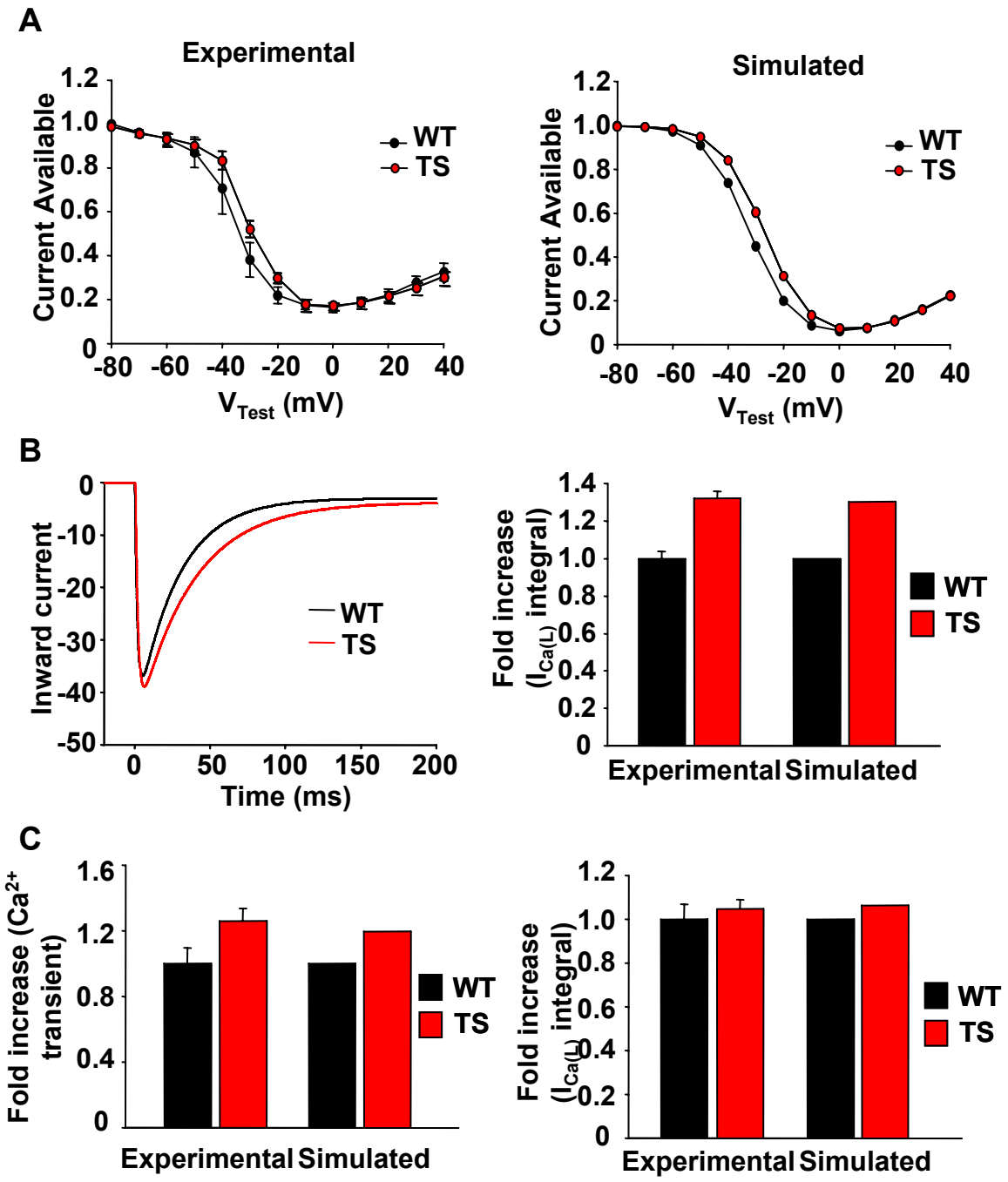

Figure 3-13: Mathematical model of WT (black) and TS (red) myocytes. **A)** Measured (*left*) and simulated (*right*) $I_{Ca(L)}$ steady-state voltage-dependent inactivation curves. **B)** Simulated $I_{Ca(L)}$ current traces during a voltage pulse to 0 mV from a holding potential of -80 mV (*left*). Measured and simulated current integrals (*right*) are determined during the pulse duration (300 ms). In simulations and experiments, Ca^{2+} was buffered with 10 mM EGTA. **C)** Measured and simulated Ca^{2+} transient amplitude (*left*) and SR Ca^{2+} content (*right*) after steady-state pacing.

(Figure 3-8A). The resulting TS LRd model with ‘CaMKII inhibition’ prevented action potential prolongation and afterdepolarizations (Figure 3-12C). These mathematical models of TS, with and without CaMKII inhibition, are consistent with experimental data from my TS ventricular myocyte model.

Discussion

TS is the first arrhythmia syndrome (LQT8) due to a genetic mutation in the $Ca_V1.2$ pore-forming α subunit [100, 101]. In comparison to cardiac Na^+ and K^+ channels, $Ca_V1.2$ has proven to be remarkably resistant to genetic disease. One key difference between Ca^{2+}, Na^+ and K^+ is the prominent role Ca^{2+} plays as a second messenger. TS patients not only have extremely profound QT interval prolongation, but also structural cardiac abnormalities, which are not typical of Na^+ or K^+ channel gene-related long QT syndrome patients. QT interval prolongation reflects increased duration of the ventricular action potential. The action potential duration prolongation in TS was attributed entirely to the defect in VDI [100], but this defect in TS VDI was ascertained in heterologous (non-myocardial) cells, where action potentials could not be directly measured. Furthermore, heterologous cells lack the highly ordered ultrastructure that is present in ventricular myocytes, for Ca^{2+} homeostasis and excitation-contraction coupling. The ventricular myocyte TS model allowed me to measure electrophysiological, intracellular Ca^{2+} handling and Ca^{2+} mediated signaling changes that occur downstream to the loss of VDI.

Despite the relatively modest reduction in $Ca_V1.2$ VDI measured in our TS model, I found action potential prolongation and spontaneous afterdepolarizations that were due to secondary activation of CaMKII. In conclusion, the shift in VDI provides the initial stimulus to trigger intracellular Ca^{2+} signaling that includes CaMKII activation. Increased CaMKII activity appears to

be necessary for the cellular phenotype of prolonged action potentials and afterdepolarizations, in so far as CaMKII inhibition prevents these phenotypes. CaMKII inhibition may be a viable alternative therapeutic approach for TS patients treated with the I_{Ca} antagonist verapamil [61]. These results showed that CaMKII amplifies Ca^{2+} entry through $Ca_V1.2$ in TS, by slowing τ_{fast}, and shifting the $V_{1/2}$ of I_{Ca} inactivation. These studies do not exclude the possibility that CaMKII inhibition could also affect other depolarizing or repolarizing currents, such as Na^+ current [105], K^+ current [67]. The findings that SR Ca^{2+} leak is increased in TS is consistent with other reports that show proarrhythmic actions of CaMKII are due to increasing SR Ca^{2+} leak [1], thereby enabling a transient inward current [116] (I_{NCX}) that triggers DADs. Thus, these data support the concept that the ryanodine receptor is a secondary proarrhythmic target for excessive CaMKII activity in TS. These data highlight how small changes in cellular Ca^{2+} entry through $Ca_V1.2$ can lead to unanticipated, maladaptive changes in Ca^{2+} activated signaling.

Interestingly a connection between CaMKII and a TS mutation was suggested based upon single channel recordings from heterologous expression of TS $Ca_V1.2$ in baby hamster kidney 6 cells [33]. These experiments found that TS $Ca_V1.2$ were more likely than WT to exhibit frequent, long openings, so called mode 2 gating that are the single channel mechanism underlying CaMKII-mediated I_{Ca} facilitation [30]. The ventricular myocytes model of TS studies add to evidence supporting a connection between TS and CaMKII by showing that CaMKII is critical for increased I_{Ca} facilitation action potential prolongation and

afterdepolarizations in our TS ventricular myocyte model. Enhanced CaMKII activity increases I_{Ca} facilitation, [17] which may cause generation of EADs [117].

Although major Ca^{2+} homeostatic proteins are conserved in ventricular myocytes across mammalian species, differences exist between species regarding the quantitative contribution of these components to the action potential [7]. Thus, one goal of future studies should be to determine if CaMKII, or other Ca^{2+}-activated signaling molecules, contribute to TS phenotypes in ventricular myocytes from other species. However, the use of the TS adult ventricular myocyte model has contributed new insights about arrhythmia mechanisms in TS, by illustrating how a concise defect in $Ca_V1.2$ gating can initiate downstream recruitment of CaMKII that ultimately enables the electrophysiological cellular disease phenotype in TS. The CNS defects of TS patients may also be due to secondary recruitment of Ca^{2+} activated signaling molecules, including CaMKII. Over-expression of CaMKII is known to interfere with neuronal growth and differentiation [76] and a constitutively active CaMKII within the mouse brain causes significantly impaired spatial memory [4]. CaMKII recruitment in TS ventricular myocytes also suggests the possibility that other disease phenotypes in TS patients (e.g. structural heart disease or mental retardation), may be initiated by defects in VDI but carried forward, indirectly, by recruitment of Ca^{2+}-dependent signaling molecules.

Methods

Cloning

The open reading frame of $Ca_V1.2$ α1c subunit (NCBI X15539) was amplified by PCR and ligated into a modified pLenti6 plasmid (Invitrogen), pLentiNB, which had the blasticidin resistance gene and promoters of the pLenti6 plasmid removed to facilitate viral packaging. An extracellular hemaglutanin epitope was added to $Ca_V1.2$ by methods previously published[2]. The dihydropyridine resistance mutation (DHP^R, T1066Y) and TS mutation (G406R) were introduced by using the PCR method Quikchange (Stratagene) as per manufacturer's protocol.

HEK293 transfection

HEK293T cells were transfected with the pLentiNB $Ca_V1.2$ WT or TS with a pIRES eGFP β_{2a} subunit using Fugene6 (Roche) as described by the manufacturer. For electrophysiology experiments, transfected HEK293T cells were detected by expression of eGFP and confirmed by inward I_{Ca}. For immunofluorescence, transfected HEK293T cells were fixed with 2% PFA and stained as described under immunofluorescence methods.

Lenti virus

The transgene plasmid pLentiNB carrying the modified $Ca_V1.2$ was transfected (Qiagen, Effectene) with the Lenti viral packaging plasmids (Invitrogen's pLP1, pLP2 and pVSVG) into HEK293FT cells (Invitrogen). Media was collected and replaced at 24, 48 and 72 hours post-transfection. The viral containing media was concentrated by either ultrafiltration (Millipore Centricon Plus-70 30kDa) or ultacentrifugation. Viral titer (transducing units per mL, TU/mL) was determined by serial dilution (10^{-3}, 10^{-4}, 10^{-5}, 10^{-6}, 10^{-7}, no virus) on HEK293 cells followed by immuno-staining (see Immunoflourescence methods) for the $Ca_V1.2$ HA epitope (anti-HA conjugated Alexa 488 Ig) and counting positively stained cells within each dilution. Viral titers achieved were between 10^5 and 10^6 TU/mL. Extracts from HEK293 cells used to produce virus were analyzed by SDS-PAGE and immunoblotting with an affinity-purified HA Ig.

Ventricular myocyte isolation, culturing and viral transduction

Adult male Sprague-Dawley rats (250-300g) were anesthetized by Avertin (2.5%) with Heparin (55 units/mL) through IP injection (0.2mL/10g). Hearts were excised, perfused retro-aortically (Langendorff) and enzymatically digested with a mixture of Collogenase (Worthington, 250 units/mL), Hyaluronidase (Sigma, 0.01%) and Protease Type XIV (Sigma, 0.0025%) in a modified tyrodes solution (0.1mM $CaCl_2$, 10mM BDM). Dissociated cardiomyocytes were washed three times in Joklik MEM (Sigma M0518) with 1% Pen/Strep and 1X ITS (Sigma) with increasing Ca^{2+} (0.25mM, 0.5mM, 0.75mM). Ventricular myocytes were plated on

glass cover slips (glass #1) coated with Geltrex (Invitrogen, thin layer) and allowed to attach for 1 hour. Cells were washed with a culture media consisting of a 50:50 mix of DMEM and F10 media with 1% Pen/Strep and 1X ITS. Attached cardiomyocytes were counted and the cell density was calculated. Lenti virus was added to the cells at a multiplicity of infection (MOI) of 1-3, and cells cultures were maintained for 24-36 hours. Cultured ventricular myocytes (WT, TS, uninfected) extracts were analyzed by SDS-PAGE and immuno-blotting with a $Ca_V1.2$ Ig (ABR).

Electrophysiology

HEK293 I_{Ca} recordings for voltage dependence of inactivation (VDI) used a two step voltage clamp protocol (repeated 0.1 Hz, resting -80mV, 25°C) with an initial conditioning step (0.8s, -50mV to +60mV, Δ10mV) followed by a test pulse (300ms, +30mV). Bath solution was in mM; 130 NMDG, 10 HEPES, 5 KCl, 15 $CaCl_2$. Pipette solution was in mM; 120 Cs methanesulfonate, 5 $CaCl_2$, 1 $MgCl_2$, 2 MgATP, 10 HEPES, 10 EGTA. Available current observed each test pulse after a given conditioning pulse was accessed a percent of the maximum current observed.

Cardiomyoycte action potentials (AP) were stimulated (2ms, 1.5-2.5nA) in current clamp mode (0.5Hz, 25°C). Bath solution was in mM; 140 NaCl, 4 HEPES, 10 Glucose, 5.4 KCl, 1.8 $CaCl_2$, 1 $MgCl_2$. Pipette solution was in mM; 120 K aspartate, 5 HEPES, 25 KCl, 4 Na_2ATP, 1 $MgCl_2$, 10 EGTA, 2 Na_2 phosphocreatine, 1 $CaCl_2$, 2 NaGTP. Recorded APs were analyzed using

ClampFit's (Axon Instruments) event detection algorithm and statistics decay time (ms) algorithm.

Cardiomoycte I_{Ba} recordings for VDI used a two step voltage clamp protocol (repeated 0.1 Hz, resting -80mV, 25°C) with an initial conditioning pulse (2.0s, -80mV to +30mV, Δ10mV) followed by a test pulse (300ms, 0mV). To record only VDI and prevent Ca^{2+} dependent inactivation, Ca^{2+} was tightly buffered through the use of Ba^{2+} as the charge carrier in the bath solution and BAPTA with no Ca^{2+} in the pipette solution. Bath solution was in mM; 137 NMDG, 10 HEPES, 10 Glucose, 1.8 $BaCl_2$, 0.5 $MgCl_2$, 25 CsCl. Pipette solution was in mM; 120 CsCl, 10 TEA, 1 MgATP, 1 NaGTP, 5 phosphocreatine, 10 HEPES, 20 BAPTA. Available current observed each test pulse after a given conditioning pulse was accessed a percent of the maximum current observed.

Cardiomyocyte I_{Ca} facilitation was recorded using a single step (300ms, 0mV) voltage clamp protocol (repeated 0.5Hz, resting -80mV, 25°C). Bath solution was in mM; 137 NMDG, 10 HEPES, 10 Glucose, 1.8 $CaCl_2$, 0.5 $MgCl_2$, 25 CsCl. Pipette solution was in mM; 120 CsCl, 3 $CaCl_2$, 10 TEA, 1 MgATP, 1 NaGTP, 5 phosphocreatine, 10 HEPES, 10 EGTA. I_{Ca} facilitation was integrated using ClampFit's area statistics (pA*ms) algorithm and normalized to cell size (pF). Inactivation time constants were calculated using ClampFit.

Immunoflourescence

HEK293 cells, cultured on coverslips (glass #1), were gently washed with PBS and fixed for 20 minutes in 2% paraformaldyhyde (25°C). Cultured adult

ventricular myocytes (WT, TS and uninfected) were paced by field stimulation (Ion Optix C-pace and C-dish, 1Hz, 35V, 2ms) for 5 minutes in Tyrodes (1.8mM $CaCl_2$, 37°C). Immediately following the pacing protocol, ventricular myocytes were fixed for 20 minutes in 2% parafomaldyhyde (25°C). Fixed cells were permeabilized for 10 minutes with PBS with 0.1% Triton X-100, 2 mg/mL BSA and 2% fish gelatin. Permeabilized cells were blocked with PBS with 2 mg/mL BSA and 2% fish gelatin. Cells were incubated overnight (4°C) in one of the following; anti-HA conjugated Alexa 488 Ig (Molecular Probes), HA Ig (Santa Cruz), pCaMKII Thr^{286} Ig (ABR), CaMKII Ig (Bers Lab) and washed. The cells incubated with HA Ig were then incubated in donkey anti-rabbit Alexa 488 Ig (Molecular Probes) at 4°C. Cells incubated with pCamKII Thr286 Ig were then incubated in donkey anti-mouse 568 (Molecular Probes). Cells incubated with CaMKII Ig were then incubated in donkey anti-rabbit 568 (Molecular Probes). Ventricular myocytes were mounted with glass coverslips and Vectashield (with or without DAPI; Vector Laboratories).

Ventricular myocyte images were collected on a Zeiss 510 Meta confocal microscope (Carl Zeiss), under 40x magnification (oil, 1.30 NA lens), with a pinhole of 1.0 airy disc (Carl Zeiss), using the Zeiss image acquisition software. HEK293 images were taken at 40x magnification using both the FITC filter and DAPI filter. All images were exported to Photoshop (Adobe) for cropping and linear adjustment of contrast.

Ca^{2+} imaging

Ventricular myocytes were loaded with Fluo-3 AM (5μM) for 20 minutes at room temperature. After 20 minutes of de-esterification, the cells were placed on recording chamber, and perfused with normal Tyrode solution (1.8 mM Ca^{2+}). Confocal Ca^{2+} imaging was performed with a laser scanning confocal microscope (LSM 510 Meta, Carl Zeiss) equipped with a NA=1.35, 63x lens. Line scan measurement of Ca^{2+} transients, SR content and sparks were all acquired at a sampling rate of 1.93 ms per line along the longitudinal axis of the myocytes. Sparks were measured under resting conditions. Steady state Ca^{2+} transients were achieved by a 30 sec pacing at 1 Hz. SR Ca^{2+} content was measured as a global Ca^{2+} release induced by 10mM caffeine exposure. All digital images were processed offline with IDL 6.0 (Research System Inc.).

Statistics

Data presented as means with SEM. Sigma Stat was used to compare two groups with a Student T-test and multiple groups with an ANOVA. Significance was set at a p value < 0.05. Categorical data between two groups was compared using a 2-tailed Fisher Exact Test with significance set at $P<0.05$.

Mathematical modeling

Mathematical models of the WT and TS myocytes are based on the Luo-Rudy dynamic model of the mammalian ventricular action potential[34, 72]. For this study, a revised formulation was incorporated for Ca^{2+} release from the

Equations

Revised formulation for I_{rel}

$$I_{Rel} = O \cdot \left([Ca^{2+}]_{Jsr} - [Ca^{2+}]_{SS}\right);$$

Where

$$\frac{dO}{dt} = -\frac{O_\infty + O}{\tau_{Irel}};$$

and

$$O_\infty = \frac{\alpha_{Rel} \cdot I_{Ca(L)}}{1 + \left(K_{Rel,\infty}/[Ca^{2+}]_{JSR}\right)^{h_{Rel}}};$$

All other parameters and equations for I_{rel} are same as in original model published by Livshitz and Rudy.

Ca^{2+} release of JSR under Ca^{2+}-overload conditions.

If buffered [csqn] > $[csqn]_{th}$

$$O = O_\infty = 6.0;$$

$$\tau_{Irel} = 10.0;$$

Where $[csqn]_{th}$ = 7.0 as in original Luo-Rudy dynamic cell model.

Nonspecific Ca^{2+}-activated current

The nonspecific Ca^{2+}-activated current was used according to the formulation in the original Luo-Rudy cell model with a reduced permeability.

$$P_{Ns(Ca)} = 1.0 \times 10^{-7}\, cm/s;$$

Mathematical model of TS action potential

L-type Ca^{2+} current

To simulate the effects of the Timothy Syndrome mutation on $I_{Ca(L)}$ channel gating, the following equation was used for steady-state voltage dependent inactivation:

$$f_\infty = \frac{1}{1 + \exp\left(\frac{V_m + 28.86}{8.0}\right)} + \frac{0.6}{1 + \exp\left(\frac{50.0 - V_m}{20.0}\right)};$$

To simulate the CaMKII-dependent effects on $I_{Ca(L)}$ facilitation, the following equation was used for the time constant of voltage-dependent inactivation:

$$\tau_f = \frac{1.35}{0.0197 \cdot \exp\left(-0.0337 \cdot (V_m + 10.0)^2\right) + 0.02};$$

Ca^{2+} leak from the SR

Increased leak from the SR due to CaMKII was simulated by increasing the conductance of I_{leak}.

sarcoplasmic reticulum and regulation by CaMKII based on the model of Livshitz and Rudy [69]. This model of SR Ca^{2+} release includes a formulation for spontaneous Ca^{2+} release from the sarcoplasmic reticulum, which occurs when the amount of Ca^{2+} bound to calsequestrin reaches threshold, as described in the original LRd model. Cells were paced to steady-state (over 15 min. pacing) at a cycle length of 700 ms using a conservative current stimulus [59]. Afterdepolarization events were monitored during a pause following steady-state pacing. Ordinary differential equations in the model were integrated numerically using the Forward Euler Method and an adaptive time step. Details on the mathematics involved in the model can be found in the Equations Section.

IV. SYNOPSIS AND FUTURE DIRECTION OF TS VENTRICULAR MYOCYTE MODEL

Implications of TS Mathematical Modeling

The initial observation of the TS mutation in heterologous cells found a loss of VDI. This loss of VDI was used in a mathematical model of a ventricular myocyte to make predictions on how this mutation would affect myocyte physiology. However, this mathematical model of TS was never tested experimentally until I developed my adult ventricular myocyte model of TS. The original modeling proved very helpful in guiding my experimental design in determining what experiments were necessary to undertake in a ventricular model of TS. The mathematical model proved helpful in interpreting our results, especially when our experimental data did not correspond with the model's predictions. Such as, we may not have examined the intracellular Ca^{2+} handling as extensively had we not had the predictions from original TS model for comparison. The initial model predicted an overload of SR Ca^{2+} and enhanced Ca^{2+} transients. Only after we observed an enhanced Ca^{2+} transient with no change in SR Ca^{2+} content did we examine spontaneous SR Ca^{2+} release. After we observed the increase in spontaneous SR Ca^{2+} release, we understood how to revise a future version of the mathematical model of TS.

The data we collected from adult TS ventricular myocytes included action potential recordings, VDI curves, I_{Ca} facilitation, Ca^{2+} transients, SR Ca^{2+} content

and spontaneous SR Ca^{2+} release. We observed changes in nearly all of these aspects of myocyte physiology. This highlights the complexity of ventricular myocyte physiology. Mathematical modeling presents an opportunity to integrate all of these data into one system where they may be analyzed collectively. Our TS mathematical model incorporated all of the experimental data including the shift in VDI, change in I_{Ca} facilitation and augmentation of intracellular Ca^{2+} handling. We found experimentally a prolongation of the action potential and DADs and our revised mathematical model of TS also showed prolonged action potentials and DADs. However, the action potential prolongation predicted in our mathematical model of TS does not correspond with the degree of action potential prolongation we observed experimentally. Two possible explanations could account for the discrepancy between the experimental data and our mathematical model. First, we may have incorrectly incorporated experimental observations into the mathematical model of TS. Second, our experiments may not have accounted all of the possible downstream affects of the TS mutation. Many of our experiments use conditions that are significantly different to those the mathematical model requires. Therefore, translating the experimental observations into the mathematical model must be done cautiously to avoid misrepresentation of the data. Perhaps with our mathematical model of TS we were too captious in extrapolating the experimental data into the mathematical model. More likely is the second explanation that the TS mutation has more widespread consequences than we measured experimentally. These could include alterations of additional ion channels that prolong the action potential due

to activation of CaMKII. We would be able to use the mathematical model and published data to better hypothesize as to which ion channels may also be affected by activated CaMKII in TS ventricular myocytes. We would then be able to test experimentally these new hypotheses and incorporate any new observations into the next revision of the mathematical model of TS.

Downstream CaMKII Phosphorylation in the TS Ventricular Myocyte Model

Our data indicates that the TS mutation leads to the activation of CaMKII and we observed many physiological changes in an adult ventricular myocyte that correspond with enhanced CaMKII activity. These include enhanced I_{Ca} facilitation, increased Ca^{2+} transient peak amplitude, faster Ca^{2+} transient decay time and increased spontaneous SR Ca^{2+} release. If our observations are associated with CaMKII activation each of these affects would correspond with phosphorylation events of involved proteins. I_{Ca} facilitation has been associated with Thr498 phosphorylation of the β_{2a} subunit of $Ca_V1.2$. However, $Ca_V1.2$ is known to be phosphorylated by CaMKII directly at Ser1512, Ser1570, Ser1922 (Chapter V) and Ser1928 (Chapter V). The increased peak Ca^{2+} transient and enhanced SR Ca^{2+} leak may be caused CaMKII phosphorylation of RYR at Ser2809 or Ser2814. A potential future direction would be to further investigate these substrates of CaMKII in TS ventricular myocytes. Faster Ca^{2+} transient decay times may be due to CaMKII phosphorylation of Thr17 on PLB that has been associated with enhanced SERCA activity. All of these CaMKII

phosphorylation events could be investigated to gain a better understanding into the downstream affects of the TS mutation.

Response of TS ventricular myocytes to adrenergic signaling

The TS $Ca_V1.2$ disrupts Ca^{2+} handling involved in excitation contraction coupling by activating CaMKII. During adrenergic stimulation PKA enhances the activity of many of the proteins we believe are phosphorylated by CaMKII in TS ventricular myocytes. The published articles on TS patients suggest more sever arrhythmias during situations of increased adrenergic stimulation. Many of the patients appear to have experienced their worst arrhythmias or cardiac arrest while at play [101]. One child had his first cardiac arrest (4 years old) while climbing onto a trampoline [100]. The same child (11years old) has severe cardiac arrhythmias once a week associated with night terrors while sleeping [100]. Another TS patient (21 years old) also has episodes of ventricular fibrillation preceded or during night terrors while sleeping [61]. Together these observations suggest adrenergic stimulation worsens the phenotype of TS. In future studies we would hypothesize that adrenergic signaling would exacerbate the TS pro-arrhythmic phenotype in ventricular myocytes. Our TS ventricular myocyte model would allow this hypothesis to be tested by measuring action potentials and intracellular Ca^{2+} handling following adrenergic stimulation.

Using a CaMKII small molecule inhibitor as a therapeutic agent to treat TS.

Current treatment for TS includes $Ca_V1.2$ antagonists such as Verapamil [61] and ICDs [61, 100, 101], both treatments help but neither reverses the TS phenotype like CaMKII inhibition did in the ventricular myocyte model of TS. Implantation of ICDs has been the most successful treatment for TS patients, but has had complications. Many of the TS patients require the ICD to pace the atrium because direct pacing of the ventricle triggered Torsades de Pointes [100]. The pharmacological treatment using a $Ca_V1.2$ antagonist improves TS patients by reducing the number of ICD shocks. However, TS patients still receive many ICD shocks and therefore there is room for improvement.

My experiments on a ventricular myocyte model of TS found that active CaMKII was responsible for the pro-arrhythmic defects. I also found that higher concentrations of the $Ca_V1.2$ antagonist, nifedipine, rescued that action potential duration and afterdepolarizations. I believe that in my experiments with high concentrations of nifedipine that enough I_{Ca} was blocked to prevent CaMKII activation. I would assume that verapamil improves TS patients by also reducing the amount of CaMKII activation. Therefore, I believe a direct inhibition of CaMKII, as opposed to indirect inhibition attained with verapamil, would yield better results in TS patients. However, an ICD may still be advisable as the long term effects of CaMKII inhibition in people remains un-studied.

CaMKII is known to have a very important role in the brain for memory. Therefore, inhibition of CaMKII could have adverse side effects associated with memory loss. However, any side effects observed from CaMKII inhibition in the

CNS would have to be balanced against the benefit of treating the life-threatening arrhythmias. The brain is protected by the blood-brain barrier and a CaMKII inhibitor may not cross this barrier or it may be altered to not cross this barrier. Furthermore, many of the adverse phenotypes associated with TS are related to defects in the brain. Potentially, inhibition of CaMKII may lessen the impact of some of these phenotypes. However, the brain, unlike the heart, requires a complex network of electrically excitable neurons that develop early in life. For TS patients the damage may already be complete after development of the brain. Additionally, other Ca^{2+} dependent signaling pathways adversely activated by the TS mutation of $Ca_V1.2$ may be responsible for the CNS defects and not CaMKII. Therefore, inhibition of CaMKII would do nothing. To better asses the impact of inhibition CaMKII for TS patients the TS $Ca_V1.2$ mutation must be studied in the context of neurons as we have done in ventricular myocytes.

CHAPTER IV

CAMKII REGULATION OF CAV1.2

Introduction

$Ca_V1.2$ I_{Ca} is regulated by many different proteins (Figure 4-1A) involved in adrenergic signaling, such as PKA, AKAP and CaMKII. CaMKII is known to dynamically affect the I_{Ca} of $Ca_V1.2$. While pacing cardiomyocytes the peak I_{Ca} increases and the $Ca_V1.2$ inactivation kinetics become slower (Figure 4-1B). These properties are collectively called I_{Ca} facilitation [3, 123]. Facilitation of wild type $Ca_V1.2$ occurs in cardiomyocytes, at least in part because facilitation requires SR Ca2+ release [113, 115]. CaMKII is also required for facilitation, because dialyzing a CaMKII inhibitory peptide (AC3-I) into cardiomyocytes prevents facilitation [30, 113].

Several lines of evidence indicate that CaMKII may phosphorylate the C-terminus of $Ca_V1.2$. CaMKII has already been shown to phosphorylate the β_{2a} subunit and CaMKII is known to phosphorylate the closely $Ca_V1.2$ related skeletal Ca^{2+} channel α1s ($Ca_V1.1$) [16]. CaMKII and PKA effects on $Ca_V1.2$ I_{Ca} parallel each other, and CaMKII activity is important for a full β-adrenergic response in the heart [126]. β-adrenergic adrenergic stimulation leads to an increase in intracellular Ca^{2+}, which activates CaMKII. The activated CaMKII phosphorylates target proteins required for complete myocardial responses to β-adrenergic stimulation. In cardiomyocytes the targets of PKA and CaMKII have

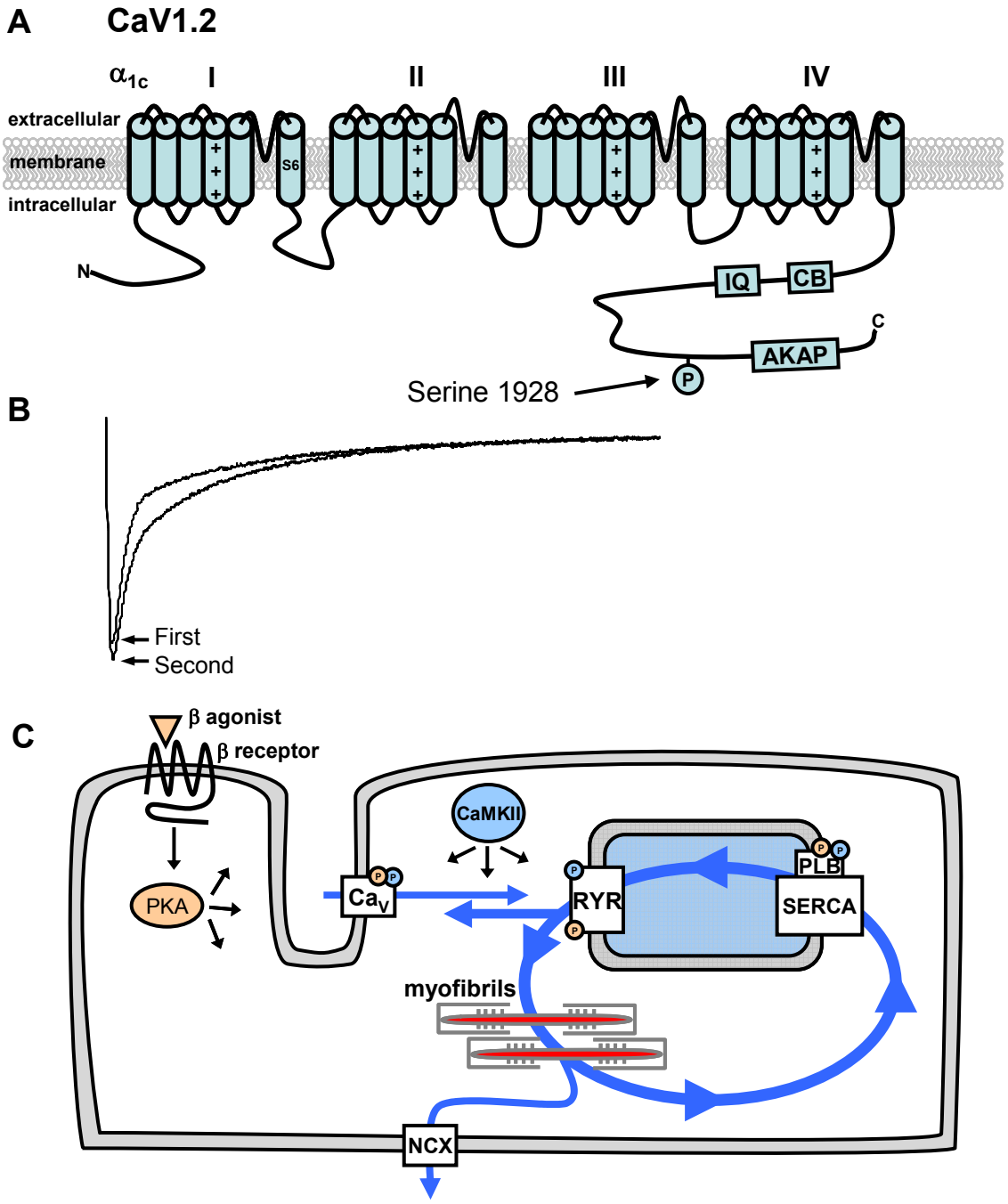

Figure 4-1: A) Schematic of $Ca_V1.2$ highlighting the PKA and PKC phosphorylation site serine 1928. **B)** $Ca_V1.2$ I_{Ca} facilitation is a CaMKII dependent property. **C)** Adrenergic signaling requires both PKA and CaMKII phosphorylation.

striking overlap and include RYR, PLB and $Ca_V1.2$ [30, 70, 103] (Figure 4-1C) Both PKA and CaMKII similarly increases the opening probability (P_O) of $Ca_V1.2$ [31]. When either PKA or CaMKII are added to an excised patch the Po of $Ca_V1.2$ increases dramatically [31]. The C-terminus of $Ca_V1.2$ is already known to be a substrate for kinases: both PKC [121] and PKA [23] phosphorylate serine 1928 of the $Ca_V1.2$ C-terminus (Figure 4-1A). This suggests that the $Ca_V1.2$ C-terminus may be a substrate for additional kinases. Together, these data point towards the $Ca_V1.2$ C-terminus as a CaMKII substrate for phosphorylation. However, the specific sites of CaMKII phosphorylation on the $Ca_V1.2$ C-terminus are not fully characterized. ***I hypothesized that CaMKII phosphorylates the C-terminus of $Ca_V1.2$.*** To address this hypothesis the C-terminus of $Ca_V1.2$ will be assessed as a substrate for CaMKII.

Results

$Ca_V1.2$ C-terminus is a CaMKII substrate

In vitro kinase assays of $Ca_V1.2$ C-terminus found that the $Ca_V1.2$ C-terminus was a substrate for CaMKII phosphorylation. GST was fused with $Ca_V1.2$ at the proximal end of the $Ca_V1.2$ C-terminus. The $Ca_V1.2$-GST fusion protein was purified using glutathione agarose beads. Following purification, the fusion protein's expression and size were confirmed by immuno-blot with an anti GST Ig. The purified GST-$Ca_V1.2$ C-terminus protein was assayed for CaMKII (100 nM) phosphorylation by *in vitro* kinase assay. The kinase assays allows for the detection of ^{32}Phosphate incorporation into a substrate from a resulting phosphorylation event. Phosphorylation by CaMKII of the $Ca_V1.2$ C-terminus was assayed by autoradiography (Figure 4-2A).

As a negative control purified GST, which is not a substrate for CaMKII, was shown to not be phosphorylated by CaMKII in the *in vitro* kinase assay (Figure 4-2A). Autophosphorylation of CaMKII was observed on the SDS-PAGE autoradiograph (Figure 4-2A) and confirms the activation of CaMKII during the kinase assay. PKA (100 nM) phosphorylation of the $Ca_V1.2$ C-terminus (Figure 4-2C) confirmed that the GST fusion protein was still able to interact as a substrate with a kinase known to phosphorylate the $Ca_V1.2$ C-terminus.

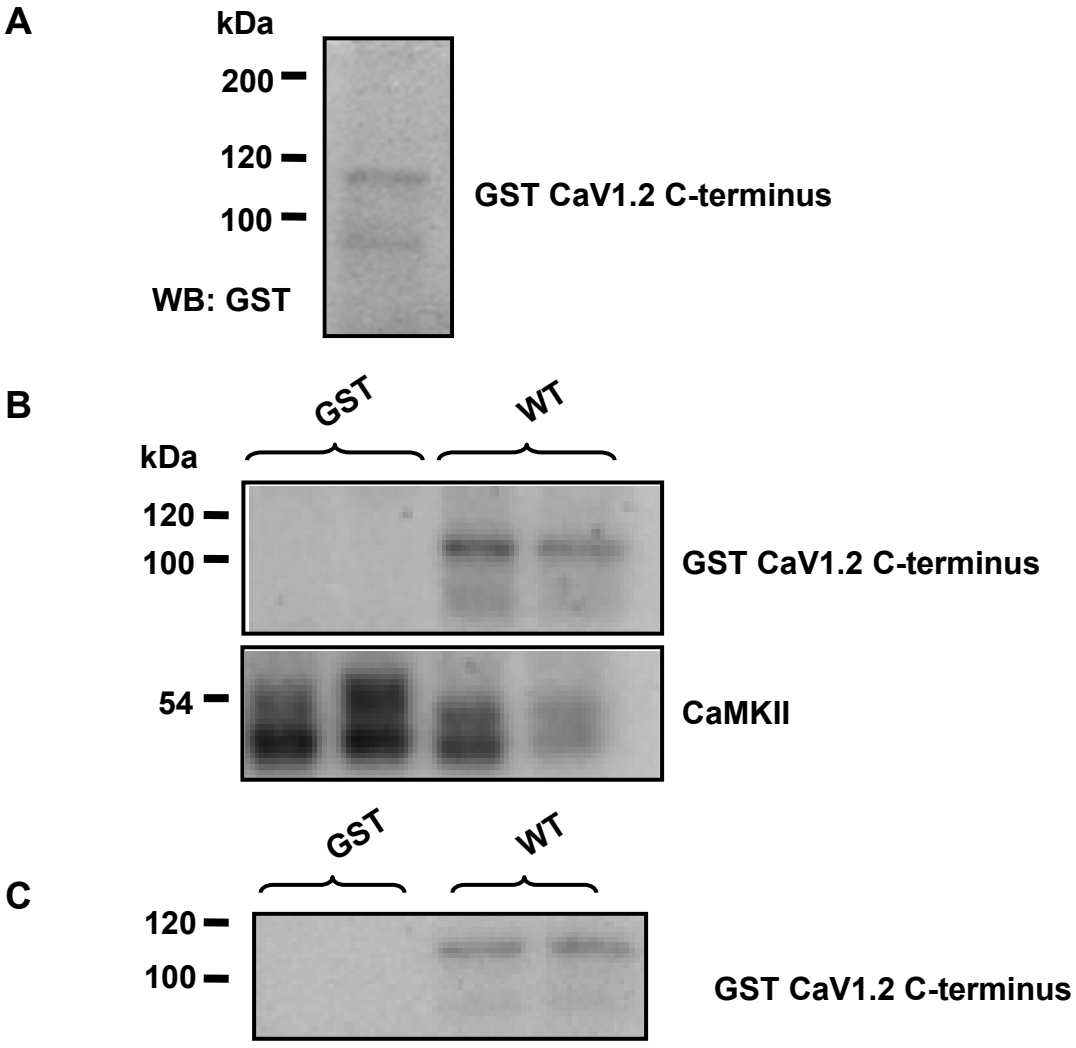

Figure 4-2: CaMKII phosphorylates the Cav1.2 C-terminus **A)** Western blot with anti-GST for CaV1.2 C-terminus GST fusion protein **B)** CaMKII *in vitro* kinase assay autoradiograph; **(top)** GST-CaV1.2 C-terminus fusion protein (WT) ^{32}P incorporation; **(bottom)** CaMKII autophosphorylation. **C)** PKA *in vitro* kinase assay autradiograph.

CaMKII phosphorylates the distal carboxy terminus of $Ca_V1.2$

Smaller portions of the $Ca_V1.2$ C-terminus were examined to refine the identification of the CaMKII phosphorylation sites. Isolation of $Ca_V1.2$ from native

tissue has suggested that the C-terminus of $Ca_V1.2$ is cleaved into two separate proteins [22, 24, 57]. The portion still associated with the channel is the proximal C-terminus (PCT) and the cleaved portion is the distal C-terminus (DCT) [57, 58] (Figure 4-3). Previous data predicted the cleavage point to be around residue 1909 (Figure 4-3) [14]. Recent work indicates that the cleavage point may be around residue 1803 [57] (Figure 4-3). Unfortunately, the specific protease has not been identified and therefore the cleavage point has not been fully characterized. The DCT was created as a GST fusion protein from residues 1909 through 2171 with GST fused on the carboxy end of the DCT.

Figure 4-3: Multiple sequence alignment between rabbit CaV1.2 C-terminus, used in experiments, and human CaV1.2 C-terminus. Gray shaded area indicates the proximal C-terminus (PCT). Blue shaded area indicates the distal C-terminus (DCT). The lighter blue represents the predicted DCT of residues 1909-2171. The darker blue represents current data on DCT, residues 1803-2171, and the dashed line is the believed cleavage site between the PCT and DCT. Green highlighted seqeunce are CaMKII predicted phosphorylation sites. (*) Marks the PKA and PKC phosphorylation site at serine 1928. Solid black line is the location that AKAP79 binds the CaV1.2 DCT.

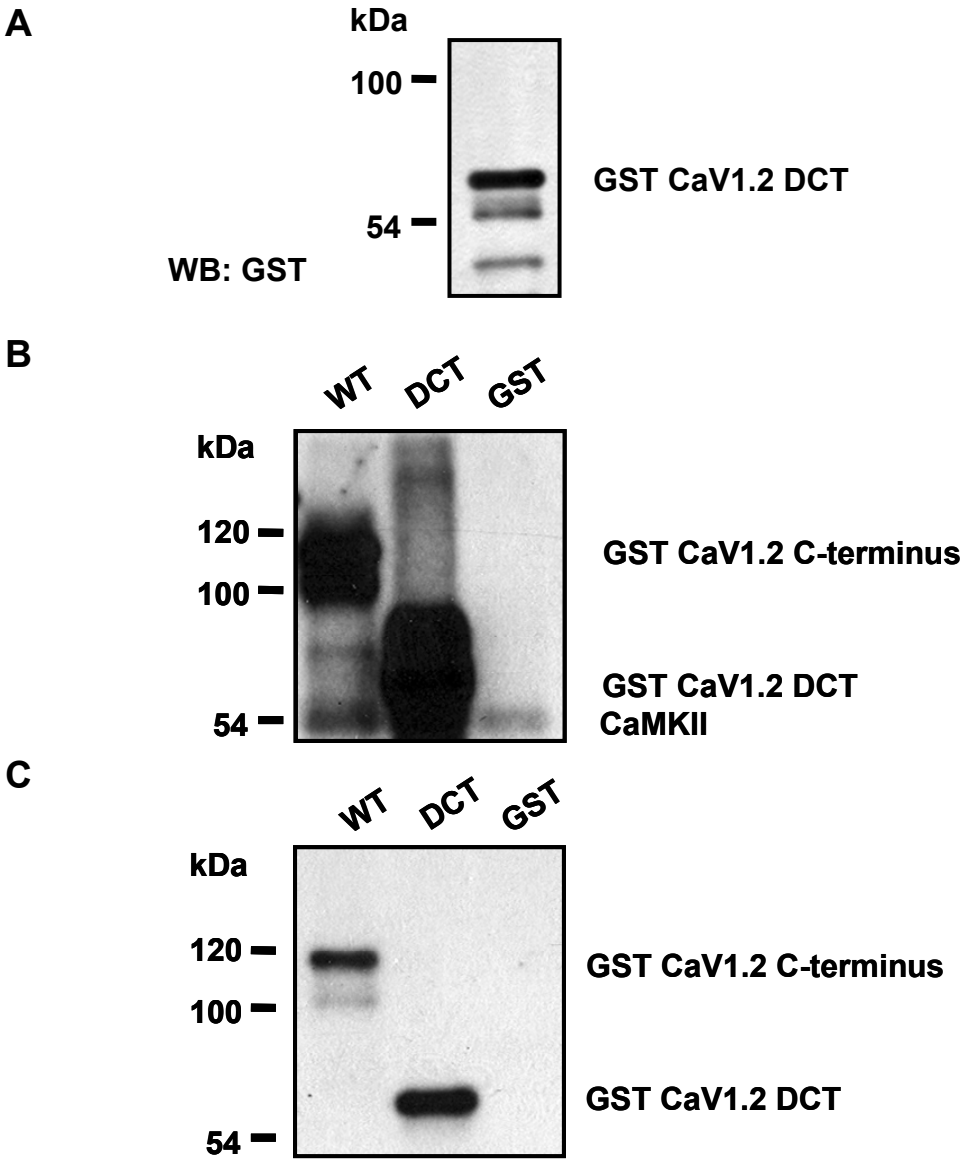

Figure 4-4: CaMKII phosphorylates the CaV1.2 distal C-terminus **A)** Western blot with anti-GST for purified CaV1.2 distal C-terminus (DCT) GST fusion protein **B)** CaMKII *in vitro* kinase assays of CaV1.2 C-terminus GST fusion protein (WT), CaV1.2 distal C-terminus GST fusion protein (DCT) and GST alone (GST) **C)** PKA *in vitro* kinase assay of WT, DCT and GST.

Sequence analysis of the $Ca_V1.2$ DCT (Figure 4-3) indicates that it would be a likely CaMKII substrate. The DCT not only contains several predicted CaMKII phosphorylation sites, but also is a focal point for kinase activity. The serine at position 1928 is known to be phosphorylated by both PKA [23, 89] and PKC [121]. Furthermore, a region of the DCT has been shown to bind an AKAP [40] that is known to associate with phosphatases that are necessary to reverse kinase mediated phosphorylation.

The $Ca_V1.2$ DCT GST fusion protein was purified with glutathione agarose beads and the protein size and expression was confirmed by western blot for GST (Figure 4-4A). *In vitro* kinase assays with CaMKII were repeated as with the $Ca_V1.2$ C-terminus GST fusion protein. The resulting autoradiograph indicates that the $Ca_V1.2$ DCT was a substrate for CaMKII phosphorylation (Figure 4-4B). As a positive control, the $Ca_V1.2$ DCT was shown to also be substrate for PKA (Figure 4-4C). The CaMKII and PKA kinase assays of the $Ca_V1.2$ C-terminus GST fusion protein were repeated as an additional positive control (Figure 4-4B, C). The autoradiograph indicates that the $Ca_V1.2$ DCT is as good or better substrate for CaMKII than the $Ca_V1.2$ C-teminus. GST was used in both CaMKII and PKA kinase assays as a negative control (Figure 4-4B, C) and was not phosphorylated by either CaMKII or PKA.

Phospho-amino acid analysis indicates a serine phosphorylation event

A phospho-amino acid analysis of $Ca_V1.2$ DCT would identify if the phosphorylation event by CaMKII was on a threonine, serine or both. The

phospho-amino acid analysis allows the separation of individual residues after hydrolysis of the peptide bonds. Phosphorylated residues can be detected by autoradiograph because of incorporation of ^{32}P from an *in vitro* kinase assay preceding the hydrolysis step. Therefore the $Ca_V1.2$ DCT was first phosphorylated by CaMKII *in vitro* and then hydrolysed. The resulting autoradiograph of the hydrolysed $Ca_V1.2$ DCT revealed three bands (Figure 4-5).

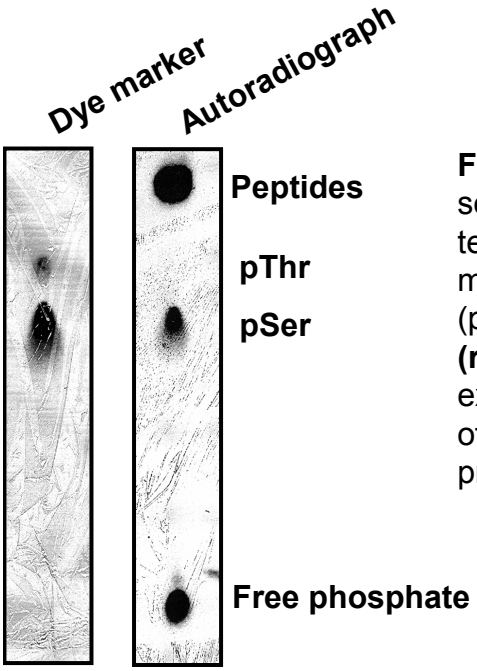

Figure 4-5: CaMKII phosphorylates a serine residue on CaV1.2 distal C-terminus. **(left)** Autoradiography of marker dye indicating phospho serine (pSer) and phospho threonine (pThr) **(right)** Autoradiograph (89 hour exposure) phospho-amino acid analysis of CaV1.2 distal C-terminus GST fusion protein.

To determine the identity of phosphorylated residues, bands found in the autoradiograph were compared to a positive control dye standard of phospho-residues. The dye standard indicates where phospho-serine and phospho-threonine would migrate. Phospho-tyrosine was omitted because CaMKII is a

serine/threonine kinase. The dye standard reveals that the CaMKII phosphorylation of $Ca_V1.2$ DCT occurs on at least one serine and not on any threonine residues (Figure 4-5).

Aside from phosphorylated residues appearing on the autoradiograph, two additional bands are present. Because hydrolysis is both incomplete and random, one band should indicate free phosphate and a second band should be unhydrolysed phosphorylated peptides.

Mass spectrometry identified several phosphorylation events

Mass spectrometry was used to identify the amino acids being phosphorylated on the $Ca_V1.2$ C-terminus GST fusion protein by CaMKII. The $Ca_V1.2$ C-terminus GST fusion protein was phosphorylated with CaMKII using either ^{32}P ATP or unlabeled ATP. The *in vitro* kinase assay with ^{32}P ATP confirmed, by autoradiograph, CaMKII phosphorylation of the $Ca_V1.2$ C-terminus. Incubating the unlabeled ATP *in vitro* kinase assay with glutathione agarose beads, the $Ca_V1.2$ C-terminus GST fusion protein was re-purified. This sample was submitted for mass spectrometry analysis by liquid chromatography MS-MS after proteolytic digestion by either trypsin or chymostrypsin, which were used to achieve a higher degree of coverage in order to identify all potential phosphorylation sites.

Analysis of the mass spectrometry data, trypsin and chymotrypsin, identified several peptides with possible phosphorylation events (Table 4-1, 4-2). The mass spectrometry data was examined for possible phosphorylation events

by identifying either a positive 80 dalton shift in mass (Table 4-1, 4-2), the addition of a phosphate group, or a negative 18 dalton shift in mass (Table 4-1, 4-2), the net mass reduction of a hydroxyl group after the loss of a phosphate group during MS-MS fragmentation. Data mining revealed two peptides with phosphorylated serines, the peptide SASLGR with serine 1922 (Figure 4-6) and the peptide ASFHLECLK with serine 1928 (Figure 4-6).

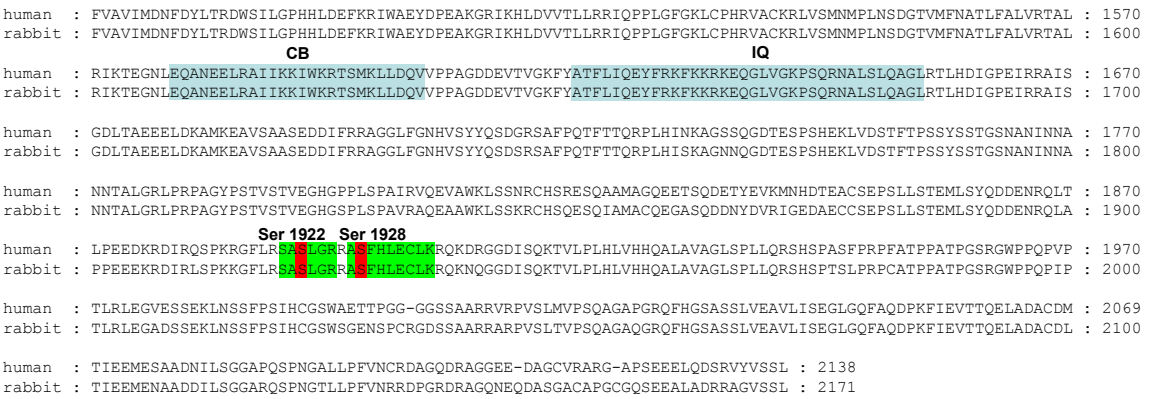

Figure 4-6: Multiple sequence alignment between rabbit CaV1.2 C-terminus, used in experiments, and human CaV1.2 C-terminus. Blue area highlights CaM binding domains. Green shows peptides identified by mass spectrometry with red indicating the residues found to be phosphorylated by CaMKII.

Table 4-1: LC-MS-MS trypsin digestion results

Peptide	P value	M/Z measured	# MS	M/Z predicted	Shift	Position	Spectra #
GWPPQPIPTLR	0.0274	671.58	2	1260.7	80.4	9	4245
NQGGDISQK	0.0227	513.98	2	945.5	80.5	6	3093
NQGGDISQK	0.0147	514.09	2	945.5	80.7	6	3788
NQGGDISQK	0.0234	514.1	2	945.5	80.7	7	3230
NQGGDISQK	0.0072	514.13	2	945.5	80.7	6	3578
NQGGDISQK	0.0205	514.16	2	945.5	80.8	6	4804
SHSPTSLPR	0.0056	532.27	2	980.5	82	0	2347

Peptide	P value	M/Z measured	# MS	M/Z predicted	Shift	Position	Spectra #
DPGRDR	0.0065	697.29	2	714.3	-18	2	2516
DPGRDR	0.0152	697.34	2	714.3	-18	1	2404
SASLGR	0.0046	572.37	3	589.3	-18	4	2034
SASLGR	0.0032	572.41	3	589.3	-18	3	1968
SASLGR	0.0051	572.41	3	589.3	-18	3	1724
SASLGR	0.0024	572.45	3	589.3	-18	3	1862
RASFHLEC(57)LK	2.21E-04	621.88	3	1259.6	-18	3	3143
SASLGRR	0.0373	364.78	3	745.4	-18	1	1771
SASLGRR	0.027	364.89	3	745.4	-18	3	1920
ASFHLEC(57)LK	5.81E-04	544	3	1103.5	-18	2	3593
ASFHLEC(57)LK	0.0024	544.01	3	1103.5	-18	2	3518
ASFHLEC(57)LK	0.0143	544.02	3	1103.5	-18	2	3448
RASFHLEC(57)LK	0.0113	415.12	3	1259.6	-17	3	3175

Table 4-2: LC-MS-MS chymotrypsin digestion results

Peptide	P value	M/Z measured	# MS	M/Z predicted	Shift	Position	Spectra #
GGDISQKTVLPL	0.0156	436.03	2	1226.7	78.4	10	3424
ADAC(57)DLTIEEMEN AADDILSGGARQSPN	0.0162	1521.92	2	2962.3	79.5	0	6500
NSSFPSIHC(57)GSW	0.0015	729.68	2	1377.5	79.8	7	4108
RASFHLEC(57)L	0.0015	606.8	2	1131.5	80.1	5	3743
KNQGGDISQ	3.75E-04	513.93	2	945.5	80.4	8	3152
ISEGLGQF	0.0434	465.89	2	849.4	80.4	8	3721
HGSASSLVEAVLISE GLGQF	8.77E-07	1041.24	2	2000	80.5	3	5877
RASFHLEC(57)L	0.0241	405.1	2	1131.5	80.8	1	2425
SHSPTSLPRPC(57)	0.0367	660.22	2	1237.5	80.9	6	2745
VEAVL	0.0231	611.33	2	529.3	81	3	4518
SPKKGFL	0.0065	857.44	2	775.4	81	6	5215
C(57)GSWSGEN	0.0297	489.42	2	895.3	81.5	0	4462

Peptide	P value	M/Z measured	# MS	M/Z predicted	Shift	Position	Spectra #
RLEGADSSEKL	6.52E-06	593.88	3	1203.6	-18	7	2596
RASFHLEC(57)L	7.95E-07	557.85	3	1131.5	-18	3	3744

In vitro kinase assay confirms CaMKII phosphorylation sites

To biochemically validate the mass spectrometry data, the serine residues, 1922 and 1928, on the $Ca_V1.2$ C-terminus GST fusion protein were mutated as either single mutations to alanine (S1922A, S1928A) or double mutations to alanines (S1922/28A). These GST fusion proteins were purified and the protein expression and size was checked by immunoblot (Figure 4-7A).

The *in vitro* kinase assays were repeated with both CaMKII and PKA. In addition to the autoradiograph, a set volume of each assay was spotted and the cpms were measured after washing away free ^{32}P ATP. To accurately compare phosphorylation levels between the mutants and wild type proteins, the pmoles of ^{32}P incorporated per pmoles of protein were calculated based upon the concentration of GST fusion protein used and cpms measured. These experiments were repeated at least three times in triplicate, using a minimum of two GST fusion protein purifications.

The *in vitro* kinase assays with CaMKII revealed an intriguing trend. Each individual serine to alanine mutation (S1922A, S1928A) had no effect on overall CaMKII phosphorylation of the $Ca_V1.2$ C-terminus GST fusion protein as compared to wild type control (Figure 4-7B, C). However, the double mutant (S1922/28A) showed a significant decrease in CaMKII phosphorylation of the $Ca_V1.2$ C-terminus (Figure 4-7B, C). PKA *in vitro* kinase assays followed a different pattern from CaMKII. Only mutations of serine 1928, the canonical PKA phosphorylation site, showed a decrease in phosphorylation levels compared to wild type (Figure 4-7D).

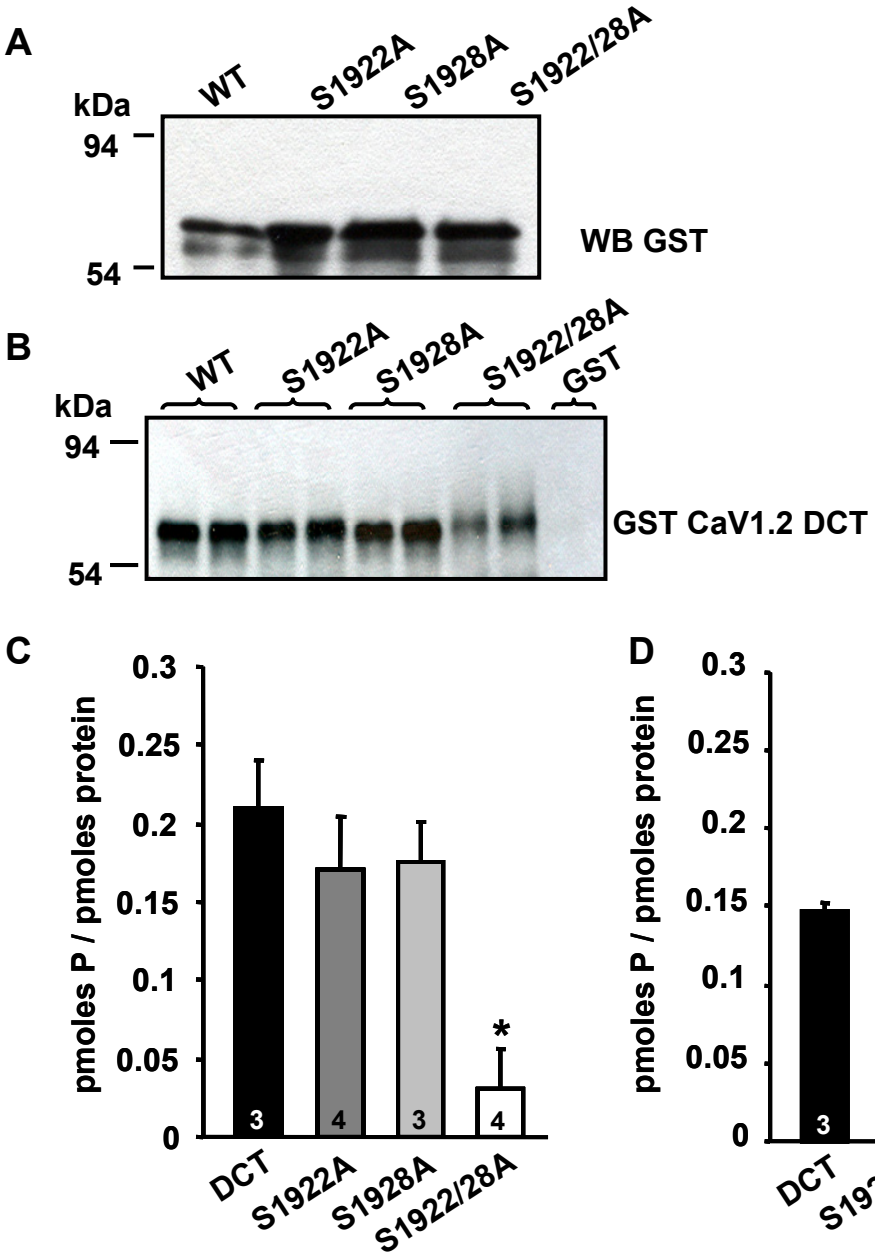

Figure 4-7: *In vitro* kinase assays on CaV1.2 distal C-terminus GST fusion proteins; wild type (DCT), serine 1922 to alanine mutation (S1922A), serine 1928 to alanine mutation (S1928A), double mutation serines 1922 and 1928 to alanines (S1922/28A). **A)** Western blot for GST of CaV1.2 distal C-terminus GST fusion proteins B) Autoradiograph of CaMKII *in vitro* kinase assay **C)** 10 nM CaMKII *in vitro* kinase assay. **D)** 10 nM PKA *in vitro* kinase assay. (* = $p<.05$)

Discussion

Implications of $Ca_V1.2$ phosphorylation studies

Interestingly, this work shows that CaMKII has the ability to phosphorylate two residues with close proximity and raises the question as to whether these sites have opposing or synergistic affects on $Ca_V1.2$ activity. The ability of CaMKII to phosphorylate serine 1922 and serine 1928 has interesting implication in relation to PKA phosphorylation of serine 1928 and $Ca_V1.2$ response to adrenergic stimulation. PLB is an example of a protein substrate where both CaMKII and PKA phosphorylate nearby sites. CaMKII phosphorylates residue threonine 17 [96] whereas PKA phosphorylates residue serine 16 [107]. The role of serine 16 and threonine 17 PLB phosphorylation is conflicted, but the it appears that either phosphorylation event releases PLB from SERCA and thereby enhances SERCA activity [60]. Another example of close proximity duel phosphorylation included CaMKII phosphorylation of Thr498 [43] and PKG of Ser494 [122] of the $Ca_V1.2$ β_{2a} subunit. These two sites on the β_{2a} subunit have opposing affects, where CaMKII phosphorylation causes an increase in I_{Ca} [43] and PKG causes a decrease in I_{Ca} [122]. A future direction would be to examine the affect CaMKII phosphorylation of serine 1922 on PKA phosphorylation of serine 1928 and if this has an impact on the response of ventricular myocyte to adrenergic signaling. Additionally, the ability of CaMKII to phosphorylate serine 1922 after PKA has phosphorylated serine 1928 could be examined. However, the role of serine 1928 during adrenergic stimulation has been questioned based

upon data showing that the C-terminus of $Ca_V1.2$ and not serine 1928 is required for $Ca_V1.2$ to respond to adrenergic signaling.

CaMKII regulation of $Ca_V1.2$

CaMKII was found to phosphorylate the $Ca_V1.2$ C-terminus at serine 1512 and serine 1570 [66] (Figure 4-8). Mutating these sites to alanine prevents voltage dependent I_{Ca} facilitation, a dynamic increase in I_{Ca} after a significant depolarizations (+160mV) [66]. The relevance of these data is questionable because the significant depolarization required for voltage dependent facilitation is not within the membrane voltages physiologically observed. Moreover, the phosphorylation sites were characterized within heterologous cells and not within ventricular myocytes where these sites may play a more important role in regulating I_{Ca}.

The $Ca_V1.2$ C-terminus is cleaved into two domains, the distal C-terminus and the proximal C-terminus [57]. The interaction of these domains affects I_{Ca} [58]. The CaMKII phosphorylation sites serine 1922 and serine 1928 are located on the distal C-terminus and serine 1512 and serine 1570 are located on the proximal C-terminus. The ability of CaMKII to phosphorylate these domains separately may be critical for the overall function of CaMKII regulation of $Ca_V1.2$ in ventricular myocytes.

CaMKII phosphorylation of the L-type Ca^{2+} channel β_{2a} subunit at thr498 (Figure 4-8) appears to be the central phosphorylation event leading to I_{Ca} facilitation [43]. Mutating Thr498 to alanine on the β_{2a} subunit prevents I_{Ca}

facilitation when expressed in adult ventricular myocytes [43]. However, the mechanism by which phosphorylation of the β_{2a} subunit changes $Ca_V1.2$ activity has yet to be elucidated. It is possible that CaMKII phosphorylation of the $Ca_V1.2$ C-terminus may play an important downstream role to Thr498 phosphorylation in I_{Ca} facilitation.

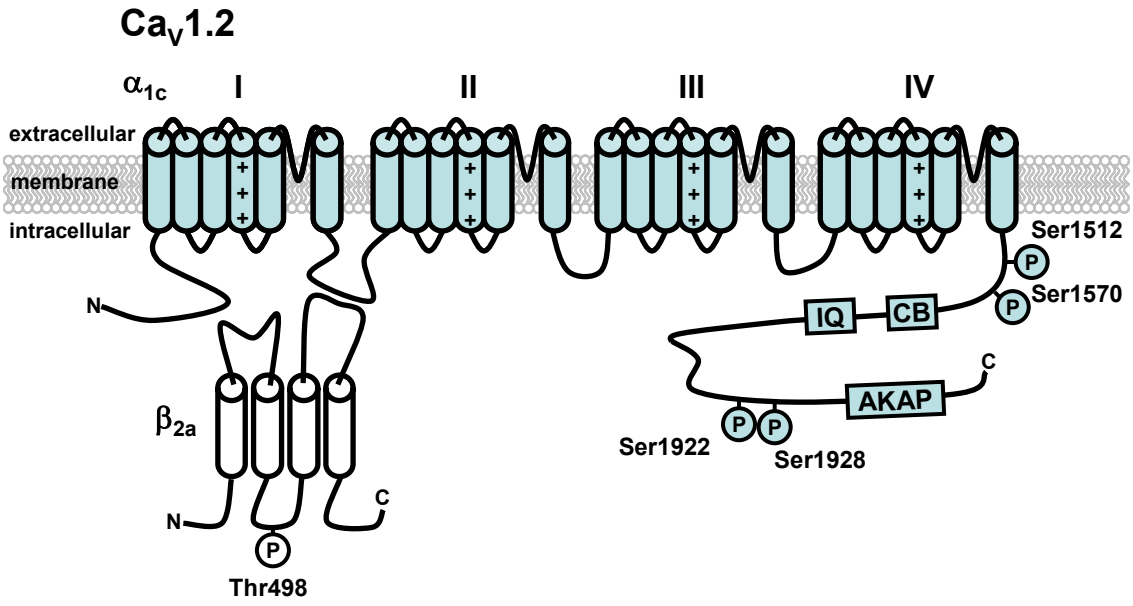

Figure 4-8: Schematic of $Ca_V1.2$ with accessory β_{2a} subunit highlighting CaMKII phosphorylation sites. CaMKII phosphorylation of Thr498 is critical for I_{Ca} facilitation.

14-3-3 predictions

Sequence analysis [118] of serine 1922 and serine 1928 reveals that phosphoserine 1922 may be 14-3-3 binding domain (Figure 4-9). 14-3-3 proteins

bind to phosphorylated targets and mediate many different cellular responses including protein trafficking. Work with the $Ca_V1.2$ distal C-terminus suggests that this domain may translocate to the nucleus and regulate gene expression [42]. The exact mechanism of the $Ca_V1.2$ distal C-terminus movement towards the nucleus remains unknown but the process is known to be Ca^{2+} dependent [42]. The CaMKII phosphorylation of serine 1922 within the distal C-terminus and subsequent interaction with 14-3-3 proteins may play a critical role in nuclear translocation of the distal C-terminus.

Phosphoserine/threonine binding group (pST_bind)

14-3-3 Mode 1			Gene Card YWHAZ	
Site	Score	Percentile	Sequence	SA
S1922	0.3165	0.117 %	KGFLRSA**S**LGRRASF	0.665

Figure 4-9: Scansite results predicting phospho-serine 1922 as a 14-3-3 binding motif.

Methods

Cloning GST fusion proteins

The C-terminus (residues 1507-2171) of $Ca_V1.2$ was cloned into the N-terminal GST fusion protein plasmid, pGEX4T, by PCR. The forward primer annealed at residues 1507 and contained a BaMHI restriction enzyme site. The reverse primer annealed at residues 2171 and contained a stop codon followed by a EcoRI restriction enzyme site. The PCR product was digested with both BaMHI and EcoRI and ligated into a pGEX4T plasmid opened with the same enzymes. The ligation was transformed into competent DH5α bacteria and plated overnight at 37°C on ampicillin containing agar plates. Colonies were picked, grown in media and screened by restriction enzyme digestion of BaMHI and EcoRI. Positively screened clones were sent for sequencing to confirm the ORF of the GST CaV1.2 C-terminus protein.

Two truncation of the GST $Ca_V1.2$ C-terminus ORF were made to create the GST $Ca_V1.2$ DCT and GST $Ca_V1.2$ PCT. The GST $Ca_V1.2$ PCT (residues 1507-1905) was created by introducing a premature stop codon by PCR mutangenesis after residue 1905. The GST $Ca_V1.2$ DCT (residues 1909-2171) was created by first introducing a second BaMHI cute site preceding residue 1909 and then digesting the resulting construct with BaMHI and performing a self ligation. Both GST $Ca_V1.2$ DCT and PCT were confirmed by sequencing the ORF.

Purification of GST fusion protein

LB media (100mL) was inoculated with bacteria transformed with a pGEX4T construct ($Ca_V1.2$ C-terminus, PCT or DCT) and incubated at 37°C overnight (16-18 hrs). The culture was added to pre-warmed media (500mL) and incubated at 37°C until the OD660 reached between 0.62 and 0.90. Protein production was induced by the addition of IPTG (final 1mM) to the bacterial culture and incubated at 30-37°C for 1-3hrs. The bacterial culture was pelleted and the spent media was discarded. The bacterial pellet was resuspended and lysed by sonication (30 seconds on and 30 seconds off at level 4 for a total of 5 min.). The lysed bacteria were pelleted by centrifugation and the supernatant was harvested. Glutathione beads were added to the supernatant and incubated at 4C for 1hr while gently shaking. The beads were collected in a column and washed several times. Bound protein was eluted by the addition of excess glutathione and collected within dialysis tubing and washed overnight. The purified protein was aliquoted and stored at -80°C. The purified protein was assessed for purity by SDS-PAGE.

Western blot of GST fusion proteins

Purified GST fusion protein was loaded (25μL of 5μM protein) into a 10% acrylamide gel with stacking and ran until dye front reached bottom of plates. Protein from the gel was transferred to a nitrocellulose membrane at 100 volts in transfer butter with 15% methanol. The membrane was blocked with 5% milk in PBS-Tween overnight at 4°C and immunoblotted with a primary antibody against

GST at 1:5000 for 2hrs at room temperature. The blot was washed 6 times with PBS-T for 15 minutes and a secondary HRP conjugated bovine anti-goat antibody at 1:5000 dilution was added at RT for 2 hours. The blot was washed and exposed to film by chemiluminescence.

In vitro kinase assays

In vitro kinase assays were performed with either CaMKII (10nM) or PKA (10nM) on purified GST fusion proteins (2μM) as substrates. Phosphorylation of the substrate was determined by the amount of ^{32}P incorporated into the substrate by measuring cpms from the reaction and by autoradiography of the reaction analyzed by SDS-PAGE. CaMKII kinase reaction consisted of 50mM HEPES, 10mM $Mg(Ac)_2$, 0.5mM $CaCl_2$, 1μM CaM, 1mM DTT and 0.4mM [^{32}P]ATP. PKA kinase reaction consisted of 50mM HEPES, 10mM $Mg(Ac)_2$, 1mM DTT and 0.4mM [^{32}P]ATP. All kinase reactions were initiated by the addition of the kinase and allowed to proceed for 20 minutes at 30°C, whereupon a sample of each reaction was spotted on P81 filter paper and each reaction was stopped by the addition of sample buffer.

Data analysis and statistics

All data reported as means with standard error of the mean (SEM). Two groups were compared using the Student T-test statistical test. Significance was set at a P value < 0.05.

Amino peptide mapping

Amino peptide mapping was performed, as previously reported[43], on *in vitro* CaMKII phosphorylated $Ca_V1.2$ DCT GST fusion protein. The radio-labeled GST fusion protein was removed from a dried Coomassie stained SDS-PAGE gel, solubilized and hydrolyzed with HCl (5.7M). Samples were run on thin layer chromatography plates with phospho-serine and phospho-threonine standards. Plates were stained to reveal the phospho standards and exposed to film.

Mass spectrometry

Purified GST fusion proteins were prepared for mass spectrometry phosphorylation analysis performing paired *in vitro* kinase assays. One sample contained [^{32}P] ATP to verify phosphorylation of the substrate and the second sample, prepared with cold ATP, was submitted for LC-MS-MS (Amy Hamm, Vanderbilt University). The program P-mod was used to analyze the spectra and identify possible phosphorylation events.

REFERENCE LIST

(1) Ai X, Curran JW, Shannon TR, Bers DM, Pogwizd SM. Ca2+/Calmodulin-Dependent Protein Kinase Modulates Cardiac Ryanodine Receptor Phosphorylation and Sarcoplasmic Reticulum Ca2+ Leak in Heart Failure. *Circ Res* 2005 December 9;97(12):1314-22.

(2) Altier C, Dubel SJ, Barrere C et al. Trafficking of L-type calcium channels mediated by the postsynaptic scaffolding protein AKAP79. *J Biol Chem* 2002 September 13;277(37):33598-603.

(3) Anderson ME, Braun AP, Schulman H, Premack BA. Multifunctional Ca2+/calmodulin-dependent protein kinase mediates Ca(2+)-induced enhancement of the L-type Ca2+ current in rabbit ventricular myocytes. *Circ Res* 1994 November;75(5):854-61.

(4) Bach ME, Hawkins RD, Osman M, Kandel ER, Mayford M. Impairment of spatial but not contextual memory in CaMKII mutant mice with a selective loss of hippocampal LTP in the range of the theta frequency. *Cell* 1995 June 16;81(6):905-15.

(5) Balke CW, Rose WC, Marban E, Wier WG. Macroscopic and unitary properties of physiological ion flux through T-type Ca2+ channels in guinea-pig heart cells. *J Physiol* 1992 October;456:247-65.

(6) Barrett CF, Tsien RW. The Timothy syndrome mutation differentially affects voltage- and calcium-dependent inactivation of CaV1.2 L-type calcium channels. *PNAS* 2008 February 4;105(6):2157-62.

(7) Bassani JW, Bassani RA, Bers DM. Relaxation in rabbit and rat cardiac cells: species-dependent differences in cellular mechanisms. *J Physiol* 1994 April 15;476(2):279-93.

(8) Bassani RA, Mattiazzi A, Bers DM. CaMKII is responsible for activity-dependent acceleration of relaxation in rat ventricular myocytes. *Am J Physiol* 1995 February;268(2 Pt 2):H703-H712.

(9) Bers DM. *Excitation-Contraction Coupling and Cardiac Contractile Force*. 2nd ed. Dordrecht, the Netherlands: Kluwer Academic Publishers; 2001.

(10) Bers DM. Cardiac excitation-contraction coupling. *Nature* 2002 January 10;415(6868):198-205.

(11) Bradshaw JM, Kubota Y, Meyer T, Schulman H. An ultrasensitive Ca2+/calmodulin-dependent protein kinase II-protein phosphatase 1 switch facilitates specificity in postsynaptic calcium signaling. *PNAS* 2003 September 2;100(18):10512-7.

(12) Brehm P, Eckert R. Calcium entry leads to inactivation of calcium channel in Paramecium. *Science* 1978 December 15;202(4373):1203-6.

(13) Brette F, Orchard C. T-Tubule Function in Mammalian Cardiac Myocytes. *Circ Res* 2003 June 13;92(11):1182-92.

(14) Bunemann M, Gerhardstein BL, Gao T, Hosey MM. Functional regulation of L-type calcium channels via protein kinase A-mediated phosphorylation of the beta(2) subunit. *J Biol Chem* 1999 November 26;274(48):33851-4.

(15) Cens T, Restituito S, Galas S, Charnet P. Voltage and Calcium Use the Same Molecular Determinants to Inactivate Calcium Channels. *J Biol Chem* 1999 February 26;274(9):5483-90.

(16) Chang CF, Gutierrez LM, Mundina-Weilenmann C, Hosey MM. Dihydropyridine-sensitive calcium channels from skeletal muscle. II. Functional effects of differential phosphorylation of channel subunits. *J Biol Chem* 1991 September 5;266(25):16395-400.

(17) Colbran RJ. Targeting of calcium/calmodulin-dependent protein kinase II. *Biochem J* 2004 February 15;378(Pt 1):1-16.

(18) Colbran RJ, Fong YL, Schworer CM, Soderling TR. Regulatory interactions of the calmodulin-binding, inhibitory, and autophosphorylation domains of Ca2+/calmodulin-dependent protein kinase II. *J Biol Chem* 1988 December 5;263(34):18145-51.

(19) Colbran RJ, Smith MK, Schworer CM, Fong YL, Soderling TR. Regulatory domain of calcium/calmodulin-dependent protein kinase II. Mechanism of inhibition and regulation by phosphorylation. *J Biol Chem* 1989 March 25;264(9):4800-4.

(20) Cruzalegui FH, Kapiloff MS, Morfin J, Kemp BE, Rosenfeld MG, Means AR. Regulation of Intrasteric Inhibition of the Multifunctional Calcium/ Calmodulin-Dependent Protein Kinase. *PNAS* 1992 December 15;89(24):12127-31.

(21) De Ferrari GM, Viola MC, D'Amato E, Antolini R, Forti S. Distinct patterns of calcium transients during early and delayed afterdepolarizations induced by isoproterenol in ventricular myocytes. *Circulation* 1995 May 15;91(10):2510-5.

(22) De Jongh KS, Merrick DK, Catterall WA. Subunits of purified calcium channels: a 212-kDa form of alpha 1 and partial amino acid sequence of a phosphorylation site of an independent beta subunit. *Proc Natl Acad Sci U S A* 1989 November;86(21):8585-9.

(23) De Jongh KS, Murphy BJ, Colvin AA, Hell JW, Takahashi M, Catterall WA. Specific Phosphorylation of a Site in the Full-Length Form of the α1 Subunit of the Cardiac L-Type Calcium Channel by Adenosine 3',5'-Cyclic Monophosphate- Dependent Protein Kinase. *Biochemistry* 1996 August 13;35(32):10392-402.

(24) De Jongh KS, Warner C, Colvin AA, Catterall WA. Characterization of the two size forms of the alpha 1 subunit of skeletal muscle L-type calcium channels. *Proc Natl Acad Sci U S A* 1991 December 1;88(23):10778-82.

(25) De Koninck P, Schulman H. Sensitivity of CaM Kinase II to the Frequency of Ca2+ Oscillations. *Science* 1998 January 9;279(5348):227-30.

(26) De Waard M, Pragnell M, Campbell KP. Ca2+ channel regulation by a conserved beta subunit domain. *Neuron* 1994 August;13(2):495-503.

(27) Delbridge LM, Bassani JW, Bers DM. Steady-state twitch Ca2+ fluxes and cytosolic Ca2+ buffering in rabbit ventricular myocytes. *Am J Physiol Cell Physiol* 1996 January 1;270(1):C192-C199.

(28) DeSantiago J, Maier LS, Bers DM. Frequency-dependent acceleration of relaxation in the heart depends on CaMKII, but not phospholamban. *J Mol Cell Cardiol* 2002 August;34(8):975-84.

(29) Dolmetsch RE, Pajvani U, Fife K, Spotts JM, Greenberg ME. Signaling to the nucleus by an L-type calcium channel-calmodulin complex through the MAP kinase pathway. *Science* 2001 October 12;294(5541):333-9.

(30) Dzhura I, Wu Y, Colbran RJ, Balser JR, Anderson ME. Calmodulin kinase determines calcium-dependent facilitation of L-type calcium channels. *Nat Cell Biol* 2000 March;2(3):173-7.

(31) Dzhura I, Wu Y, Colbran RJ, Corbin JD, Balser JR, Anderson ME. Cytoskeletal disrupting agents prevent calmodulin kinase, IQ domain and voltage-dependent facilitation of L-type Ca2+ channels. *J Physiol* 2002 December 1;545(Pt 2):399-406.

(32) Erickson JR, Joiner ML, Guan X et al. A dynamic pathway for calcium-independent activation of CaMKII by methionine oxidation. *Cell* 2008 May 2;133(3):462-74.

(33) Erxleben C, Liao Y, Gentile S et al. Cyclosporin and Timothy syndrome increase mode 2 gating of CaV1.2 calcium channels through aberrant phosphorylation of S6 helices. *PNAS* 2006 March 7;103(10):3932-7.

(34) Faber GM, Rudy Y. Action Potential and Contractility Changes in [Na+]i Overloaded Cardiac Myocytes: A Simulation Study. *Biophys J* 2000 May 1;78(5):2392-404.

(35) Faber GM, Silva J, Livshitz L, Rudy Y. Kinetic Properties of the Cardiac L-Type Ca2+ Channel and Its Role in Myocyte Electrophysiology: A Theoretical Investigation. *Biophys J* 2007 March 1;92(5):1522-43.

(36) Findlay I. Physiological modulation of inactivation in L-type Ca2+ channels: one switch. *J Physiol (Lond)* 2004 January 15;554(2):275-83.

(37) Fukunaga K, Kobayashi T, Tamura S, Miyamoto E. Dephosphorylation of autophosphorylated Ca2+/calmodulin-dependent protein kinase II by protein phosphatase 2C. *J Biol Chem* 1993 January 5;268(1):133-7.

(38) Ganesan AN, Maack C, Johns DC, Sidor A, O'rourke B. Beta-adrenergic stimulation of L-type Ca2+ channels in cardiac myocytes requires the distal carboxyl terminus of alpha1C but not serine 1928. *Circ Res* 2006 February 3;98(2):e11-e18.

(39) Ganesan AN, O'rourke B, Maack C, Colecraft H, Sidor A, Johns DC. Reverse engineering the L-type Ca(2+) channel alpha(1c) subunit in adult cardiac myocytes using novel adenoviral vectors. *Biochem Biophys Res Commun* 2005 April 8;329(2):749-54.

(40) Gao T, Yatani A, Dell'Acqua ML et al. cAMP-dependent regulation of cardiac L-type Ca2+ channels requires membrane targeting of PKA and phosphorylation of channel subunits. *Neuron* 1997 July;19(1):185-96.

(41) Gerhardstein BL, Puri TS, Chien AJ, Hosey MM. Identification of the sites phosphorylated by cyclic AMP-dependent protein kinase on the beta 2 subunit of L-type voltage-dependent calcium channels. *Biochemistry* 1999 August 10;38(32):10361-70.

(42) Gomez-Ospina N, Tsuruta F, Barreto-Chang O, Hu L, Dolmetsch R. The C Terminus of the L-Type Voltage-Gated Calcium Channel CaV1.2 Encodes a Transcription Factor. *Cell* 2006 November 3;127(3):591-606.

(43) Grueter CE, Abiria SA, Dzhura I et al. L-type Ca2+ channel facilitation mediated by phosphorylation of the beta subunit by CaMKII. *Mol Cell* 2006 September 1;23(5):641-50.

(44) Guo T, Zhang T, Mestril R, Bers DM. Ca2+/Calmodulin-Dependent Protein Kinase II Phosphorylation of Ryanodine Receptor Does Affect Calcium

Sparks in Mouse Ventricular Myocytes. *Circ Res* 2006 August 18;99(4):398-406.

(45) Haase H, Kresse A, Hohaus A et al. Expression of calcium channel subunits in the normal and diseased human myocardium. *J Mol Med* 1996 February;74(2):99-104.

(46) Hadley RW, Hume JR. An intrinsic potential-dependent inactivation mechanism associated with calcium channels in guinea-pig myocytes. *J Physiol (Lond)* 1987 August 1;389(1):205-22.

(47) Hagemann D, Bohlender J, Hoch B, Krause EG, Karczewski P. Expression of Ca2+/calmodulin-dependent protein kinase II delta-subunit isoforms in rats with hypertensive cardiac hypertrophy. *Mol Cell Biochem* 2001 April;220(1-2):69-76.

(48) Hagemann D, Kuschel M, Kuramochi T, Zhu W, Cheng H, Xiao RP. Frequency-encoding Thr17 phospholamban phosphorylation is independent of Ser16 phosphorylation in cardiac myocytes. *J Biol Chem* 2000 July 21;275(29):22532-6.

(49) Handrock R, Schroder F, Hirt S, Haverich A, Mittmann C, Herzig S. Single-channel properties of L-type calcium channels from failing human ventricle. *Cardiovasc Res* 1998 February;37(2):445-55.

(50) Hanley RM, Means AR, Kemp BE, Shenolikar S. Mapping of calmodulin-binding domain of Ca2+/calmodulin-dependent protein kinase II from rat brain. *Biochemical and Biophysical Research Communications* 1988 April 15;152(1):122-8.

(51) Hardman J, Limbird L, Gilman A. *Goodman and Gilman's Pharmacological Basis of Therapeutics*. 10 ed. New York: McGraw-Hill Medical Publishing Division; 2001.

(52) He M, Bodi I, Mikala G, Schwartz A. Motif III S5 of L-type calcium channels is involved in the dihydropyridine binding site. A combined radioligand binding and electrophysiological study. *J Biol Chem* 1997 January 31;272(5):2629-33.

(53) Hess P, Lansman JB, Tsien RW. Different modes of Ca channel gating behaviour favoured by dihydropyridine Ca agonists and antagonists. *Nature* 1984 October 11;311(5986):538-44.

(54) Hille B. *Ion Channels of Excitable Membranes*. 3rd ed. Sinauer Associates; 2008.

(55) Hoch B, Meyer R, Hetzer R, Krause EG, Karczewski P. Identification and expression of delta-isoforms of the multifunctional Ca2+/calmodulin-

dependent protein kinase in failing and nonfailing human myocardium. *Circ Res* 1999 April 2;84(6):713-21.

(56) Hoelz A, Nairn AC, Kuriyan J. Crystal structure of a tetradecameric assembly of the association domain of Ca2+/calmodulin-dependent kinase II. *Mol Cell* 2003 May;11(5):1241-51.

(57) Hulme JT, Konoki K, Lin TW et al. Sites of proteolytic processing and noncovalent association of the distal C-terminal domain of CaV1.1 channels in skeletal muscle. *Proc Natl Acad Sci U S A* 2005 March 25.

(58) Hulme JT, Yarov-Yarovoy V, Lin TWC, Scheuer T, Catterall WA. Autoinhibitory control of the CaV1.2 channel by its proteolytically processed distal C-terminal domain. *J Physiol (Lond)* 2006 October 1;576(1):87-102.

(59) Hund TJ, Kucera JP, Otani NF, Rudy Y. Ionic Charge Conservation and Long-Term Steady State in the Luo-Rudy Dynamic Cell Model. *Biophysical Journal* 2001 December 1;81(6):3324-31.

(60) Inui M, Chamberlain BK, Saito A, Fleischer S. The nature of the modulation of Ca2+ transport as studied by reconstitution of cardiac sarcoplasmic reticulum. *J Biol Chem* 1986 February 5;261(4):1794-800.

(61) Jacobs A, Knight BP, McDonald KT, Burke MC. Verapamil decreases ventricular tachyarrhythmias in a patient with Timothy syndrome (LQT8). *Heart Rhythm* 2006 August;3(8):967-70.

(62) January CT, Riddle JM. Early afterdepolarizations: mechanism of induction and block. A role for L-type Ca2+ current. *Circ Res* 1989 May;64(5):977-90.

(63) Kanaseki T, Ikeuchi Y, Sugiura H, Yamauchi T. Structural features of Ca2+/calmodulin-dependent protein kinase II revealed by electron microscopy. *J Cell Biol* 1991 November 1;115(4):1049-60.

(64) Kolodziej SJ, Hudmon A, Waxham MN, Stoops JK. Three-dimensional Reconstructions of Calcium/Calmodulin-dependent (CaM) Kinase IIalpha and Truncated CaM Kinase IIalpha Reveal a Unique Organization for Its Structural Core and Functional Domains. *J Biol Chem* 2000 May 5;275(19):14354-9.

(65) Lai Y, Nairn AC, Gorelick F, Greengard P. Ca2+/calmodulin-dependent Protein kinase II: Identification of Autophosphorylation Sites Responsible for Generation of Ca2+/calmodulin-independence. *PNAS* 1987 August 15;84(16):5710-4.

(66) Lee TS, Karl R, Moosmang S et al. Calmodulin Kinase II Is Involved in Voltage-dependent Facilitation of the L-type Cav1.2 Calcium Channel: IDENTIFICATION OF THE PHOSPHORYLATION SITES. *J Biol Chem* 2006 September 1;281(35):25560-7.

(67) Li J, Marionneau C, Zhang R et al. Calmodulin Kinase II Inhibition Shortens Action Potential Duration by Upregulation of K+ Currents. *Circ Res* 2006 November 10;99(10):1092-9.

(68) Lindemann JP, Jones LR, Hathaway DR, Henry BG, Watanabe AM. beta-Adrenergic stimulation of phospholamban phosphorylation and Ca2+-ATPase activity in guinea pig ventricles. *J Biol Chem* 1983 January 10;258(1):464-71.

(69) Livshitz LM, Rudy Y. Regulation of Ca2+ and electrical alternans in cardiac myocytes: role of CAMKII and repolarizing currents. *Am J Physiol Heart Circ Physiol* 2007 June 1;292(6):H2854-H2866.

(70) Lokuta AJ, Rogers TB, Lederer WJ, Valdivia HH. Modulation of cardiac ryanodine receptors of swine and rabbit by a phosphorylation-dephosphorylation mechanism. *J Physiol* 1995 September 15;487 (Pt 3):609-22.

(71) Lou LL, Lloyd SJ, Schulman H. Activation of the multifunctional Ca2+/calmodulin-dependent protein kinase by autophosphorylation: ATP modulates production of an autonomous enzyme. *Proc Natl Acad Sci U S A* 1986 December;83(24):9497-501.

(72) Luo CH, Rudy Y. A dynamic model of the cardiac ventricular action potential. I. Simulations of ionic currents and concentration changes. *Circ Res* 1994 June;74(6):1071-96.

(73) Maier LS, Zhang T, Chen L, DeSantiago J, Brown JH, Bers DM. Transgenic CaMKII{delta}C Overexpression Uniquely Alters Cardiac Myocyte Ca2+ Handling: Reduced SR Ca2+ Load and Activated SR Ca2+ Release. *Circ Res* 2003 May 2;92(8):904-11.

(74) Marks ML, Whisler SL, Clericuzio C, Keating M. A new form of long QT syndrome associated with syndactyly. *Journal of the American College of Cardiology* 1995 January;25(1):59-64.

(75) Marx SO, Reiken S, Hisamatsu Y et al. PKA phosphorylation dissociates FKBP12.6 from the calcium release channel (ryanodine receptor): defective regulation in failing hearts. *Cell* 2000 May 12;101(4):365-76.

(76) Masse T, Kelly PT. Overexpression of Ca2+/Calmodulin-Dependent Protein Kinase II in PC12 Cells Alters Cell Growth, Morphology, and Nerve

Growth Factor-Induced Differentiation. *J Neurosci* 1997 February 1;17(3):924-31.

(77) Maune JF, Klee CB, Beckingham K. Ca2+ binding and conformational change in two series of point mutations to the individual Ca(2+)-binding sites of calmodulin. *J Biol Chem* 1992 March 15;267(8):5286-95.

(78) McDonald TF, Pelzer S, Trautwein W, Pelzer DJ. Regulation and modulation of calcium channels in cardiac, skeletal, and smooth muscle cells. *Physiol Rev* 1994 April;74(2):365-507.

(79) Meyer T, Hanson PI, Stryer L, Schulman H. Calmodulin Trapping by Calcium-Calmodulin-Dependent Protein Kinase. *Science* 1992 May 22;256(5060):1199-202.

(80) Ozawa T, Sasaki K, Umezawa Y. Metal ion selectivity for formation of the calmodulin-metal-target peptide ternary complex studied by surface plasmon resonance spectroscopy. *Biochimica et Biophysica Acta (BBA) - Protein Structure and Molecular Enzymology* 1999 October 12;1434(2):211-20.

(81) Payne ME, Fong YL, Ono T et al. Calcium/calmodulin-dependent protein kinase II. Characterization of distinct calmodulin binding and inhibitory domains. *J Biol Chem* 1988 May 25;263(15):7190-5.

(82) Pelzer D, Pelzer S, McDonald TF. Properties and regulation of calcium channels in muscle cells. *Rev Physiol Biochem Pharmacol* 1990;114:107-207.

(83) Peterson BZ, DeMaria CD, Yue DT. Calmodulin is the Ca2+ sensor for Ca2+-dependent inactivation of 1-type calcium channels. *Neuron* 1999 March;22(3):549-58.

(84) Picht E, DeSantiago J, Huke S, Kaetzel MA, Dedman JR, Bers DM. CaMKII inhibition targeted to the sarcoplasmic reticulum inhibits frequency-dependent acceleration of relaxation and Ca2+ current facilitation. *J Mol Cell Cardiol* 2007 January;42(1):196-205.

(85) Pinna LA, Ruzzene M. How do protein kinases recognize their substrates? *Biochim Biophys Acta* 1996 December 12;1314(3):191-225.

(86) Pragnell M, De Waard M, Mori Y, Tanabe T, Snutch TP, Campbell KP. Calcium channel beta-subunit binds to a conserved motif in the I-II cytoplasmic linker of the alpha 1-subunit. *Nature* 1994 March 3;368(6466):67-70.

(87) Priebe L, Beuckelmann DJ. Simulation Study of Cellular Electric Properties in Heart Failure. *Circ Res* 1998 June 15;82(11):1206-23.

(88) Priori SG, Corr PB. [Variations in arrhythmogenic response to catecholamines in acute myocardial ischemia]. *Cardiologia* 1991 March;36(3):229-35.

(89) Puri TS, Gerhardstein BL, Zhao XL, Ladner MB, Hosey MM. Differential effects of subunit interactions on protein kinase A- and C-mediated phosphorylation of L-type calcium channels. *Biochemistry* 1997 August 5;36(31):9605-15.

(90) Roden DM, Lazzara R, Rosen M, Schwartz PJ, Towbin J, Vincent GM. Multiple Mechanisms in the Long-QT Syndrome: Current Knowledge, Gaps, and Future Directions. *Circulation* 1996 October 15;94(8):1996-2012.

(91) Schroder F, Handrock R, Beuckelmann DJ et al. Increased availability and open probability of single L-type calcium channels from failing compared with nonfailing human ventricle. *Circulation* 1998 September 8;98(10):969-76.

(92) Schuster A, Lacinova L, Klugbauer N, Ito H, Birnbaumer L, Hofmann F. The IVS6 segment of the L-type calcium channel is critical for the action of dihydropyridines and phenylalkylamines. *EMBO J* 1996 May 15;15(10):2365-70.

(93) Schworer CM, Colbran RJ, Keefer JR, Soderling TR. Ca2+/calmodulin-dependent protein kinase II. Identification of a regulatory autophosphorylation site adjacent to the inhibitory and calmodulin-binding domains. *J Biol Chem* 1988 September 25;263(27):13486-9.

(94) Schworer CM, Colbran RJ, Soderling TR. Reversible generation of a Ca2+-independent form of Ca2+(calmodulin)- dependent protein kinase II by an autophosphorylation mechanism. *J Biol Chem* 1986 July 5;261(19):8581-4.

(95) Shields SM, Ingebritsen TS, Kelly PT. Identification of protein phosphatase 1 in synaptic junctions: dephosphorylation of endogenous calmodulin-dependent kinase II and synapse-enriched phosphoproteins. *J Neurosci* 1985 December 1;5(12):3414-22.

(96) Simmerman HK, Collins JH, Theibert JL, Wegener AD, Jones LR. Sequence analysis of phospholamban. Identification of phosphorylation sites and two major structural domains. *J Biol Chem* 1986 October 5;261(28):13333-41.

(97) Soldatov NM, Oz M, O'Brien KA, Abernethy DR, Morad M. Molecular Determinants of L-type Ca2+ Channel Inactivation. SEGMENT EXCHANGE ANALYSIS OF THE CARBOXYL-TERMINAL CYTOPLASMIC MOTIF ENCODED BY EXONS 40-42 OF THE HUMAN alpha 1C SUBUNIT GENE. *J Biol Chem* 1998 January 9;273(2):957-63.

(98) Song LS, Guia A, Muth JN et al. Ca(2+) signaling in cardiac myocytes overexpressing the alpha(1) subunit of L-type Ca(2+) channel. *Circ Res* 2002 February 8;90(2):174-81.

(99) Song LS, Sobie EA, McCulle S, Lederer WJ, Balke CW, Cheng H. Orphaned ryanodine receptors in the failing heart. *Proceedings of the National Academy of Sciences* 2006 March 14;103(11):4305-10.

(100) Splawski I, Timothy KW, Decher N et al. Inaugural Article: Severe arrhythmia disorder caused by cardiac L-type calcium channel mutations. *PNAS* 2005 June 7;102(23):8089-96.

(101) Splawski I, Timothy KW, Sharpe LM et al. CaV1.2 Calcium Channel Dysfunction Causes a Multisystem Disorder Including Arrhythmia and Autism. *Cell* 2004 October 1;119(1):19-31.

(102) Splawski I, Yoo DS, Stotz SC, Cherry A, Clapham DE, Keating MT. CACNA1H Mutations in Autism Spectrum Disorders. *J Biol Chem* 2006 August 4;281(31):22085-91.

(103) Tada M, Kirchberger MA, Repke DI, Katz AM. The stimulation of calcium transport in cardiac sarcoplasmic reticulum by adenosine 3':5'-monophosphate-dependent protein kinase. *J Biol Chem* 1974 October 10;249(19):6174-80.

(104) Thandroyen FT, Morris AC, Hagler HK et al. Intracellular calcium transients and arrhythmia in isolated heart cells. *Circ Res* 1991 September 1;69(3):810-9.

(105) Wagner S, Dybkova N, Rasenack EC et al. Ca2+/calmodulin-dependent protein kinase II regulates cardiac Na+ channels. *J Clin Invest* 2006 December;116(12):3127-38.

(106) Wang SQ, Wei C, Zhao G et al. Imaging Microdomain Ca2+ in Muscle Cells. *Circ Res* 2004 April 30;94(8):1011-22.

(107) Wegener AD, Simmerman HK, Lindemann JP, Jones LR. Phospholamban phosphorylation in intact ventricles. Phosphorylation of serine 16 and threonine 17 in response to beta-adrenergic stimulation [published erratum appears in J Biol Chem 1989 Sep 15;264(26):15738]. *J Biol Chem* 1989 July 5;264(19):11468-74.

(108) Wehrens XHT, Lehnart SE, Reiken SR, Marks AR. Ca2+/Calmodulin-Dependent Protein Kinase II Phosphorylation Regulates the Cardiac Ryanodine Receptor. *Circ Res* 2004 April 2;94(6):e61-e70.

(109) Weidmann S. Resting and action potentials of cardiac muscle. *Ann N Y Acad Sci* 1957 August 9;65(6):663-78.

(110) Weidmann S. Membrane excitation in cardiac muscle. *Circulation* 1961 August;24:499-505.

(111) Witcher DR, Kovacs RJ, Schulman H, Cefali DC, Jones LR. Unique phosphorylation site on the cardiac ryanodine receptor regulates calcium channel activity. *J Biol Chem* 1991 June 15;266(17):11144-52.

(112) Wu Y, Colbran RJ, Anderson ME. Calmodulin kinase is a molecular switch for cardiac excitation-contraction coupling. *Proc Natl Acad Sci U S A* 2001 February 27;98(5):2877-81.

(113) Wu Y, Dzhura I, Colbran RJ, Anderson ME. Calmodulin kinase and a calmodulin-binding 'IQ' domain facilitate L-type Ca2+ current in rabbit ventricular myocytes by a common mechanism. *J Physiol* 2001 September 15;535(Pt 3):679-87.

(114) Wu Y, Kimbrough JT, Colbran RJ, Anderson ME. Calmodulin kinase is functionally targeted to the action potential plateau for regulation of L-type Ca2+ current in rabbit cardiomyocytes. *J Physiol* 2004 January 1;554(Pt 1):145-55.

(115) Wu Y, MacMillan LB, McNeill RB, Colbran RJ, Anderson ME. CaM kinase augments cardiac L-type Ca2+ current: a cellular mechanism for long Q-T arrhythmias. *Am J Physiol* 1999 June;276(6 Pt 2):H2168-H2178.

(116) Wu Y, Roden DM, Anderson ME. Calmodulin kinase inhibition prevents development of the arrhythmogenic transient inward current. *Circ Res* 1999 April 30;84(8):906-12.

(117) Wu Y, Temple J, Zhang R et al. Calmodulin kinase II and arrhythmias in a mouse model of cardiac hypertrophy. *Circulation* 2002 September 3;106(10):1288-93.

(118) Yaffe MB, Leparc GG, Lai J, Obata T, Volinia S, Cantley LC. A motif-based profile scanning approach for genome-wide prediction of signaling pathways. *Nat Biotechnol* 2001 April;19(4):348-53.

(119) Yan GX, Rials SJ, Wu Y et al. Ventricular hypertrophy amplifies transmural repolarization dispersion and induces early afterdepolarization. *Am J Physiol Heart Circ Physiol* 2001 November 1;281(5):H1968-H1975.

(120) Yang D, Zhu WZ, Xiao B et al. Ca2+/Calmodulin Kinase II-Dependent Phosphorylation of Ryanodine Receptors Suppresses Ca2+ Sparks and Ca2+ Waves in Cardiac Myocytes. *Circ Res* 2007 February 16;100(3):399-407.

(121) Yang L, Liu G, Zakharov SI et al. Ser1928 is a common site for cav1.2 phosphorylation by protein kinase C isoforms. *J Biol Chem* 2005 January 7;280(1):207-14.

(122) Yang L, Liu G, Zakharov SI, Bellinger AM, Mongillo M, Marx SO. Protein Kinase G Phosphorylates Cav1.2 {alpha}1c and {beta}2 Subunits. *Circ Res* 2007 August 31;101(5):465-74.

(123) Yuan W, Bers DM. Ca-dependent facilitation of cardiac Ca current is due to Ca-calmodulin-dependent protein kinase. *Am J Physiol* 1994 September;267(3 Pt 2):H982-H993.

(124) Yue DT, Herzig S, Marban E. Beta-adrenergic stimulation of calcium channels occurs by potentiation of high-activity gating modes. *Proc Natl Acad Sci U S A* 1990 January;87(2):753-7.

(125) Zeng J, Rudy Y. Early afterdepolarizations in cardiac myocytes: mechanism and rate dependence. *Biophysical Journal* 1995 March 1;68(3):949-64.

(126) Zhang R, Khoo MS, Wu Y et al. Calmodulin kinase II inhibition protects against structural heart disease. *Nat Med* 2005 April;11(4):409-17.

(127) Zuhlke RD, Pitt GS, Deisseroth K, Tsien RW, Reuter H. Calmodulin supports both inactivation and facilitation of L-type calcium channels. *Nature* 1999 May 13;399(6732):159-62.

(128) Zuhlke RD, Reuter H. Ca2+-sensitive inactivation of L-type Ca2+ channels depends on multiple cytoplasmic amino acid sequences of the alpha1C subunit. *Proc Natl Acad Sci U S A* 1998 March 17;95(6):3287-94.